



HAL
open science

Interactions physiques de bicouches lipidiques déposées sur un coussin de polymères pour l'incorporation de protéines

Jean Goder

► **To cite this version:**

Jean Goder. Interactions physiques de bicouches lipidiques déposées sur un coussin de polymères pour l'incorporation de protéines. Biological Physics [physics.bio-ph]. Université Paris sciences et lettres, 2019. English. NNT: 2019PSLEE090 . tel-04941979

HAL Id: tel-04941979

<https://theses.hal.science/tel-04941979v1>

Submitted on 12 Feb 2025

HAL is a multi-disciplinary open access archive for the deposit and dissemination of scientific research documents, whether they are published or not. The documents may come from teaching and research institutions in France or abroad, or from public or private research centers.

L'archive ouverte pluridisciplinaire **HAL**, est destinée au dépôt et à la diffusion de documents scientifiques de niveau recherche, publiés ou non, émanant des établissements d'enseignement et de recherche français ou étrangers, des laboratoires publics ou privés.

THÈSE DE DOCTORAT
DE L'UNIVERSITÉ PSL

Préparée à l'Ecole Normale Supérieure

Physical interactions of cushioned supported lipid bilayers for protein incorporation

Soutenu par

Jean Goder

Le 18 décembre 2019

Ecole doctorale n° 564

Physique en Ile de France

Spécialité

Biophysique

Dirigée par **Stephen Donaldson**
et **Eric Perez**



Composition du jury :

Elisabeth, Charlaix PR, Université Grenoble Alpes	<i>Présidente</i>
Thierry, Charitat PR, Institut Charles Sadron	<i>Rapporteur</i>
Pierre, Nassoy DR, Laboratoire Photonique, Numérique et Nanosciences	<i>Rapporteur</i>
Lorena, Redondo-Morata CR, Institut Pasteur Lille	<i>Examineur</i>
Gustavo, Luengo Chercheur, L'Oréal	<i>Examineur</i>
Eric, Perez DR-Emérite, ENS	<i>Directeur de thèse</i>
Stephen, Donaldson Superviseur, ENS	<i>Invité</i>

Acknowledgement

I would like to express my deepest gratitude to all the people who have contributed to the successful completion of my PhD journey. This research and the degree itself would not have been possible without their guidance, support, and encouragement.

First and foremost, I would like to thank my supervisor, **Dr. Stephen Donaldson** from LabEx ENS. His profound knowledge, invaluable advice, and constant support have been instrumental in helping me navigate the complexities of my experiments and overcome challenging research hurdles. I am truly grateful for his patience and mentorship throughout this process.

I would also like to extend my sincere thanks to my thesis director, **Dr. Eric Perez**, for his thought-provoking discussions about my thesis subject. His insights and guidance encouraged me to critically think and develop effective strategies to approach and tackle this project.

I am grateful to the **M3 team at ENS** for their warm welcome, collaborative spirit, and the many stimulating discussions that enriched my research experience. I would like to specifically acknowledge **Sophie Favier**, **Aymeric Chorlay**, and **Clémence Gruget**, who were not only colleagues but also companions during this challenging journey. Our shared discussions about research and the ups and downs of the PhD process have been invaluable, both scientifically and personally.

Furthermore, I would like to extend my appreciation to the other PIs for their advice and insightful contributions to various scientific questions that arose during my work: **Dr. Frédéric Pincet, Dr. Christine Gourier, Dr. Wladimir Urbach, and Dr. Rachid Thiam**. Their expertise and suggestions helped refine my approach and deepen my understanding.

On a personal note, I would like to thank my **family** for their unwavering financial and emotional support throughout the years. Their belief in me and constant encouragement have been a cornerstone of my success, and I could not have completed this journey without them.

Finally, I extend my heartfelt gratitude to all my friends, collaborators, and everyone else who contributed to this thesis, directly or indirectly. Their presence, kindness, and encouragement provided the strength I needed to persevere and achieve this milestone.

Abstract

Supported Lipid bilayers (SLBs), lipid bilayers that are directly deposited on a solid substrate, are generally used as models of biological membranes for the study of membrane interactions involving proteins and receptors. A primary problem with these model membranes is the fact that transmembrane proteins cannot interact physiologically due to unfavourable interactions induced by the proximity of the solid support. Another synthetic membrane used for studying transmembrane is the Suspended Lipid Bilayer (SLIM), a thin, planar lipid bilayer that is suspended across an opening or microfabricated structure, such as a microfluidic channel or a hole in a substrate.

However, its limitation is that it cannot be used in parallel with Surface force Apparatus (SFA) and Atomic Force Apparatus techniques, where a solid substrate is necessary. This research investigates the development and characterization of cushioned supported lipid bilayers (CSLBs) as an advanced model system to overcome the limitations of traditional membrane systems for studying biological membranes and transmembrane proteins. By introducing a polymer cushion between the solid substrate and lipid bilayer, this research aims to create a biomimetic model that preserves the mobility, flexibility, and natural dynamics of membrane components, providing a more physiologically relevant platform for investigating lipid-protein interactions and membrane fusion events.

The cushioned bilayers were constructed using polyethylene glycol (PEG), a hydrophilic and biocompatible polymer. Two variants of bifunctional PEG were utilized: DSPE-PEG-Thiol for gold substrates and DSPE-PEG-Silane for mica and glass substrates. The

polymer cushion serves to lift the lipid bilayer off the solid substrate, minimizing undesirable substrate-membrane interactions and enabling transmembrane proteins to retain their functional properties. To fabricate the cushioned bilayers, two methods were explored: self-assembled monolayers (SAMs) and Langmuir-Blodgett (LB) deposition techniques. While SAMs resulted in inhomogeneous polymer layers with three-dimensional aggregates, the LB technique provided precise control over polymer and lipid deposition, leading to uniform and defect-free cushions. The Langmuir-Blodgett (LB) technique was pivotal in fabricating CSLBs with high precision. This method allowed the deposition of amphiphilic molecules onto solid substrates at controlled molecular densities. The LB technique involved the formation of a monolayer at the air-water interface, with the hydrophobic tails oriented towards the air. Substrate preparation included a meticulous step of maintaining the molecular area constant during deposition, ensuring homogeneity. Atomic force microscopy (AFM) in tapping mode, which is a scanning probe technique used to image and analyze surface properties at the nanoscale, confirmed the structural integrity of these polymer cushions, showing a thickness of approximately 7 nm for the PEG layer.

The lipid bilayers were subsequently deposited onto the polymer cushions in a two-step process: a mixed lipid-PEG monolayer was deposited as the inner layer, followed by a pure lipid outer layer. High-resolution AFM imaging revealed smooth, defect-free bilayer surfaces, confirming the successful fabrication of cushioned bilayers. The lateral mobility of lipids within the bilayers was measured using fluorescence recovery after photobleaching (FRAP), which is a technique used to study the dynamics of molecular

diffusion and interactions within biological systems. It involves photobleaching a specific region of fluorescently labeled molecules with a high-intensity laser and then monitoring the recovery of fluorescence over time as unbleached molecules move into the bleached area. The results showed that lipid diffusion varied depending on the phase state of the bilayer, with diffusion coefficients increasing significantly in the fluid phase compared to the gel phase. Specifically, fluid-phase bilayers exhibited diffusion coefficients in the range of $4.3 \times 10^8 \text{ cm}^2/\text{s}$, demonstrating their suitability for dynamic studies of membrane processes. Additionally, the ability to modulate lipid mobility by adjusting the polymer cushion composition highlights the versatility of the CSLB system for various experimental conditions.

To assess the functional potential of CSLBs, membrane interaction studies were performed using the surface force apparatus (SFA), is a scientific instrument used to measure the forces between two surfaces in close-proximity, often with nanometer precision. It is commonly used to study adhesion, friction, lubrication, and the properties of thin films or confined liquids. The technique relies on precisely controlled movement of surfaces and accurate detection of force and distance to explore intermolecular and intersurface interactions. Force-distance measurements demonstrated that the polymer cushion effectively decoupled the lipid bilayer from the substrate, allowing the bilayers to deform and interact under physiologically relevant conditions. The SFA experiments revealed that membrane hemi-fusion, a critical intermediate state in membrane fusion, occurred only when both bilayer leaflets were in a fluid phase. This observation underscores the importance of lipid fluidity for facilitating membrane fusion processes,

consistent with the behavior of biological membranes. The thickness of the polymer cushion was measured to be approximately 20 nm in aqueous conditions, further validating its structural and functional properties.

The biological relevance of CSLBs was demonstrated by incorporating Synaptotagmin-1 (Syt1), a transmembrane protein involved in calcium-triggered synaptic vesicle fusion. Traditional SLBs restrict transmembrane protein activity due to the rigid substrate, but CSLBs allowed Syt1 to retain its physiological behavior. Force measurements using SFA showed that the interaction energy between Syt1 and an opposing membrane was significantly reduced compared to previous studies using SLBs. The energy per molecule decreased from 17.6 ± 1.4 kBT in SLBs to 2.7 ± 0.6 kBT in CSLBs, indicating that the polymer cushion dissipates energy during protein-membrane interactions. This finding highlights the importance of the cushioned bilayer system in enabling the natural conformational flexibility of transmembrane proteins during membrane fusion events.

Compared to other synthetic lipid membrane technologies, CSLBs offer significant advantages in preserving physiological membrane dynamics. Suspended lipid bilayers, while effective in eliminating substrate interactions, suffer from instability and are less suitable for long-term studies. Similarly, hybrid lipid bilayers composed of tethered lipid layers on solid substrates provide some flexibility but still impose constraints on protein mobility and functionality. Giant unilamellar vesicles (GUVs), which mimic cellular membranes in their spherical architecture, allow for detailed studies of curvature effects and membrane fusion events; however, their lack of structural stability and limited compatibility with force-based measurements restricts their use for precise quantitative

studies. CSLBs overcome these limitations by combining the stability of SLBs with the flexibility and fluidity of suspended and vesicular systems. The introduction of a polymer cushion allows for both long-term stability and physiological lipid-protein interactions, making CSLBs a superior platform for studying membrane fusion, protein mobility, and dynamic processes under controlled conditions.

In the context of neuronal traffic pathways, the CSLB system was employed to study synaptic vesicle fusion, a highly dynamic process involving the SNARE protein complex and Syt1. The research captured critical intermediate states of vesicle docking and fusion, providing insights into the mechanisms governing calcium-triggered neurotransmitter release. By mimicking the biophysical environment of neuronal membranes, CSLBs enabled the investigation of protein dynamics, lipid-protein interactions, and energy dissipation during membrane fusion. These findings contribute to a deeper understanding of the molecular mechanisms underlying neurotransmission, with potential implications for studying other membrane-associated processes such as viral entry, immune responses, and drug delivery.

In conclusion, this research presents CSLBs as a robust and versatile platform for studying biological membranes and transmembrane proteins under physiologically relevant conditions. By overcoming the limitations of traditional SLBs, the cushioned bilayer system provides a more biomimetic environment that preserves the mobility, flexibility, and dynamic interactions of membrane components. Comparisons with alternative synthetic membrane technologies, such as suspended bilayers, hybrid bilayers, and GUVs, highlight the unique strengths of CSLBs in providing both stability and

physiological relevance. The successful integration of functional proteins, combined with precise control over bilayer structure and lipid mobility, establishes CSLBs as a valuable tool for investigating complex biological processes such as membrane fusion, protein interactions, and neuronal traffic pathways. Future work could expand the application of CSLBs to other areas of biophysics and biomedical research, offering new opportunities for studying membrane dynamics and developing novel therapeutic strategies.

Keywords: Cushioned supported lipid bilayers, synthetic membrane models, Langmuir-Blodgett technique, transmembrane proteins, membrane fusion, surface force apparatus, Synaptotagmin-1, neuronal traffic pathways, lipid mobility, polyethylene glycol, giant unilamellar vesicles, hybrid lipid bilayers

Résumé

Les bicouches lipidiques supportées (SLBs), des bicouches lipidiques directement déposées sur un substrat solide, sont généralement utilisées comme modèles de membranes biologiques pour l'étude des interactions membranaires impliquant des protéines et des récepteurs. Un problème majeur avec ces membranes modèles réside dans le fait que les protéines transmembranaires ne peuvent pas interagir de manière physiologique en raison des interactions défavorables induites par la proximité du support solide. Une autre membrane synthétique utilisée pour étudier les protéines transmembranaires est la bicouche lipidique suspendue (SLIM), une fine bicouche lipidique plane suspendue au-dessus d'une ouverture ou d'une structure microfabriquée, telle qu'un canal microfluidique ou un trou dans un substrat. Cependant, sa limitation réside dans son incompatibilité avec des techniques comme l'appareil de force de surface (SFA) et les techniques à force atomique, où un substrat solide est nécessaire.

Cette recherche explore le développement et la caractérisation des bicouches lipidiques supportées et amorties (CSLBs) comme un système modèle avancé pour surmonter les limitations des systèmes membranaires traditionnels dans l'étude des membranes biologiques et des protéines transmembranaires. En introduisant un coussin polymère entre le substrat solide et la bicouche lipidique, cette recherche vise à créer un modèle biomimétique qui préserve la mobilité, la flexibilité et les dynamiques naturelles des composants membranaires, offrant une plateforme plus pertinente sur le plan

physiologique pour étudier les interactions lipides-protéines et les événements de fusion membranaire.

Les bicouches amorties ont été construites à l'aide de polyéthylène glycol (PEG), un polymère hydrophile et biocompatible. Deux variantes de PEG bifonctionnel ont été utilisées : DSPE-PEG-Thiol pour les substrats en or et DSPE-PEG-Silane pour les substrats en mica et en verre. Le coussin polymère soulève la bicouche lipidique du substrat solide, minimisant les interactions indésirables entre le substrat et la membrane, et permettant aux protéines transmembranaires de conserver leurs propriétés fonctionnelles. Pour fabriquer les bicouches amorties, deux méthodes ont été explorées : les monocouches auto-assemblées (SAMs) et les techniques de dépôt Langmuir-Blodgett (LB). Bien que les SAMs aient donné des couches polymères hétérogènes avec des agrégats tridimensionnels, la technique LB a permis un contrôle précis du dépôt de polymères et de lipides, aboutissant à des coussins homogènes et sans défauts.

La technique Langmuir-Blodgett (LB) a été essentielle pour fabriquer des CSLBs avec une grande précision. Cette méthode a permis le dépôt de molécules amphiphiles sur des substrats solides à des densités moléculaires contrôlées. La technique LB implique la formation d'une monocouche à l'interface air-eau, avec les queues hydrophobes orientées vers l'air. La préparation des substrats comprenait une étape méticuleuse consistant à maintenir constante la surface moléculaire pendant le dépôt, garantissant l'homogénéité. La microscopie à force atomique (AFM) en mode tapotement, une technique de sonde à balayage utilisée pour imager et analyser les propriétés de surface à l'échelle nanométrique,

a confirmé l'intégrité structurelle de ces coussins polymères, montrant une épaisseur d'environ 7 nm pour la couche de PEG.

Les bicouches lipidiques ont ensuite été déposées sur les coussins polymères en deux étapes : une monocouche mixte lipides-PEG a été déposée comme couche interne, suivie d'une couche externe purement lipidique. Des images AFM haute résolution ont révélé des surfaces de bicouches lisses et sans défauts, confirmant la fabrication réussie des bicouches amorties. La mobilité latérale des lipides dans les bicouches a été mesurée à l'aide de la récupération de fluorescence après photoblanchiment (FRAP), une technique utilisée pour étudier la dynamique de diffusion moléculaire et les interactions dans les systèmes biologiques. Les résultats ont montré que la diffusion lipidique variait selon l'état de phase de la bicouche, avec des coefficients de diffusion augmentant significativement dans la phase fluide par rapport à la phase gel. En particulier, les bicouches en phase fluide présentaient des coefficients de diffusion de l'ordre de $4,3 \times 10^8 \text{ cm}^2/\text{s}$, démontrant leur aptitude à des études dynamiques des processus membranaires. De plus, la capacité à moduler la mobilité lipidique en ajustant la composition du coussin polymère souligne la polyvalence du système CSLB pour diverses conditions expérimentales.

Pour évaluer le potentiel fonctionnel des CSLBs, des études d'interaction membranaire ont été réalisées à l'aide de l'appareil de force de surface (SFA), un instrument scientifique utilisé pour mesurer les forces entre deux surfaces à proximité, souvent avec une précision nanométrique. Les mesures force-distance ont démontré que le coussin polymère découplait efficacement la bicouche lipidique du substrat, permettant aux bicouches de se déformer et d'interagir dans des conditions physiologiquement pertinentes. Les

expériences SFA ont révélé que l'hémifusion membranaire, un état intermédiaire critique dans la fusion membranaire, ne se produisait que lorsque les deux feuilletts de la bicouche étaient en phase fluide. Cette observation souligne l'importance de la fluidité lipidique pour faciliter les processus de fusion membranaire, conformément au comportement des membranes biologiques. L'épaisseur du coussin polymère a été mesurée à environ 20 nm en conditions aqueuses, validant encore ses propriétés structurales et fonctionnelles.

La pertinence biologique des CSLBs a été démontrée par l'incorporation de la Synaptotagmine-1 (Syt1), une protéine transmembranaire impliquée dans la fusion des vésicules synaptiques déclenchée par le calcium. Les SLBs traditionnelles restreignent l'activité des protéines transmembranaires en raison de la rigidité du substrat, mais les CSLBs ont permis à Syt1 de conserver son comportement physiologique. Les mesures de force réalisées avec le SFA ont montré que l'énergie d'interaction entre Syt1 et une membrane opposée était significativement réduite par rapport aux études précédentes utilisant des SLBs. L'énergie par molécule est passée de $17,6 \pm 1,4$ kBT dans les SLBs à $2,7 \pm 0,6$ kBT dans les CSLBs, indiquant que le coussin polymère dissipe l'énergie lors des interactions protéine-membrane.

Comparées à d'autres technologies de membranes lipidiques synthétiques, les CSLBs offrent des avantages significatifs en préservant la dynamique physiologique des membranes. Les bicouches lipidiques suspendues, bien qu'efficaces pour éliminer les interactions avec le substrat, souffrent d'instabilité et sont moins adaptées aux études à long terme. De même, les bicouches lipidiques hybrides, composées de couches lipidiques attachées à des substrats solides, offrent une certaine flexibilité mais imposent encore des

contraintes à la mobilité et à la fonctionnalité des protéines. Les vésicules unilamellaires géantes (GUVs), qui imitent les membranes cellulaires dans leur architecture sphérique, permettent des études détaillées des effets de courbure et des événements de fusion membranaire ; cependant, leur manque de stabilité structurelle et leur compatibilité limitée avec les mesures basées sur la force restreignent leur utilisation pour des études quantitatives précises.

Les CSLBs surmontent ces limitations en combinant la stabilité des SLBs avec la flexibilité et la fluidité des systèmes suspendus et vésiculaires. L'introduction d'un coussin polymère permet à la fois une stabilité à long terme et des interactions lipides-protéines physiologiques, faisant des CSLBs une plateforme supérieure pour l'étude de la fusion membranaire, de la mobilité des protéines et des processus dynamiques dans des conditions contrôlées.

Mots-clés : Bicouches lipidiques supportées avec coussin, modèles de membranes synthétiques, technique de Langmuir-Blodgett, protéines transmembranaires, fusion membranaire, appareil à forces de surface, Synaptotagmine-1, voies de trafic neuronal, mobilité lipidique, polyéthylène glycol, vésicules unilamellaires géantes, bicouches lipidiques hybrides.

Table of contents

Acknowledgement	1
Abstract	3
Résumé	9
Table of contents	14
Chapter 1:	16
Introduction	16
1. Membrane model system	21
1.1 Lipid monolayer	23
1.2 Lipid Vesicles	23
1.3 Supported lipid bilayer	25
1.4 The need for better membrane model	25
2. Neuronal traffic pathway.....	26
2.1 Synaptotagmin-1: the calcium sensor of neurotransmission.....	29
2.2 Synaptotagmin measurements on solid supported lipid bilayer	30
3. Thesis outline	31
Chapter 2:	33
Primary Techniques for Surface Preparation and Characterisation	33
1. Langmuir Blodgett deposition technique	33
1.1 The Teflon Boat.....	35
1.2 The Teflon Barrier	36
1.3 The Substrate Holder	37
2. Atomic Force Microscopy Technique	39
2.1 The atomic force microscope	39
2.2 AFM Tapping Mode	41

3. Confocal microscopy and the Fluorescence Recovery After Photo-bleaching (FRAP)	43
3.1 Confocal microscopy	44
3.2 Fluorescence Recovery After Photo-bleaching (FRAP)	46
4. The Surface Force Apparatus (SFA)	50
4.1 SFA - Mica surfaces preparation	51
4.2 SFA - Surface translation mechanism	52
4.3 SFA - Lens separating distance measurement principle	53
4.4 SFA - Force measurement principle	55
4.5 SFA – Energy interaction between surfaces	56
4.6 SFA – A typical SFA force run	57
Chapter 3:	60
Development of cushioned supported lipids bilayer and its structural characterisation	60
1. Polyethylene Glycol (PEG)	60
2. Self Assembled Monolayer (SAM) chemistry	62
2.1 PEG cushion Height	63
2.2 Exposure to air	64
2.3 Preparation optimisation	66
3. Langmuir Blodgett Depositions	67
4. Outer lipid leaflet Lateral diffusion	72
5. Cushioned supported membrane surface characterisation by AFM	80
Chapter 4:	91
Surface Force measurements on different Cushioned supported bilayer systems	91
1. Force measurements on an asymmetric system	94
2. Force measurements on a symmetric system	99
3. Force measurements on a Hybrid system with Protein incorporated	104
Conclusion	112
Bibliography	118

Chapter 1:

Introduction

Living things (human beings, animals and plants) are made of complex machineries like in a car. And like in a car, they have different parts (building blocks) that work in harmony together to make everything work smoothly. In order to maintain, repair and/or improve the harmonious mechanism of these complex machines, we need to understand how each part works individually to further understand how they work together on the bigger scale.

In living things, cells are the building blocks of this complex machinery. The study of cells has been a challenging, active area of research since the seventeenth century, when Robert Hooke first observed them through his compound microscope (Alberts et al. 2008). The human body is composed of trillions of cells, each with their own specific functionality. Figure 1 shows the levels of structural organisation of the human body. From the top to bottom, the complexity increases: molecules, organelles, cells, tissues, organs, organ systems and organism. In order for one to fully understand the complexity of the human body, one needs to start by understanding the basic unit of this huge complex architecture.

Cells are enclosed by a membrane, called the plasma membrane, which separates the intercellular matrix (cytoplasm) from the extracellular space. Similar separation is also found within eukaryotic cells, represented in Figure 2, where tiny specialised cellular structures called organelles have membranes delimiting them from the cytoplasm. Even if, they are not all exactly the same membrane (in term of composition, structure, etc...) they do have some similar characteristics such as their thickness (thinner than the size of a cell), and their role as a barrier.

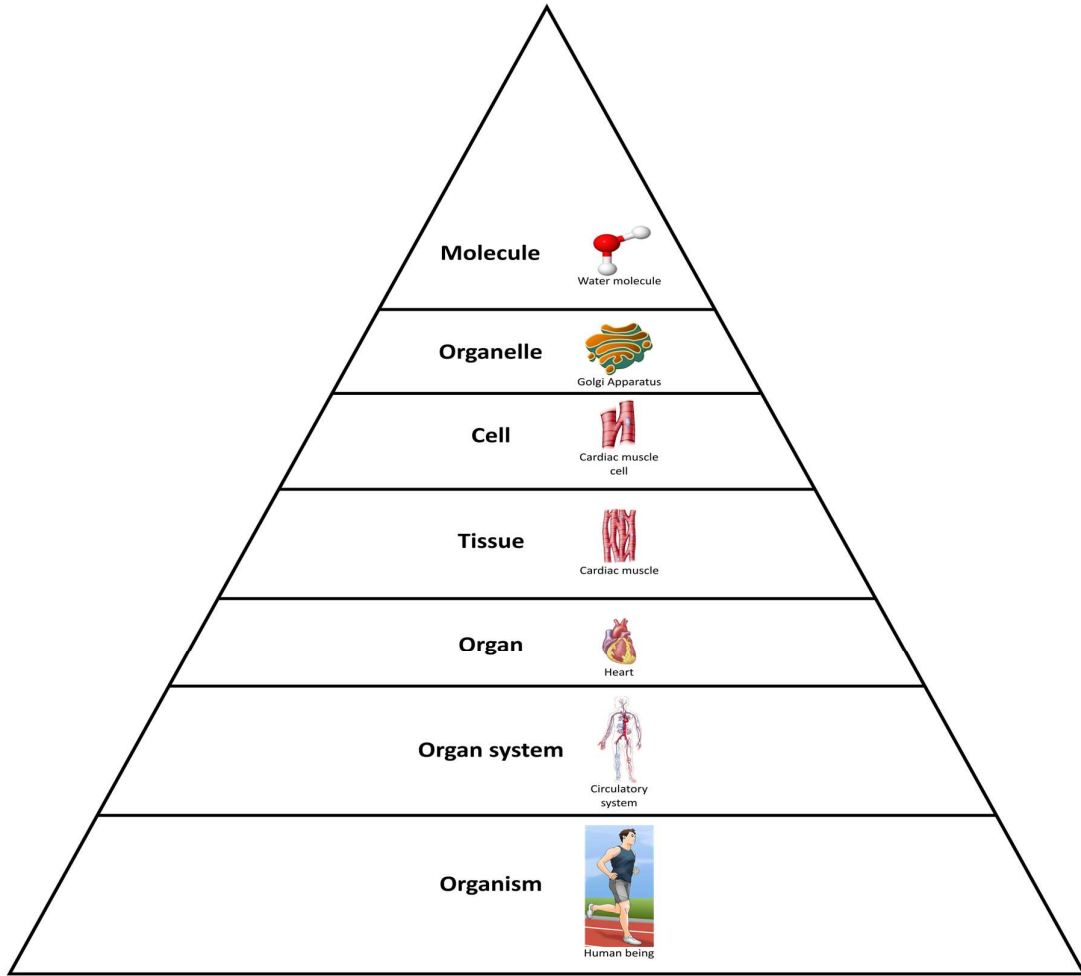


Figure 1: shows the levels of structural organisation of the human body. The organisation of the body is shown in terms of increased complexity from the molecules to the human organism.

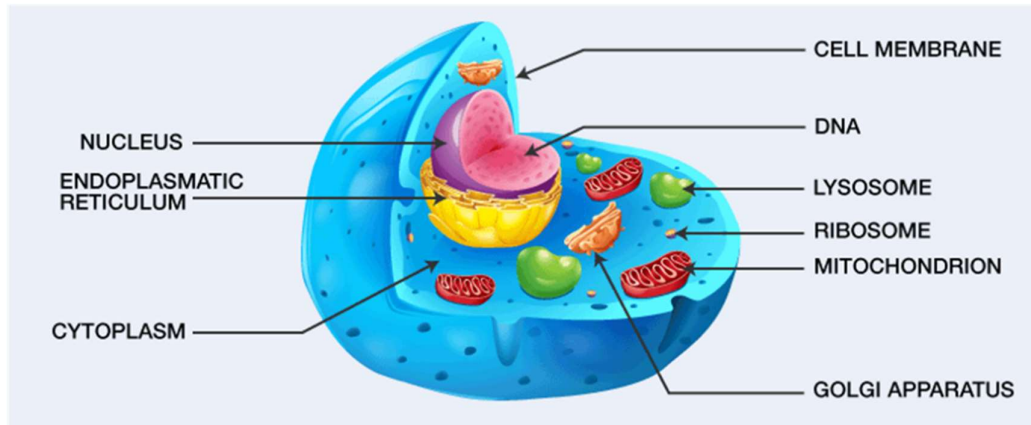


Figure 2: shows a cell, the fundamental unit of life. Image extracted from <https://byjus.com/biology/cells>

Structural separation is essential for eukaryotes. However, to ensure the smooth functioning of the cells and the organisms, all these entities should be able to interact and communicate with each other and their environment. Therefore, this means that the membranes, necessary for the structure of these entities and separating them from their environment, must allow these entities to interact and cannot be rigid barriers. So the principal characteristic of a biological membrane means that it must be flexible, deformable and fluid. In these membranes, there are the presence of ionic channels and ionic pumps that allows the cell and the organelles to regulate the ionic concentration of their environment by diffusion or active transport respectively (Berg et al. 2019). These structures allow the transfer of small molecules only.

From time to time the cell and organelles need to transfer bigger molecules and substances around. Since the membranes are flexible, deformable and fluid, they allow for other means of transfer processes. Endocytosis is a cellular mechanism, where the

substances to be transferred are surrounded by the cell membrane, which then buds off inside the cell to form a vesicle containing substances. Then, in order to transfer the substances, the next process is called exocytosis, where the vesicle fuses with the cell membrane releasing its content beyond the cell membrane. In order for these two processes to happen, the cell membrane should be able to deform. Membranes generally do not fuse spontaneously because of the high energy cost. There are specialised proteins that produce the machinery necessary for them fuse.

In this thesis, we are interested in the mechanisms behind membrane fusion. It is not only inside the cell, through the process of exocytosis, that membrane fusion is important but there are also other processes that rely on the same mechanism. For example in fertilization, membrane fusion needs to happen between a sperm and an oocyte in order for genetic materials of the sperm to be transferred to the oocyte. It is the same case for viral infections. The virus membrane envelop has to fuse with the plasma membrane of the host cell in order to deliver its content and thus infecting it.

Therefore it is important to fully comprehend the mechanism behind membrane fusion in the different parts of a living thing.

1. Membrane model system

To go on studying the process behind membrane fusion and the different proteins involved in this process, we firstly need a proper model for a biological membrane.

In 1972, a model for the plasma membrane was proposed called the “Fluid Mosaic Model” (Singer and Nicolson 2016). This model states that membranes are made of phospholipids bilayer that have incorporated with cholesterol, proteins, and carbohydrates that contribute to the membrane’s fluidity nature. This structural assembly allows the membrane to perform multiple functions such as molecules detection, cell adhesion and membrane fusion.

In 1997, an improved model of the “Fluid Mosaic Model” for the plasma membrane structure was proposed by adding the concept of lipid micro-domains, called “lipid rafts”. In this model, the membrane lipids are phase-separated and re-organised into lateral micro-domains (lipid rafts) with a specific composition and a molecular dynamic that are different to the composition and the dynamic of the surrounding liquid crystalline phase (Eeman and Deleu 2010). Therefore, an extensive understanding of all the plasma membrane’s components and their synergistic functions can lead to a better understanding of all living organisms, and also plays a crucial role in the future of biological advancement.

Biological membranes have a huge variety of lipids and proteins, making it nearly impossible to determine their exact composition in a cell. Nevertheless, their main components are well defined which are the lipids and proteins.

Lipids are small amphiphilic molecules, with a hydrophilic head and hydrophobic tails. They are the major components of the lipid bilayer constituting the biological membrane. Lipid bilayers are sheet-like recruitment of thousands of amphiphilic lipid molecules held together by the hydrophobic interactions between the acyl chains in their tails. Based on their chemical structures, membrane lipids can be classified in three groups: glycerol-based lipids (phospholipids), ceramide-based sphingolipids and sterols.

Since an actual biological membrane is as complex as explained earlier, scientists have built model membrane with more simplicity in order to gradually understand the role of each lipid and protein in the biological membrane. With these model membranes, we are able to study the structure and functions of type of lipids, effect of curvature membrane protein complexes, ion channels, also study the interactions of lipids with drugs or other nanoparticles (Szoka 1980). Model systems used to this day are: lipid monolayers, lipid vesicles and supported lipid bilayers. All these different systems have their own advantages and disadvantages, but they all mimic the lipid arrangement of biological cell membrane.

1.1 Lipid monolayer

A lipid monolayer is just a sheet of lipid, half of a bilayer. It is formed by spreading amphiphilic molecules on the surface of a liquid. This model provides a simple way of observing the effect of introducing different lipids to monolayer and studying lipid-lipid interactions by varying different parameters such as temperature, the composition of the subphase, and the nature and the packing of the spread molecules. These studies are often done using a Langmuir-Blodgett trough (instrument explained in detail in the next chapter). With this instrument, we measure the surface pressure (Π) of the monolayer film at the interface as a function of the mean molecular area (A). From this, we get information about the lipids phase from the compression isotherms and this allows the study of lipid mixtures for phenomena such as phase separation. The limit with this model is that we only study a monolayer and not the other phenomena that may happen in a bilayer.

1.2 Lipid Vesicles

Lipid vesicles or liposomes are the simplest models that are very close to cell membranes. They are spherical lipid bilayers with an internal aqueous compartment and can be made in different sizes; SUVs (small unilamellar vesicles, 20-50 nm in diameter), LUVs (large unilamellar vesicles, 100-500 nm in diameter) and GUVs (giant unilamellar vesicles, 10-100 μm in diameter). GUVs are the closest in terms of size to that of actual cells and are

usually grown using well defined mixtures of pure lipids (Mouritsen et al. 2012). This model can be used with a technique called micropipette manipulation, in which the contact angle between the two GUVs can be measured (as shown in Figure 3) and related to the adhesion energy of the vesicle as described in (Gourier et al. 2005; Bouar et al. 2001). This technique along with the GUVs lipid model, allows the measurement of force during membrane fusion with different proteins incorporated in them. The limitation with this model is that we cannot fully replicate the composition of actual biological membranes since their lipids and proteins composition is so complex.

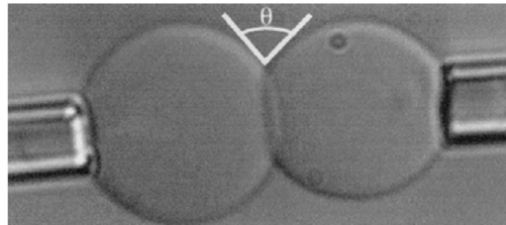


Figure 3: shows two osmotically controlled GUVs held with micropipettes by aspiration and observed using interference contrast microscopy. In order to control the tension of the vesicle bilayers, a suction pressure is applied to the micropipettes. One of them (left) is pressurised into a tight-rigid sphere with large bilayer tension, whereas the adherent vesicle (right) is held with low pressure and remains deformable. The adhesion energy W_{adh} is obtained by measuring the contact angle θ_c of the two GUVs and the tension τ_m on the membrane (θ): $W_{adh} = \tau_m(1 - \cos \theta_c)$. Extracted from (Bouar et al. 2001).

1.3 Supported lipid bilayer

Supported lipid bilayers (SLBs) are the most stable membrane models. They are made by depositing a lipid bilayer on supported solid surfaces such as mica, glass or silicon wafers with the lipid polar headgroups of the first monolayer facing the surface while the lipid headgroups of the second monolayer face the aqueous medium. Comparing this model to the vesicle one, the supported bilayer is simpler to prepare and to control the lipid composition in each monolayer. SLBs are an excellent model to study the physic-chemical properties of the cell membrane and they are accessible to a wide variety of techniques. They were used in the investigation of drugs interactions with cell membranes in terms of structures, morphology and surface chemistry. These interactions were investigated using techniques such as X-ray scattering, scanning electron microscope (SEM), atomic force microscopy (AFM), Surface Force Apparatus (SFA) and more.

1.4 The need for better membrane model

However, the Supported Lipid Bilayer (SLB) model as great as it is, has a big disadvantage when it comes to study transmembrane proteins. The SLBs are not suitable for physiological studies of transmembrane proteins as the extra residues of the transmembrane proteins are pinned down between the bilayer and its support, thus preventing the proteins to move freely or even extend properly during an interaction with another apposing lipid bilayer. In recent years, new models were developed in order to

resolve these issues, like the suspended lipid bilayer (Heo et al. 2019) and the cushioned supported lipid bilayer. These two membranes models allow transmembrane proteins to be biochemically active within the membrane.

This thesis is centred on developing the cushioned supported lipid bilayer with model lipid mixtures and then more biologically relevant assays. This model consists of depositing a thin layer (~5 -10 nm) polymer cushion between the bilayer and its support. By doing so the bilayer will be slightly lifted up from the solid substrate allowing it to accommodate transmembrane proteins with all their physiological characteristics preserved such as mobility, flexibility and extension, thus, making the lipid bilayer more bio-chemically active. Using the developed system, we will investigate the mechanisms of membrane fusion in the synapses with actual transmembrane proteins.

2. Neuronal traffic pathway

The present work was done within a team interested in the mechanism of membrane fusion within the Neuronal traffic pathway, where all the brain activities happens; thoughts, feelings, sensations and actions. For this to happen, two neurons need to communicate with each other via chemical release, which happens at specialised cell junctions called synapses. How the synaptic vesicles fuse with the plasma membrane of the neuron to release neurotransmitters and also how calcium ions trigger this process,

has been the subject of intense research. Several key proteins such as SNAREs (Soluble NSF (N-ethylmaleimide-sensitive factor) Attachment Protein Receptors) (Figure 4A) proteins along with SM (Sec1/Munc 18-like) (Figure 4B) proteins are the usual fusion machinery for different intracellular fusion processes. However, for the release of neurotransmitters, there is a need for a fast, calcium-triggered fusion process which is governed by additional proteins such as Synaptotagmin (Figure 4D) and Complexin (Figure 4C).

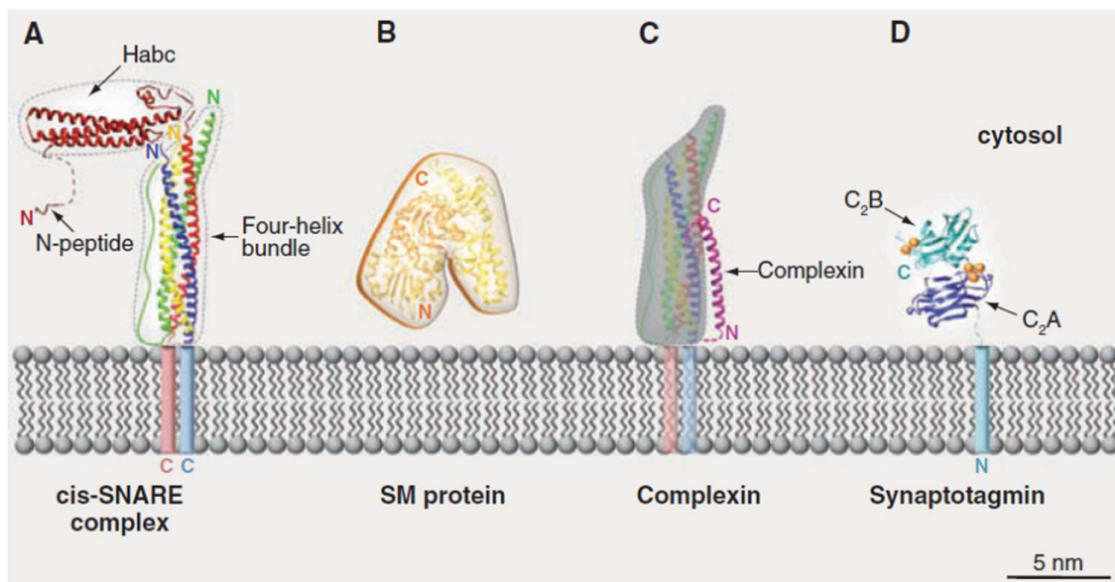


Figure 4: Illustrate the main structures involved in the fusion process. (A): SNARE complex of VAMP/Synaptobrevin (blue helix), syntaxin-1 (red helix) and SNAP-25 (green and yellow helices for the N- and C-terminal domains, respectively). (B) Munc18. (C) Complexin, bound to the SNARE complex (purple). (D) Synaptotagmin. Extracted from (Südhof and Rothman 2009).

The essence of the membrane fusion machinery for neurotransmission is formed by a set of three membrane proteins called the SNARE proteins (Südhof and Rothman 2009). This machinery involves the zippering of the “SNAREpin” complex which is formed by the

binding of one v-SNARE protein (synaptobrevin-2) in the synaptic vesicle (transport vesicle) and two t-SNARE proteins (SNAP-25 and Syntaxin-1) in the plasma membrane of the neuron (target membrane) (Söllner et al. 1993). The assembling of the SNAREpin is the force generator behind the membrane fusion: the zippering of the SNAREs (as shown in Figure 5) releases about 35 $k_B T$ of energy per SNAREpin (Li et al. 2007) which is converted into a force that pulls the two apposing bilayers closer together and fuse them.

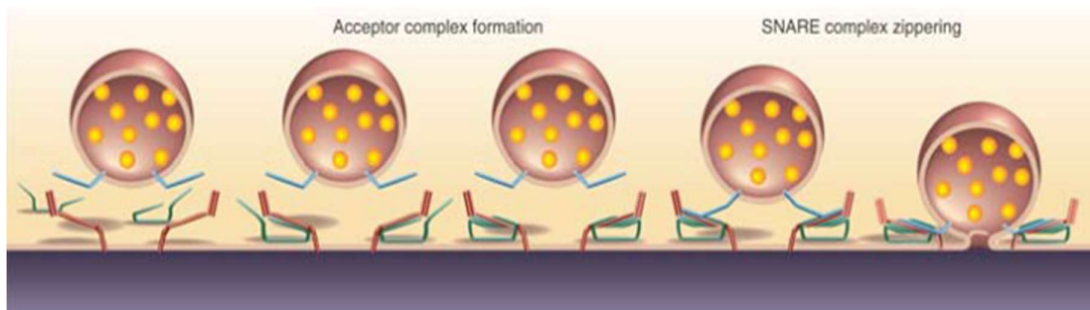


Figure 5: Illustrates of the SNARE-mediated fusion. Three α -helices (t-SNAREs) from the plasma membrane (two SNAP-25 and one syntaxin-1) combine with a fourth α -helix (v-SNARE) from the synaptic vesicle (synaptobrevin-1) to form the SNAREpin. The zippering of the SNAREpin proceeds, generating a force which pulls the 2 bilayers together which then eventually force them to fuse. Extracted from (Palfreyman and Jorgensen, n.d.).

In a more physiological situation, the SNAREs need to be enabled for fusion. This is achieved with the addition of proteins such as SM protein Munc18 and Munc13. They are involved in the initial set up of the SNAREs for assembly and more (Jahn and Fasshauer 2012).

In order to spontaneously complete fusion, SNARE proteins generally take 0.1 to 1 second (Weber et al. 1998). The release of neurotransmitters is estimated to be between the milli- to the micro- seconds range (Schweizer and Augustine 1998), 1000 to 10 000 times

faster than expected from the SNAREs alone. This means there are other proteins involved in this process.

2.1 Synaptotagmin-1: the calcium sensor of neurotransmission

Another protein involved in the release of neurotransmitters is the calcium sensor membrane proteins called synaptotagmin. In the 1960's, it was revealed that calcium-triggered ultrafast synaptic vesicle fusion (Katz and Miledi 1969). It was found that the calcium sensor involved in the neurotransmission is the protein called Synaptotagmin.

Synaptotagmin proteins are composed of an N-terminal transmembrane region, a linker of variable length and two calcium-binding modules, the C2 domains, labelled C2A and C2B. There are 15 isoforms of this protein in mammals, localised to the synaptic and secretory vesicles or the plasma membrane (Corbalan-garcia and Gómez-fernández 2014). Synaptotagmin-1 is the most important isoform for triggering release of neurotransmitters. In our work, we are going to use this protein to test our developed cushioned supported bilayer and compared to the work of Dr. Gruget briefly described next.

2.2 Synaptotagmin measurements on solid supported lipid bilayer

The work of Dr. Gruget was primarily using the surface force apparatus (SFA) to measure the interaction of synaptotagmin-1 (Syt1) during membrane fusion. During this study, the supported lipid bilayer model was used and instead of the full length Syt1, modified versions with the transmembrane part replaced by 12-histidine residues tag was used. If the full length Syt1 was used with this SLB model, the extra residues of the transmembrane proteins would be pinned between the bilayer and its support. Therefore, with the 12-histidine residues replacing the transmembrane domain, Syt1 will be able to bind to the Ni-NTA lipids in the outer layer of the SLB and thus allowing Syt1 to diffuse freely. Moreover, in this format 2-3 histidines bind to 1 molecule of Ni-NTA lipid found on the outer layer of one of the supported bilayers. In this work, the binding energy of membrane anchored Syt1 to an anionic membrane was directly measured. The measurements were performed in different ionic compositions of the buffer. Syt1 has a binding energy of ~ 6 kBT, ~ 10 kBT and ~ 18 kBT, respectively in presence of EGTA, Mg^{2+} and Ca^{2+} in the buffer. Moreover, molecular rearrangements measured during confinement are more dominant in Ca^{2+} and Mg^{2+} and suggest that Syt1 initially binds through C2B, and then reorients the C2 domains into preferred binding configurations. This work provides energetic and mechanistic details of the Syt1 Ca^{2+} -activation process in synaptic transmission (Gruget et al. 2018).

3. Thesis outline

In this thesis, we aimed to fabricate a cushioned supported lipid bilayer (CSLB) model system that would mimic the membrane of a cell with all its physiological properties (flexibility, fluidity, deformation, and interactions). In chapter 2, we explained in detail the different equipments we used in this project to make the CSLBs and characterise them. From the Langmuir film balance (to deposit monolayer of lipid on substrates and make the CLSBs) to the surface force apparatus (to measure the intermolecular forces between two molecularly smooth surfaces that bear CLSBs), we also detailed the confocal microscope (to observe fluorescent surface and measure the diffusion coefficient of lipids within the CLSBs) and the atomic force microscope (to measure surface topography).

In chapter 3, we started the fabrication of the CSLBs using self assembly monolayer (SAM) to adsorb a thin layer of polyethylene glycol (PEG) polymer. We observed through atomic force microscopy (AFM) that, with this method, we could not obtain a homogeneous coverage of the substrate and because of the presence of 3D aggregates that would produce long distance repulsions and therefore make the CLSBs unsuitable for surface force measurements. We then used a different method named the Langmuir Blodgett deposition technique to form the CLSB. We have used it in an unconventional way by depositing a first monolayer (the inner monolayer) that was a lipid/PEG mixture, followed

by the deposition of a second monolayer of pure lipid (the outer monolayer). With it, we were able to obtain a homogeneous membrane and control the ratio of PEG molecules in the inner layer of the membrane. These CSLBs were subjected to fluorescence recovery after photobleaching (FRAP) measurements to observe their diffusion rate and probe which one has the highest mobility. Moreover, using high resolution AFM, we were able to image the CSLBs' surface topography and observe a relationship between lipid fluidity and membrane structure.

Finally, in chapter 4, we used surface force apparatus (SFA) with the CSLBs in three different configurations: an asymmetric one (in which a CSLB was facing a clean mica surface), a symmetric one (in which two CSLBs were facing each other) and a protein anchored configuration (in which a CSLB was bearing a protein and faced a solid supported lipid bilayer). The asymmetric configuration measurements give us structural information; the thickness of the CSLBs in aqueous medium and the average distance between two neighbouring PEG molecules tethered on the same mica surface. The symmetric configuration measurements give us information about the interaction between two membranes and the conditions for which they would hemifuse without any fusogenic proteins. Finally, the protein anchored configuration measurements enabled us to understand the behaviour of Syt1, a calcium sensor protein for neurotransmission. With the CSLB model, this has allowed us to observe the interaction in a more physiological manner and compare our findings with that obtained by (Gruget et al. 2018).

Chapter 2:

Primary Techniques for Surface Preparation and Characterisation

In this chapter, we discuss the preparation of the cushioned supported lipid bilayer and the different techniques to characterise them.

1. Langmuir Blodgett deposition technique

The Langmuir Blodgett is the technique we used in this work to produce lipids bilayer surfaces. This technique is named after Dr. Irving Langmuir and his research assistant Dr. Katharine Blodgett. In the 1930s, during their study on surface chemistry, observing monolayer at the air-water interface to learn about the nature of intermolecular forces, they refined a method to transfer such monolayer onto solid support (G. Roberts 2006). In chapter 2 section 1, we will explain in detail, how we transferred a homogenous monolayer of amphiphilic molecules onto solid substrate at a constant molecular density.

Phospholipids dissolve readily in chloroform and commonly form self-assembled structures in water due to their amphiphilic nature. When depositing a few drops of phospholipids solution in chloroform onto the surface of water, the molecules spontaneously spread and form a monolayer at the air/water interface. This phospholipids monolayer orients with their hydrophobic tails oriented towards the air.

Throughout this work, we used a homemade Langmuir film balance which was designed in the 1994 by Dr. Eric Perez and Dr. Joe Wolfe (Perez and Wolfe 1994). It consists of a Teflon coated trough, 25 cm long and 15 cm wide, which is filled with aqueous buffer. A schematic representation of this Langmuir film balance is shown in Figure 6. This instrument is made up of three major parts working in unison:

- I. A Fixed Teflon boat, that measures the surface tension of a monolayer,
- II. A Teflon barrier, that can vary the molecular area of the amphiphilic molecules,
and
- III. A substrate holder, which passes the substrate through the monolayer.

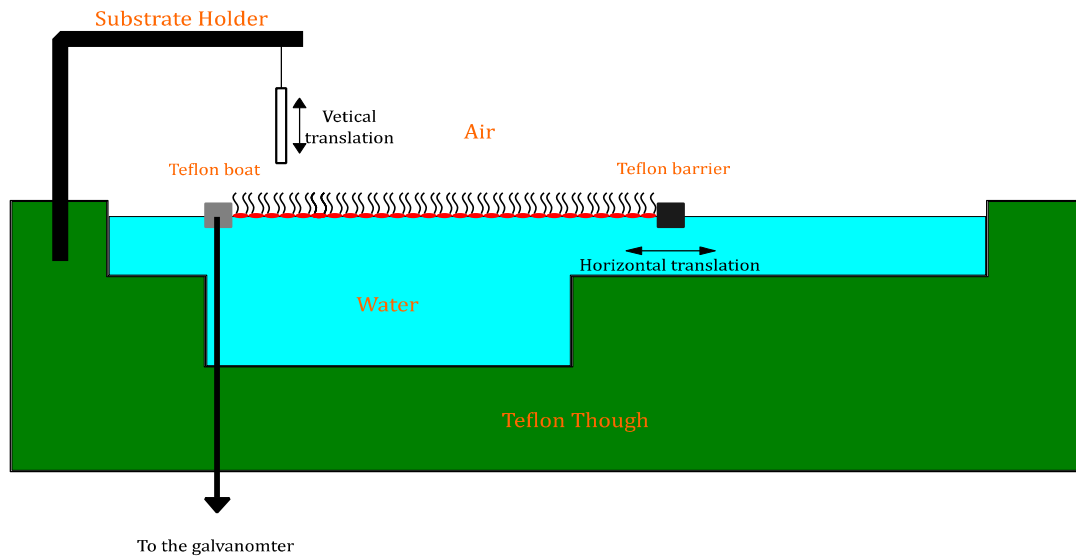


Figure 6: Schematic representation of the Langmuir balance used in the Lab

1.1 The Teflon Boat

When lipids are deposited between the barrier and the boat, a horizontal force, $F = \pi (L + d)$, is applied on the boat by the monolayer: where π , is the surface pressure of the monolayer (in mN/m), L , is the width of the boat (in m) and d , is the distance between the end of the boat and the fixed support (in m) as shown in Figure 7 . This force is transmitted to the galvanometer through the displacement of a mobile stainless-steel needle connecting the boat to the galvanometer. To return the needle to its original position, the galvanometer sends a current, I to counter the force exerted by the monolayer. This current intensity, I (in mA), after calibration, is proportional to the surface pressure of the monolayer, π (in mN/m). The proportionality coefficient α ($\alpha = 0.75 \text{ Nm}^{-1}/\text{A}$ for our Langmuir film balance) is obtained using known weights and a lever,

which produces a horizontal force. The surface pressure of a monolayer is given by the following equation:

$$\pi = \alpha(I - I_0) \quad (\text{Eq 2.1.1})$$

Where I_0 (in mA) is the intensity in the absence of monolayer at the air/water interface.

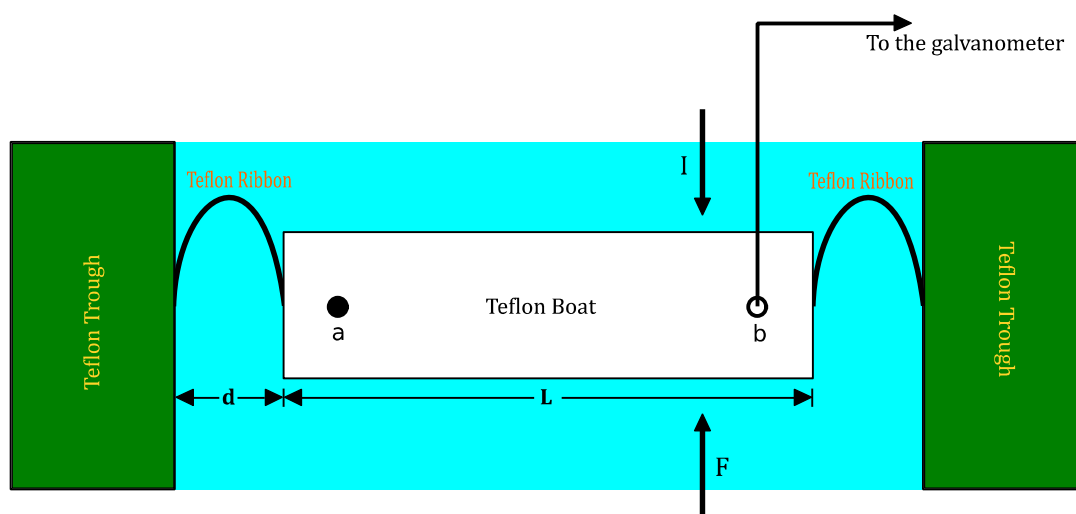


Figure 7: Schematic diagram of the Teflon Boat: (a) fixed stainless steel needle; (b) moving stainless steel needle connected to a galvanometer; Teflon Ribbon attaching the boat to the trough. This schematic diagram shows most of the features but is not to scale.

1.2 The Teflon Barrier

On the other side, a Teflon barrier determines the total area occupied by the monolayer. This is done by varying the horizontal position X of the barrier, which is probed by an optical coder. The molecular area σ of the amphiphilic molecules is related to the barrier's position X (in nm) and the width of the trough l (in nm) by:

$$\sigma = \frac{XI}{N_{\text{molecules}}} \quad (\text{Eq 2.1.2})$$

Where σ is in nm^2 and $N_{\text{molecules}}$ is the number of molecules deposited at the air-water interface.

1.3 The Substrate Holder

A vertical translation performed by a mobile substrate holder allows a surface to cross the air-water interface, and to deposit one or several monolayer. The simultaneous unison of the mobile substrate holder, the Teflon barrier and the current sent by the galvanometer is done computationally. During the deposition of a monolayer on a substrate, the surface pressure is maintained to a constant value set at a preset current, I_c . This value is reached by the horizontal translation of the barrier to the position where the measured current I matches I_c . The substrate is extracted, at a constant rate of 2 mm/s from the water, crossing the air-water interface to the air as shown in Figure 8. During this step the polar heads of the amphiphilic molecules bind to the surface, which becomes hydrophobic. To achieve a homogeneous deposition, it is important to keep the molecular area of the monolayer constant during the whole extraction, which is done through a feed-back loop. This means that the loss of molecules that bind to the surface is compensated by constantly compressing the monolayer. To obtain a bilayer, another monolayer is deposited on top of the first one but in reverse. This time, the amphiphilic

molecules bind to the first monolayer through their hydrophobic tails, in order to prevent the latter from contacting water.

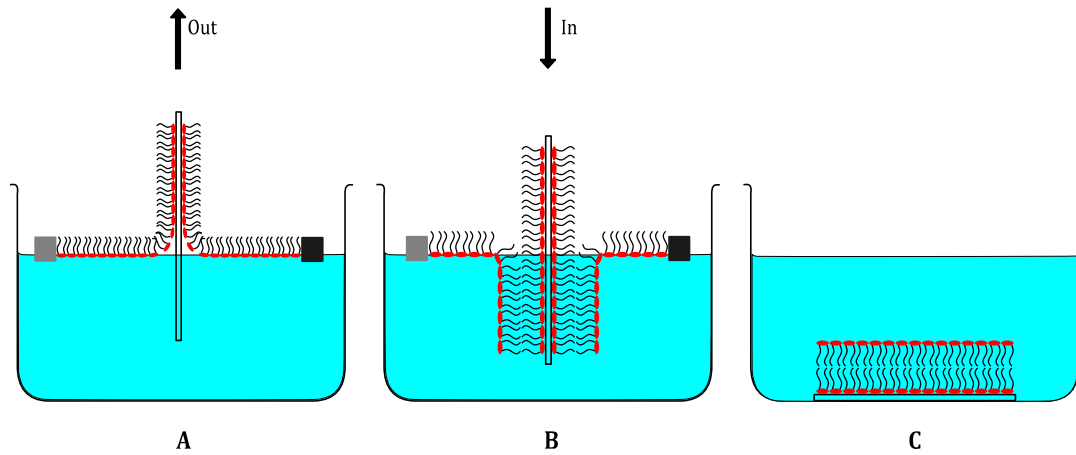


Figure 8: Illustrates the preparation of supported bilayer using the Langmuir-Blodgett; A. is the deposition of the 1st layer starting the surface inside the basin, B. is the deposition of the 2nd layer where we bring back the surface in the basin, and C. Shows a lipids bilayer on top of a solid substrate after deposition kept in aqueous medium.

2. Atomic Force Microscopy Technique

2.1 The atomic force microscope

The Atomic Force Microscope (AFM) is another piece of equipment we used in this work. It is a type of high resolution scanning probe microscope that has atomic resolutions of 10^{-10} m. The atomic force microscope was pioneered in 1986 by Nobel Prize Winner Gerd Binnig along with Calvin Quate and Christoph Gerber. In chapter 2 section 2.1, we will explain in detail, how we used the AFM to obtain a topographical image of the surface we produced during this work.

The atomic force microscope is made up of different parts that can be seen in Figure 9:

- I. A tip at the end of a spring cantilever with a spring constant k ,
- II. A laser directed onto the back of the cantilever, reflecting onto a photodiode detector, and
- III. A sample holder that can move in the x, y and z direction with the aid of a piezoelectric scanning tube.

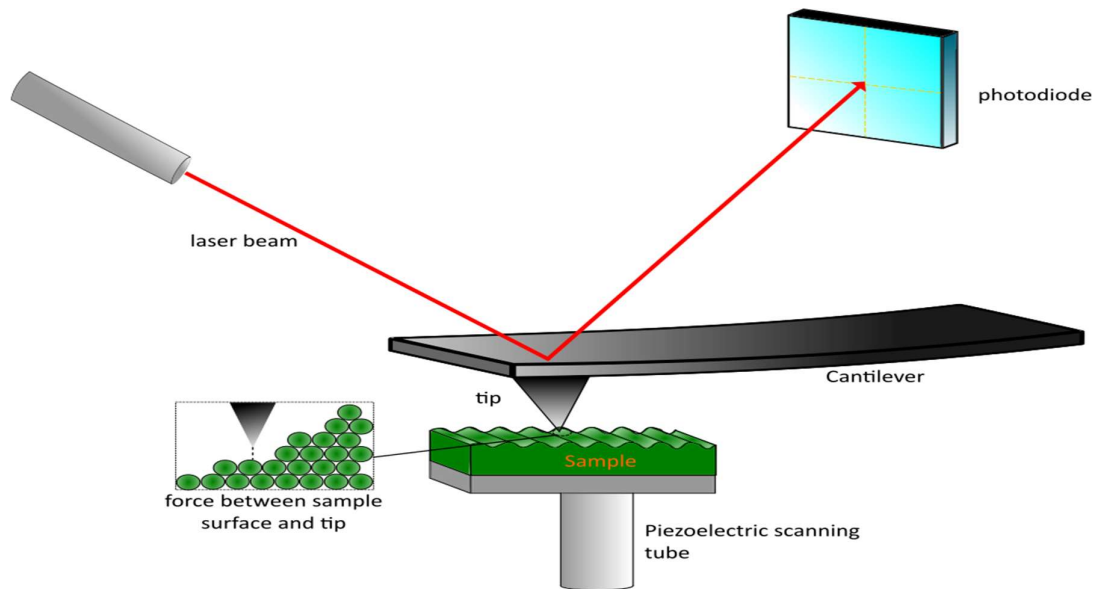


Figure 9 : is a schematic of a typical Atomic Force Microscope (AFM)

This instrument is based on the principle that when the tip is brought within atomic separating distance to the sample, interactive forces (electrostatic, magnetic, capillary, Van der Waals) are developed between the atoms of the tip and those of the sample surface. As the tip move across the sample surface, the interactions drive the cantilever to jump up and down with the changes in the profile of the surface. Thus, by measuring the deflection of the cantilever, the topography of the sample can be imaged (Jagtap and Ambre 2005).

Assuming the cantilever acts like a spring with a spring constant k , we can characterize the interactive force generated between the tip and the surface with Hooke's Law.

$$F = - k \cdot d_z \quad (\text{Eq 2.2.1})$$

Where F is the force (in N), k is the cantilever spring constant (in N/m) and d_z is the bending of the spring (in m). By measuring the variation of the reflected laser beam on the back of the cantilever tip using a photo diode detector, we were able to monitor the separation between the tip and the sample and thus, measuring the interaction force. In order to keep this force to a preset value, the sample holder is moved up and down via the piezoelectric scanning tube. Finally, a three-dimensional image of the sample surface can be constructed by recoding the cantilevers motion in the z-direction as a function of the sample's x and y position.

The AFM can be operated in three modes; contact mode, tapping mode and non-contact mode. Since we used mostly tapping mode in our characterization of our surfaces, the following explains this mode.

2.2 AFM Tapping Mode

While the AFM contact mode works by dragging the tip across the surface and the AFM non-contact mode works by vibrating the tip above the surface without allowing the tip and the sample to be in contact, the AFM tapping mode is the intermediate between the two. This mode is the appropriate one for soft samples like ours as it has an atomic resolution with a low applied force.

In the AFM tapping mode, the cantilever tip is oscillated near its resonance frequency and is lowered slowly onto the sample. The tip makes contact with the surface for a very short period in each oscillating cycle. The tip-sample interactions shift the amplitude, resonance frequency and phase angle of the oscillating cantilever. The amplitude of the cantilever is modulated such that the probe maintains sufficient energy for the tip to touch the surface and pull out without damaging or deforming the surface. With the AFM tapping mode, we obtained two types of profile; height profile and Phase profile.

Height profile

The height profile gives us images of the roughness of the sample surface. As the tip scans across the surface, the vertical position of the latter is recorded by measuring the changes in the height (z-axis length) of the piezoelectric scanning tube. The input voltage to the piezoelectric scanning tube is proportional to the length by which the tube moves up and down to maintain the force extended between the tip and the sample constant. The change in height gives us a topographical 2D map of the sample surface. The height profile is satisfactory to measure the height of the surface features but does not show distinct edges of these features.

Phase profile

The phase profile shows the change in the phase offset between the input drive signal to the piezoelectric scanning tube and the oscillating cantilever. The phase offset between the two is set to zero, when the cantilever is made to oscillate freely in air. As the probe tip interacts with the sample surface, there is a change in the phase offset of the oscillating cantilever by some angle with respect to the phase offset of the input drive signal. As the tip moves across the surface, it encounters area of differing elasticity, which gives rise to changes in phase offset between the two signals. These changes are the results of the amounts of damping experienced by the probe tip. The phase profile gives us an image of the stiffness of the surface.

3. Confocal microscopy and the Fluorescence Recovery After

Photo-bleaching (FRAP)

In this work, as mentioned earlier, the goal is to develop an artificial membrane system that can both diffuse freely and harbour transmembrane proteins while keeping their structural characteristics. Using confocal microscopy combined with the Fluorescence Recovery After Photo-bleaching (FRAP) technique, we were able to measure the lateral diffusion coefficient of the lipids in the upper leaflet of our cushioned supported lipid bilayer.

3.1 Confocal microscopy

Confocal microscopy is an optical imaging technique with an increased spatial resolution and contrast of its images. In comparison to conventional light microscopy technique, confocal microscopy uses adjustable pinholes to block out-of-focus light during image acquisition. The principle of this technique was introduced by Marvin Minsky in 1957 to overcome the limitations encountered in the traditional wide-field fluorescence microscopy.

The experiments have been done on a Leica confocal microscope model *Leica TCS SP5 II*. A detailed and complete explanation of the microscope functioning can be found in its manual (*Leica TCS SP5 Leica TCS SP5 X User Manual*, n.d.), but here we provide a brief overview of the technique. In confocal microscopy, the observed samples are stained with a fluorescent dye. A laser beam is reflected onto a section of the sample by a dichroic mirror as shown in the schematic in Figure 10. The fluorescent molecules are excited by the laser beam and on the way back to their ground state emit photons of a longer wavelength. These photons pass through the dichroic mirror and into a photomultiplier tube as detector.

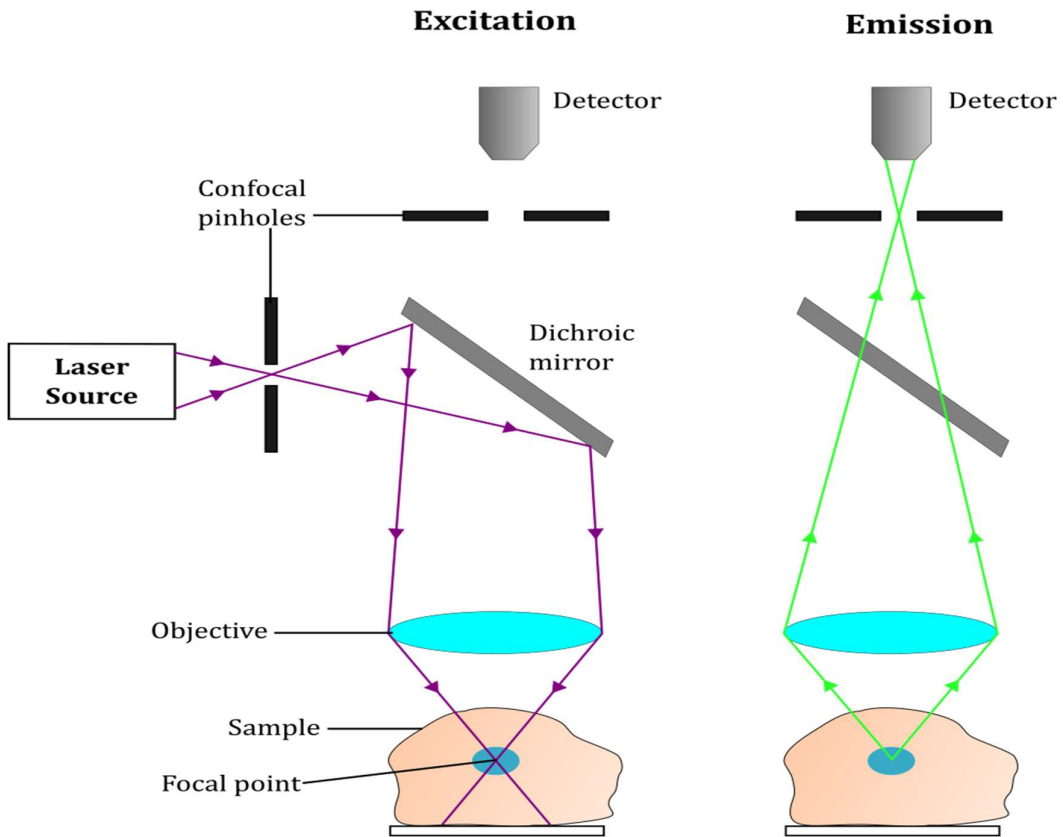


Figure 10: illustrates the principle of confocal microscopy. A laser source excites section of the sample with a short wavelength laser beam. Photons of longer wavelength are emitted from the sample and are detected by a detector after passing through a dichroic mirror. Pinholes are used to eliminate out-of-focused light.

In confocal microscopy, the image contrast is increased with the help of a pinhole in the path of the emitted beam between the objective and the detector as shown in Figure 11. The pinhole blocks the light beams coming from above and below the region of interest, thus compiling only fluorescence coming from a specific slice of the specimen. By varying the z-direction of the specimen, several focused sliced images were taken and using imaging software, a three dimensional image of the specimen can be constructed. Confocal microscopy is not only used for imaging but can also be used for the lateral

diffusion measurement of lipids using the technique called Fluorescence Recovery After Photo-bleaching (FRAP).

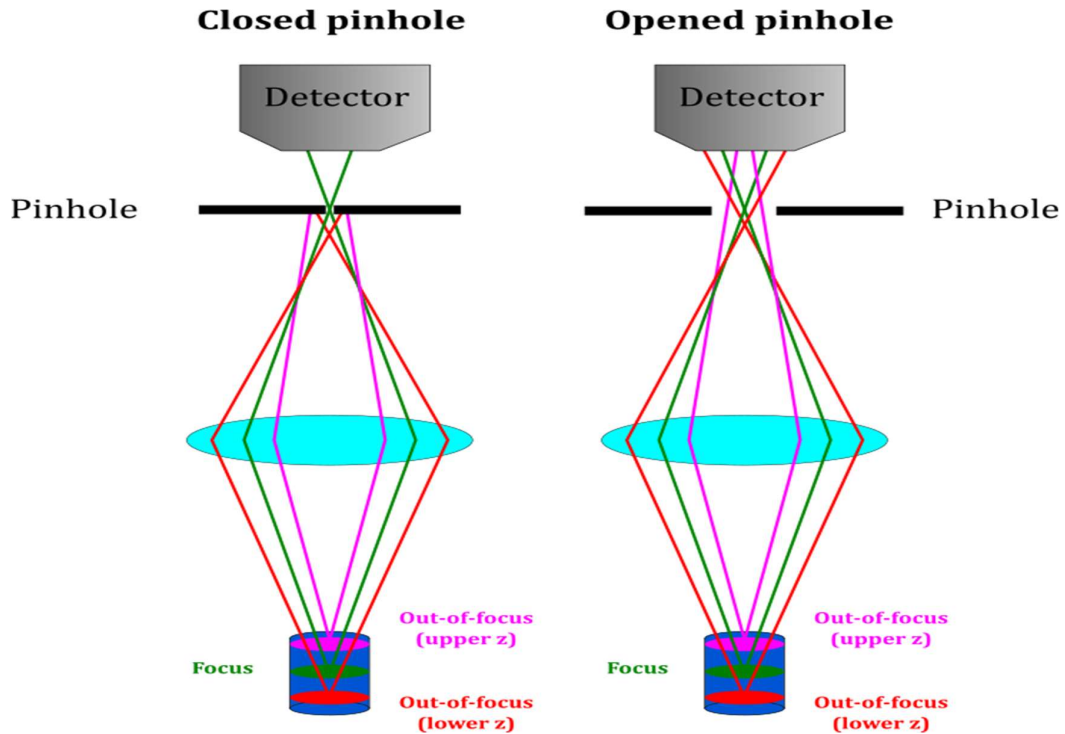


Figure 11: illustrates how emissions from out of focus planes are blocked by the pinhole.

3.2 Fluorescence Recovery After Photo-bleaching (FRAP)

Fluorescence recovery after photo-bleaching is a common method to study the diffusion of lipids and proteins in artificial and cellular membrane systems. FRAP is a technique, where a dark spot (zero fluorescence intensity) is created and the replenishment of that spot with fluorescent molecules is observed over time. The technique is well documented and explained in (Pincet et al. 2016). A typical FRAP experiment consist of 3 phases; the

pre-bleaching phase, bleaching phase and post-bleaching. The pre-bleaching phase is when a few frames (time for the microscope to take an image) recorded before bleaching, necessary for the data normalization. The bleaching phase is when a region of interest (ROI) on the surface is exposed to a high-intensity (100%) laser beam for 0.2-0.6 s (depending on the fluorescent dye) leaving behind a dark spot as shown in Figure 12 top. In the post-bleaching phase, the fluorescence recovery at that particular region is monitored over time. This recovery results from the isotropic diffusion of unbleached molecules towards the ROI and the bleached molecules out. The monitored recovery gives rise to a normalized fluorescence intensity as a function of time as shown in Figure 12 bottom. The shape of the curve depends not only on the mobility of the fluorescent molecules but also on the form and size of the bleached area.

In this work, we used mostly the disk-shaped bleaching geometry with different diameter sizes. The recovery process for such geometry is described by the following equation:

$$I(t) = I_0 + \sum (I_{n\infty} - I_0) e^{-\frac{2\tau_n}{t}} \left(J_0 \left(\frac{2\tau_n}{t} \right) + J_1 \left(\frac{2\tau_n}{t} \right) \right) \quad (\text{Eq 2.3.1})$$

Where I_0 is the fluorescence intensity just after the bleach, J_0 and J_1 are the modified Bessel functions of order 0 and 1, $I_{n\infty}$ is the intensity contribution of the species n at $t = \infty$ and τ_n is the characteristic diffusion time of the species n . Detailed behind the above equation is given in (Soumpasis 1983).

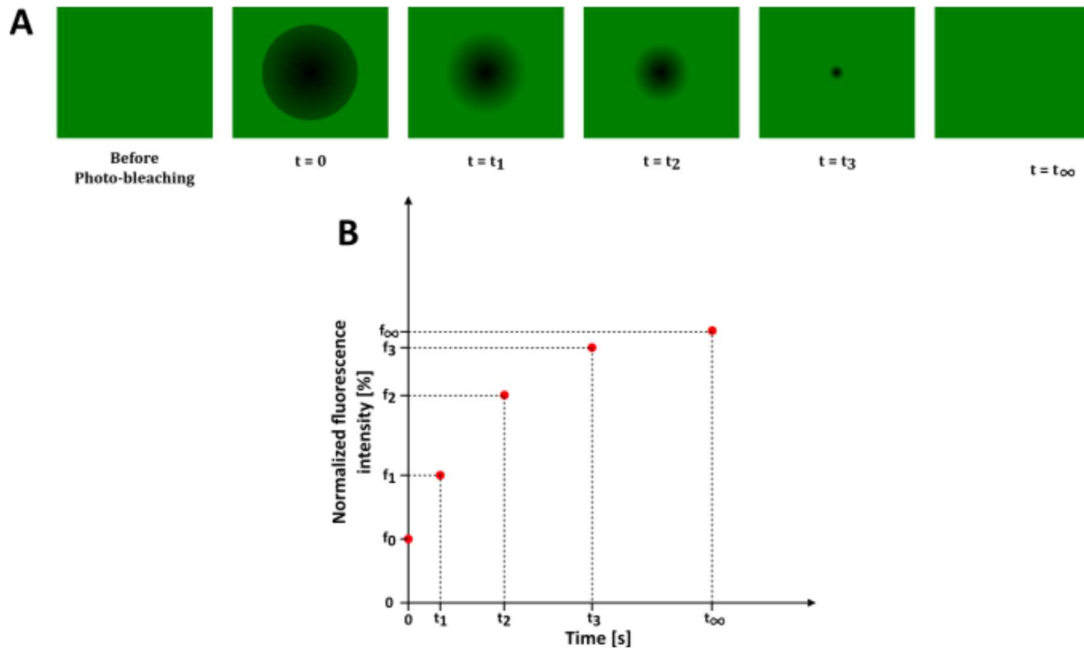


Figure 12: Illustration of a FRAP experiment. (A) are the timed frame images taken by the microscope before and after photo bleaching. Time $t=0$ is the 1st image taken just after photo bleaching. (B) is the Normalized fluorescence intensity versus Time curve for a particular Region of Interest (ROI). Each point is equivalent to the fluorescent intensity obtained for that time frame image.

In a disk-shaped geometry, the diffusion coefficient D is related to the characteristic diffusion time τ as follows:

$$D = \frac{d^2}{16\tau} \quad (\text{Eq 2.3.2})$$

Where the D is the diffusion coefficient (in $\mu\text{m}^2/\text{s}$), τ is the characteristic diffusion time (in s) and d is the diameter of the region of interest ROI (in μm).

We used in silico simulations to accurately fit each set of FRAP data at different diameter of ROI, in order to extract the three parameters I_0 , I_{∞} and τ . By plotting the average

16τ values against their corresponding d^2 , the inverse gradient of the linear fitting of the data points is equivalent to the diffusion coefficient. Since we assumed that the lipids diffusion in our work is mainly governed by Brownian motion, the linear fitting of the data has to go through the origin as shown in Figure 13.

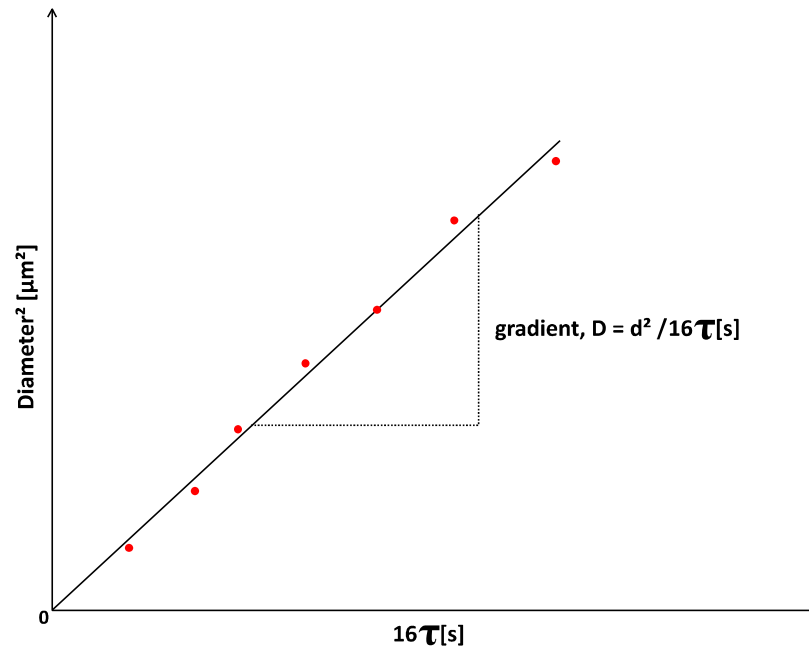


Figure 13: Illustrate a d^2 vs 16τ linear fit. As we assume that the whole process in the study is govern by Brownian motion, the gradient of the line passing through the origin gives us the diffusion coefficient of the lipids on the bilayer.

From Figure 13, we can say that the higher the gradient, the higher the diffusion coefficient, meaning that the lipid on the membrane surface diffuse faster.

4. The Surface Force Apparatus (SFA)

The purpose of this study was to understand the mechanism behind membrane fusion and the surface force apparatus (SFA) is an excellent device to simulate this interaction. The SFA used in this work is a replica of the “Mark II” model developed in 1978 by Jacob Israelachvili (Jacob N Israelachvili and Adams 1978). This equipment enables the measurement of intermolecular forces between two atomically flat surfaces in a controlled vapour, aqueous and non-aqueous environment. The SFA uses Hooke’s Law (Eq 2.2.1) to measure the force, and it uses the Fringes of Equal Chromatic Order (FECO) (Eq 2.4.1) to measure the separating distance, with an accuracy of 2×10^{-7} N and 1 \AA respectively. In Figure 14, a schematic of the device is represented. In this chapter 2 section 4, the primary aspects of an SFA experiment will be discussed, including surface preparation and the force-distance measurements.

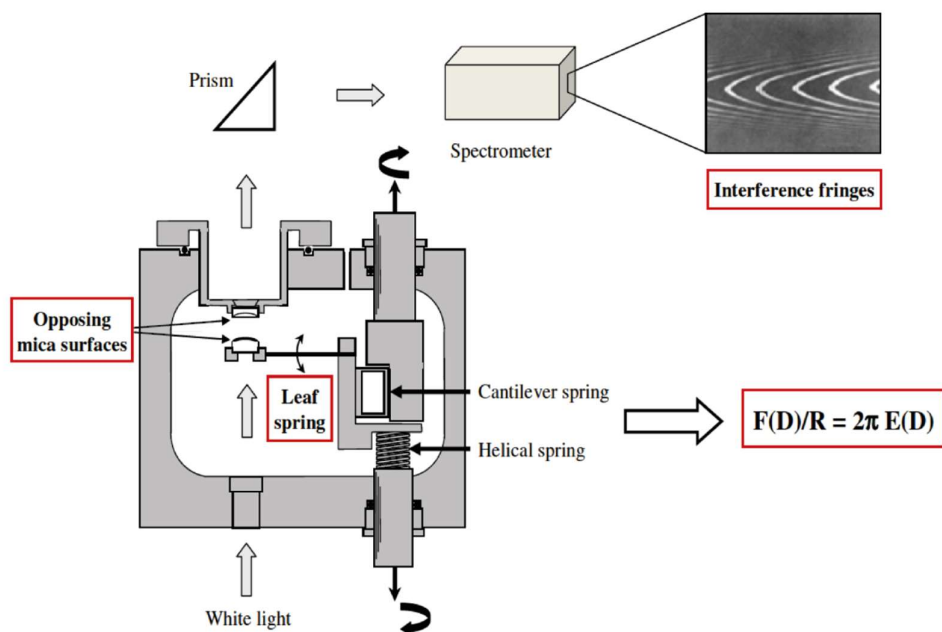


Figure 14: Schematic representation of the Mark II Surface Force Apparatus (SFA) used in this study. Two back-silvered mica substrates are glued on two lenses set up in crossed-cylinder geometry. The separating distance between the two lenses is measured accurately from the constructive interference pattern created by the light reflecting through them. The force is measured simultaneously by the deflection of the cantilever spring and its spring constant. The combined set up allows the measurement of the free interaction energy, E between surfaces as a function of their separation distance, D . Extracted from (Perez et al. 2008)

4.1 SFA - Mica surfaces preparation

In this study, mica was used as our preferred substrate due to the high probability of obtaining atomically flat surfaces of $\sim 2 \text{ cm}^2$ area and a few micrometers in thickness. This is accomplished by repeatedly cleaving a thick mica sheet ($\sim 1 \text{ mm}$) into thinner sheets until getting the desired thickness. This is a crucial step in the preparation as contamination at this step would cause the failure of the force-distance measurements. Mica is easily contaminated due to its high surface energy after cleaving and to avoid that, the entire preparation is done inside a laminar flow hood. Using a clean needle, mica

is cleaved until an appropriate thickness (~ 2 to 4 microns) is achieved, indicated by the colourful light interferences on the sheet. A heated platinum wire is then used to cut pieces of mica with uniform thickness. These pieces are transferred onto a larger clean mica sheet on which they readily adhere due to Van der Waals forces, protecting them from further contamination. The sheet is then back-silvered with ~ 55 nm thickness of silver inside a vacuum Edwards evaporator. At the start of every experiment, these mica surfaces are glued on two plano-convex cylindrical lenses with the silver facing the glue. After curing under UV light for an hour, the lenses are set up in the SFA chamber in cross-cylinder geometry.

4.2 SFA - Surface translation mechanism

Inside the SFA, one of the lenses moves up and down, while the other is fixed to the upper side of the chamber. The mobile lens is attached to a bending spring used for the force measurements. The SFA has two different translation mechanisms for the bottom lens; the “coarse level” and the “finer level”. The coarse level provides a quick positioning of the lenses with an accuracy of about $1\ \mu\text{m}$, used commonly at the beginning and end of the experiment. The finer level on the other hand, displaces the lens with a resolution of $1\ \text{nm}$. This is done by the differential spring system as shown in Figure 15. This system consists of a flexible helical spring pushed against a spring cantilever that is approximately 1000 times stiffer. Therefore, a $1\ \mu\text{m}$ compression of the helical spring bends the cantilever by $1\ \text{nm}$, resulting in movement of the lower lens by $1\ \text{nm}$.

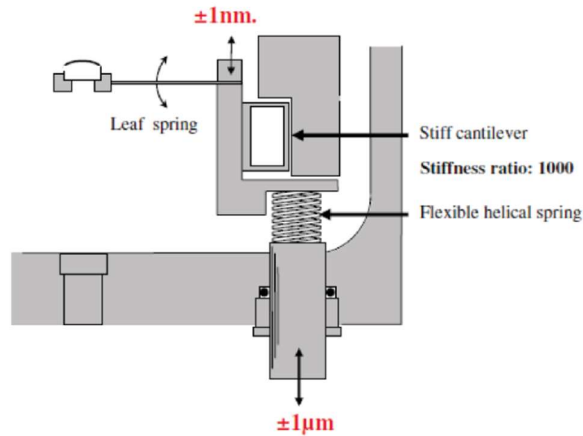


Figure 15: Differential spring system to displace the bottom lens up or down the chamber. Extracted from (Perez et al. 2008)

4.3 SFA - Lens separating distance measurement principle.

When white light is shone perpendicularly on the two silvered mica surfaces, various wavelengths are reflected and transmitted across the different interfaces that form a Fabry-Perot interferometer. The coating of silver covering the mica substrate is adjusted to allow 1% of the incident light to be transmitted, while reflecting the rest. Inside the spectrometer, the transmitted light from the interferometer is split in several fringes, each corresponding to a specific Chromatic order. These fringes are called Fringes of Equal Chromatic Order (FECO). The fringes appear as curved interference patterns as shown in Figure 16. The wavelengths are classified by their order of interference n . In the SFA experiment, the interference pattern at contact in air, as shown in Figure 16 top, is used as the zero reference distance and the position of fringes, λ_n^0 is recorded. When the surfaces are separated by a distance D , each fringe λ_n^D is shifted towards longer

wavelengths by $\Delta\lambda_n$. This shift $\Delta\lambda_n$ and the separating distance D are related as followed (J. N. Israelachvili 1973):

$$\tan (2\pi\mu D/\lambda_n^D) = \frac{2\left(\frac{\mu_{mica}}{\mu}\right) \sin \left[\frac{1-\lambda_n^0/\lambda_n^D}{1-\lambda_n^0/\lambda_{n-1}^0} \pi \right]}{\left(1+\left(\frac{\mu_{mica}}{\mu}\right)^2\right) \cos \left[\frac{1-\lambda_n^0/\lambda_n^D}{1-\lambda_n^0/\lambda_{n-1}^0} \pi \right] \pm \left(\left(\frac{\mu_{mica}}{\mu}\right)^2-1\right)} \quad (\text{Eq 2.4.1})$$

where, λ_n^D (in nm) is the wavelength of the n th ordered fringe at distance D (in nm), λ_n^0 and λ_{n-1}^0 (in nm) are the wavelengths of the n and $n-1$ ordered fringes respectively when the mica interfaces are in contact, μ_{mica} is the refractive index of mica (= 1.60) and μ is the refractive index of the media sandwiched between the two mica sheets. The + sign refers odd order fringes (n odd) and the – sign refers to even order fringes (n even).

The interference pattern can be observed by eye through an eye piece on the side of the spectrometer and the exact position of the fringes of the whole spectrum is precisely recorded with a CCD camera.

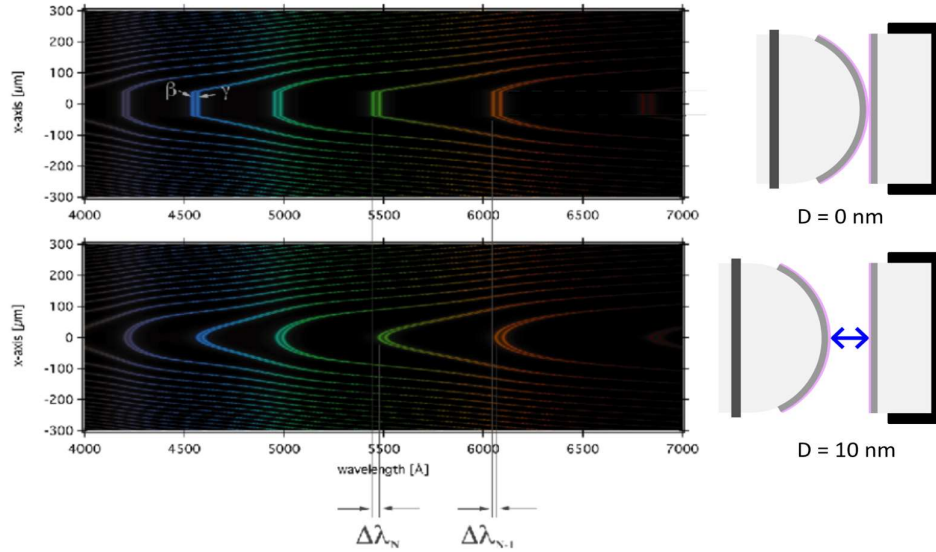


Figure 16: Fringes of Equal Chromatic Order (FECO) of two mica surfaces; in contact (top) or separated (bottom) here by 10nm. Each fringe comes as a doublet of β - and γ - components due to the birefringence of mica. The distance of the fringe and the minimum equates to the separating distance between the two surfaces. In contact, the fringe's shape shows the surface contact shape.

4.4 SFA - Force measurement principle

In an SFA experiment, the force measurement is proportional to the bending of the cantilever holding the lower (mobile) surface. During the measurement, the cantilever is moved up and down at a slow, quasi-static velocity (1-5 nm/s). The calibration is done at long range, where there is no interaction force, by measuring the distance between the two surfaces as a function of the motor displacement. In that regime, where there is no interaction force, the displacement of the mobile surface is governed only by the displacement of the motor. When there is an interaction force, whether attractive or repulsive, the mobile surface displaces faster or slower than the calibration. The exact force is calculated simply by the principle of Hooke's law:

$$F = k(\Delta x) \quad (\text{Eq 2.4.2})$$

where, k is the spring constant (in Nm^{-1}) and Δx is difference between the actual distance and the imposed distance of the lower surface, as shown in Figure 17, such that a positive force corresponds to a repulsion and a negative force corresponds to an attraction.

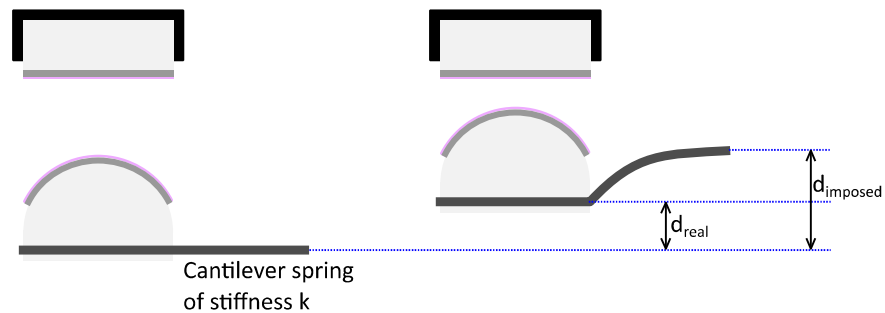


Figure 17: SFA force measurement. When there is a force exerted between the two surfaces, the displacement enforced by the motor's movement on the cantilever (d_{imposed}) differs from that of the real displacement of the surfaces (d_{real}). The force measured is given by: $F = k(d_{\text{imposed}} - d_{\text{real}})$

4.5 SFA – Energy interaction between surfaces

During a SFA experiment, the force F and the distance D between the two opposite surfaces are measured and recorded simultaneously. From these sets of data, we can extrapolate for the interaction free energy per unit area, E , between the surfaces on account of the specific geometry of the SFA. The two cylindrical lenses, of the same radius of curvature R , are arranged in cross-cylinder geometry, equivalent to a sphere/plane geometry with a good approximation. In this setting, the Derjaguin approximation

(Derjaguin, Muller, and Toporov 1975) relates the Force, $F(D)$ and the interaction free energy per unit area, $E(D)$ both as a function of the distance between the two surfaces:

$$\frac{F(D)}{2\pi R} = E(D) \quad (\text{Eq 2.4.3})$$

Which is only true if the separating distance, D is much smaller than the radius of curvature of the lenses ($D \ll R$) and that the force decreases sufficiently rapidly with distance (at least in $1/D^2$). In our experimental study, the radius of curvature of both lenses is 2 cm and the measurement range distance is between 0 to 200 nm.

4.6 SFA – A typical SFA force run

In the SFA experiments, curves of force normalized by the surface radius of curvature F/R are plotted as a function of the separation distance, D as shown in Figure 18. SFA experiments consist of a collection of consecutive approach and separation runs of the two surfaces. On the approach and separation run, the mobile surface is moved towards or away from the fixed surface slowly. At each point (corresponding to the steps by which the motor moved the mobile surface), the distance and its equivalent force is recorded. When there is no adhesion or hysteresis between the surfaces, the separation curve profile overlaps perfectly that of the approach. However, in case of adhesion, the curve profiles differ. If there is an adhesion, during the separation run, the surfaces stay in

contact until the pulling force induced by the separation movement is sufficient to separate them. This only happens when the gradient of the surface force is larger than the cantilever's spring constant. At that moment, the cantilever experiences an adhesive jump away from contact. The jumping distance ΔD_{jump} and the adhesion force F_{ad} are related as follows:

$$F_{\text{ad}} = k\Delta D_{\text{jump}} \quad (\text{Eq 2.4.4})$$

Where k is the spring constant of the cantilever (in N/m).

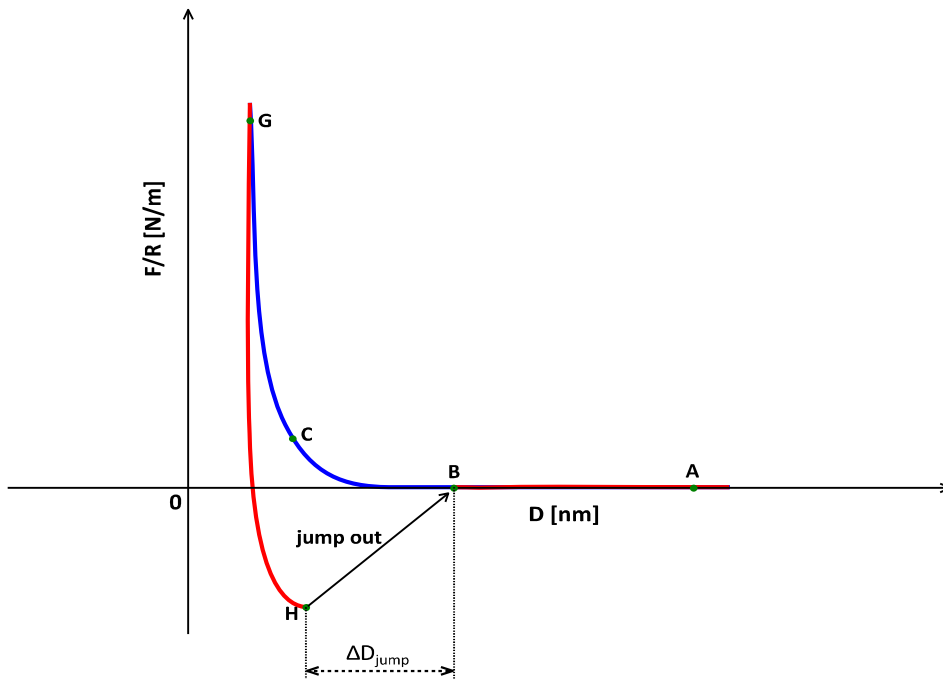


Figure 18: Illustrates a typical SFA force Vs distance curve. The path $A \rightarrow B \rightarrow C \rightarrow G$ represents the approach run of the two surfaces from a long distance till contact. As for the separating run, there are two possibilities; the separation run overlap the approach run by going through $G \rightarrow C \rightarrow B \rightarrow A$, indicating a fully repulsive run with no adhesion or hysteresis, and if the approach run goes through $G \rightarrow H \rightarrow B \rightarrow A$, there has been an adhesion force between the surfaces. The adhesion force F_{ad} is related to the measured jump distance of the two lenses from contact ΔD_{jump} as followed: $F_{ad} = k\Delta D_{jump}$, with k the spring constant as the force gradient.

Chapter 3:

Development of cushioned supported lipids bilayer and its structural characterisation

The aim of this project was to create an artificial membrane on a solid substrate, having the same behaviour of the lipid bilayer in a cell. The idea was to form a neutral polymer cushion between the substrate and the membrane to reduce the interaction between them. In this chapter, we go through the different methods we used to create the artificial membrane and how we analysed their effectiveness.

1. Polyethylene Glycol (PEG)

A favourable polymer for cushioning lipid membrane and transmembrane proteins should meet the following criteria (Wagner and Tamm 2000):

- It should be hydrophilic and should interact neither with the lipid membrane nor with transmembrane proteins, and

- It should be chemically linked to the bilayer at one end and on the solid substrate (glass or mica) at the other end, in order to increase the durability of the cushion.

Polyethylene glycol (PEG) was the polymer used in our work, corresponding to the criteria mentioned above. We used 2 types of bi-functionalized PEG: 1,2-distearoyl-sn-glycero-3-phosphoethanolamine – polyethylene – Thiol (DSPE-PEG-Thiol) or (DPT) Figure 19 (A) and 1,2-distearoyl-sn-glycero-3-phosphoethanolamine – polyethylene – silane (DPSE-PEG-Silane) or (DPS) Figure 19 (B), both with an average molecular weight of 5000 Da. DSPE is an 18 carbon saturated phospholipid with high hydrophobicity. The lipid head is attached to one end of the PEG polymer. As for the other end of the PEG, it is attached to either a thiol or a silane molecule depending if the substrate used is gold covered for thiol and simply glass or mica for silane.

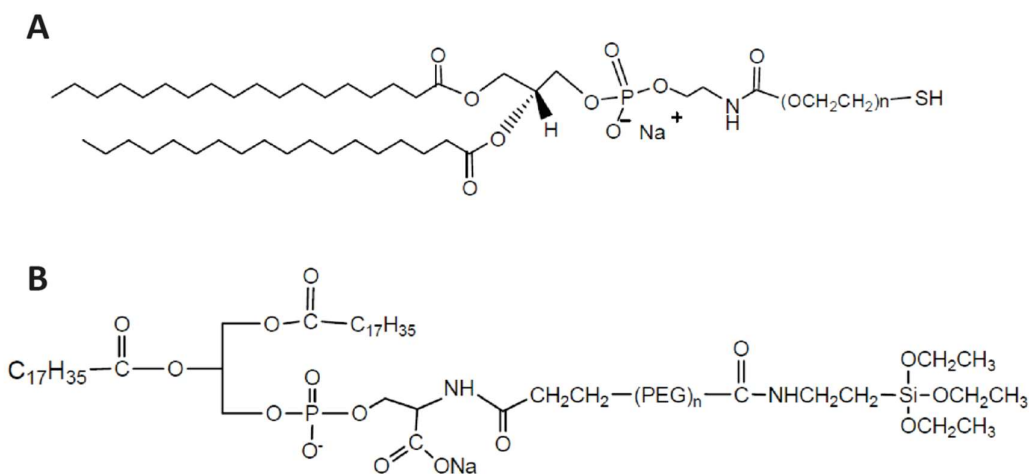


Figure 19: Illustrates the bi-functionalised Polyethylene glycol molecules used during the project; (A) 1,2-distearoyl-sn-glycero-3-phosphoethanolamine – polyethylene – Thiol and (B) 1,2-distearoyl-sn-glycero-3-phosphoethanolamine – polyethylene – silane

2. Self Assembled Monolayer (SAM) chemistry

The first method, used in order to create this artificial fluid membrane, was to use self-assembled monolayer (SAM), to form a polymer monolayer on a substrate, and vesicle fusion to create a lipid bilayer on top of the polymer. Self assembly is a process where organic molecules are high assembled spontaneously onto a noble metal surface by chemisorptions (Prashar 2012). This method consists of immersing a substrate, for a previously determined time period, into a solution containing the organic molecules as illustrated in Figure 20. In this work, DSPE-PEG-thiol was first used to react with gold covered mica.

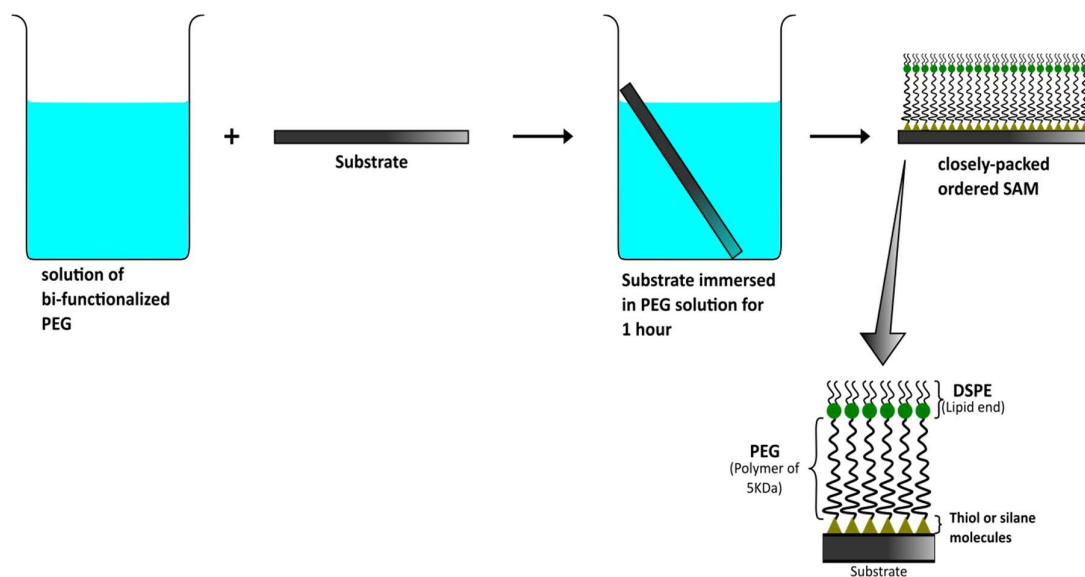


Figure 20: Illustration of the Self assembly monolayer process. This process involve immersing the substrate for a determine amount of time to obtain a monolayer coverage of the substrate.

Using Atomic Force Microscopy technique described in chapter 2, we observed the first monolayer deposited on the gold covered mica substrate with tapping mode in air. During this study, the following questions were investigated:

- What is the actual height of the PEG cushion monolayer?
- What is the best condition to preserve the monolayer surface prepared?
- And finally, optimising the time of immersion of the substrate and the concentration of the DPT solution, in order to obtain a good monolayer on the surface.

2.1 PEG cushion Height

In this investigation, after gluing gold covered mica onto a piece of glass (mica facing the glue), the substrate was immersed into a 2.5 mg/mL DPT solution for 1 hour. During the deposition, the substrate was partially immersed. With tapping mode AFM imaging, we observed the interface between the immersed and non-immersed zones, as shown in Figure 21. We analyzed the height profile on both parts and calculate the average height of the PEG cushion to be $\sim 7 \pm 1$ nm.

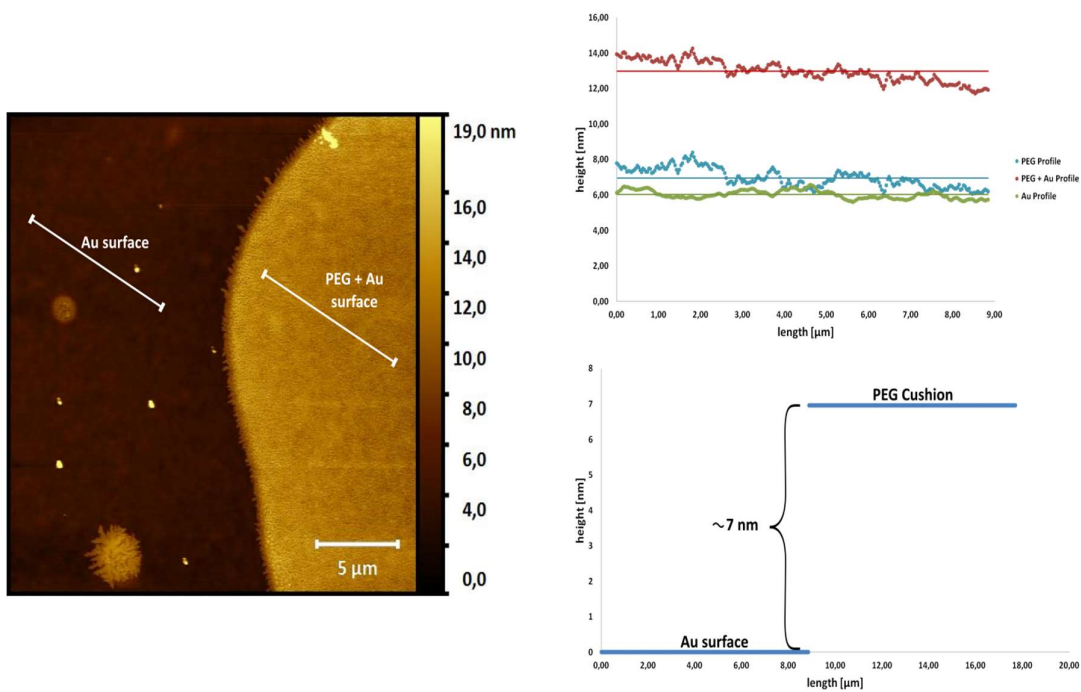


Figure 21: Illustrates tapping mode AFM images (25μm by 25μm) (in air) of DSPE-PEG-Thiol on gold covered mica and how we determine the height of the cushion. The image of the left shows the edge of the cushion. On the top right, the graphs show the height profile of the different surfaces present on the image; in green Au surface, in red PEG on Au and in blue PEG only. On the bottom right, the graph is the result of putting the gold surface as our zero reference height to obtain the actual height of the cushion.

2.2 Exposure to air

During the investigation, we also observed the long term effect of exposing the surfaces to air. As it can be observed in Figure 22, after 24 hours of exposure to air, the polymer on the gold surface starts to crystallise (snow flake shaped). During the immersion period, PEG molecules are tethered, via thiol at the end of the PEG, to the surface of the substrate and the molecules of the pegylation solution (95% ethanol and 5% water) are trapped between the PEG chains. Over time, the molecules of the pegylation solution evaporate, allowing the PEG chains to interact leading to nucleation and to finally form crystals after

24 hrs. We found out that keeping the surface in a solvent resolved that issue, for example in ethanol as shown in Figure 23.

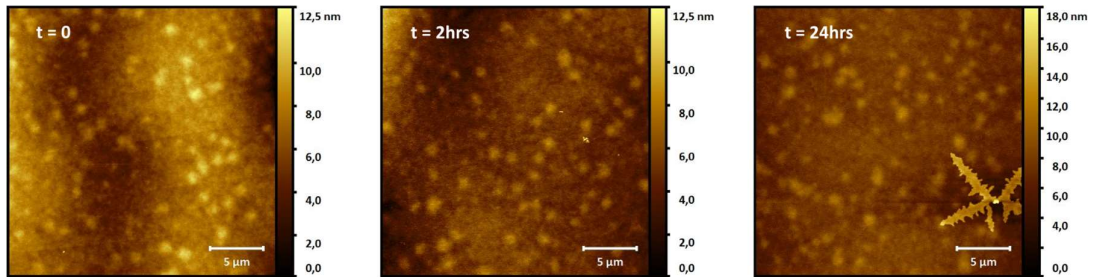


Figure 22: Illustrates tapping mode AFM images (25µm by 25µm) (in air) of DSPE-PEG –Thiol surfaces. From Left to right, the image shows the effect of air exposure to the surface. After 24 hours in air, there are signs of PEG crystallisation in the shape of a snow flake.

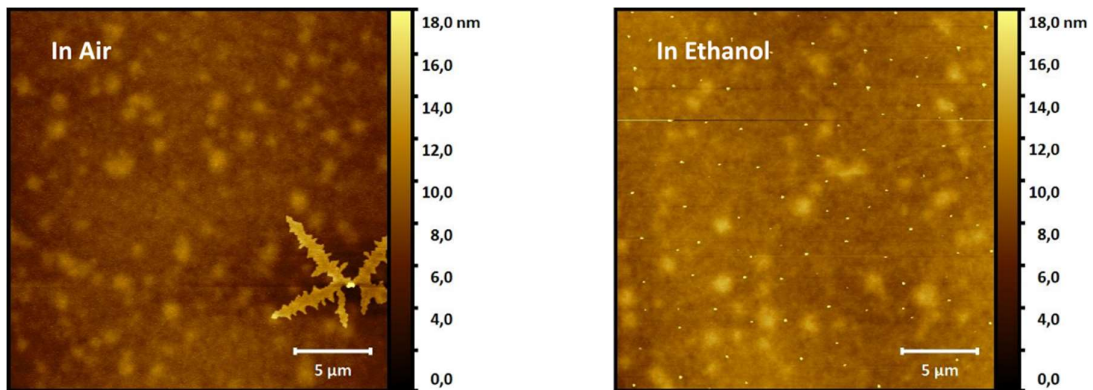


Figure 23: shows the same surfaces preparation of PEG cushion but conserved for 24hrs in 2 different environmental conditions; on the left in air and on the right in ethanol. These are 25µm by 25µm images.

2.3 Preparation optimisation

The last observations made in this investigation, concerned the relationship between the immersion condition during SAM method and the height of the polymer thickness deposited. SAM deposition depends on 2 conditions; the time of immersion of the substrate and the concentration of the PEG solution in which the latter is immersed. Figure 24 displays 4 images representing 4 surfaces made in different preparation conditions. The goal of this study was to improve the SAM conditions in order to have only a homogeneous monolayer of PEG covering the substrate. As measured earlier above, we expect that a thin layer of PEG should be around 7 nm in thickness. In Figure 24, we can observe some bright spots that represent objects of at least 14 nm in thickness according to their scale. This means that the bright spots could represent layer stacking of PEG. It is observed that at low concentration and short immersion time, that there are less bright spot, thus we are getting closer to a thin monolayer of PEG. But, there are still a few more layers stacking, which may cause stray long distance forces issues when used in the surface force apparatus, technique described in chapter 2 section 4.

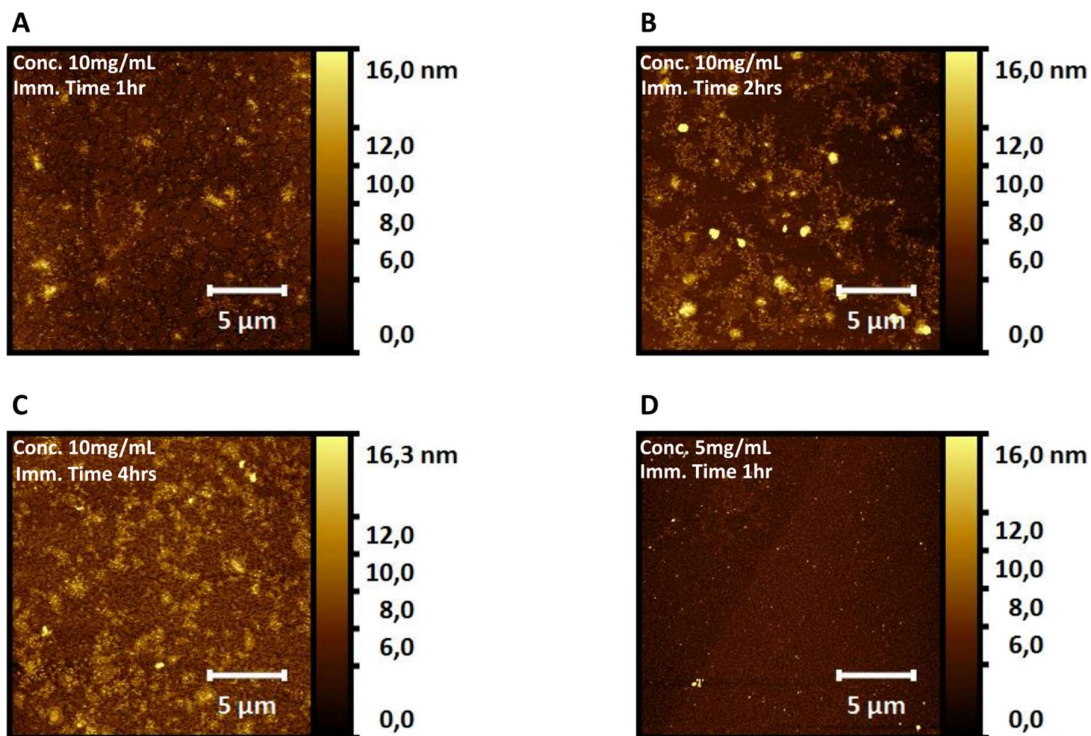


Figure 24: shows the effect of PEG solution concentration and time of Immersion of the substrate on the surface preparation. The images A, B and C are surfaces prepared with the same PEG solution concentration but different time of immersion. The images A and D are surfaces with the same time of immersion but different PEG solution concentration. These are 20μm by 20μm images.

It is crucial that the membranes produced are reproducible without any loose particles as seen on the AFM images above. Another membrane preparation method had been designed to improve the production.

3. Langmuir Blodgett Depositions

The next method used in our work, was described in chapter 2 section 1; the Langmuir Blodgett deposition technique. It was the most efficient method of preparation as it allowed us to accurately control each monolayer composition and density, deposited on

the surface with a uniform coverage. As mentioned in chapter 2 section 1, each monolayer in the cushioned supported bilayer was deposited at a precise surface pressure. To determine that surface pressure, isothermal compression experiments were performed on the different lipid compositions used throughout the work.

On the air-water interface, amphiphilic molecules are free to move on the aqueous surface. As the area covered by the molecules decreases, the molecules diffusing freedom decreases, forcing the molecules to interact with each other and leading to an increase of the surface pressure π . By monitoring the evolution of the surface pressure, π of the amphiphilic monolayer with respect to its molecular area σ , we obtained pressure-area isotherms of the monolayer. Depending on the nature of the molecules, different phase transitions can be viewed. In Figure 25, a typical isotherm of a monolayer is shown. A region with a constant gradient indicates that the monolayer is in a homogenous phase, whereas a region, with a change in gradient, indicates a phase transition at that pressure.

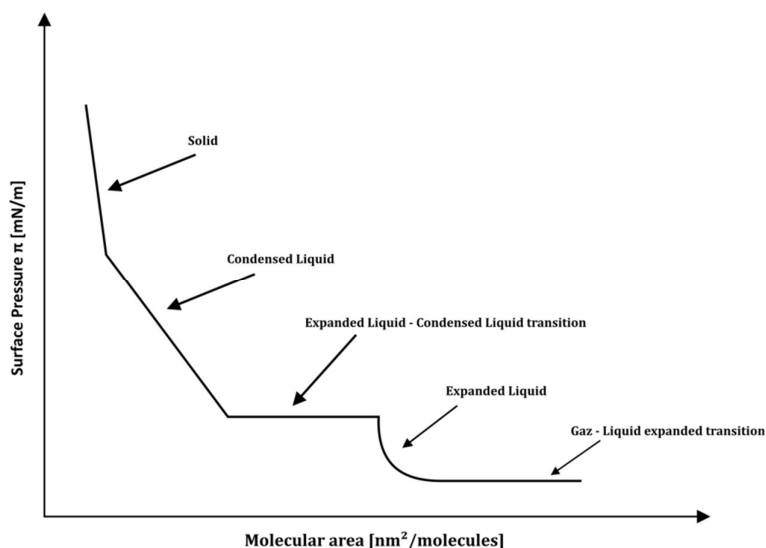


Figure 25: Illustrates a standard isotherm of an amphiphilic monolayer

The first set of isothermal compression experiments is a replica of the work by (Wagner and Tamm 2000). This study examined mixtures of 1-Palmitoyl-2-oleoyl-sn-glycero-3-phosphocholine (POPC) and DSPE-PEG-Silane (DPS) to observe the effect of adding PEG-lipid to the monolayer. In Figure 26, on the left are the average experimental isothermal curves obtained as 0 mol%, 1 mol%, 5 mol% and 10 mol% of DPS is added to the POPC monolayer. On the right, are the published curves by Wagner and Tamm. Both sets of curves have the same trend but, there is a shift in their molecular area. This is due to the fact that during our experiments, the concentration of amphiphilic molecules present in the monolayer was miscalculated due to uncertainty in organic solvent volume.

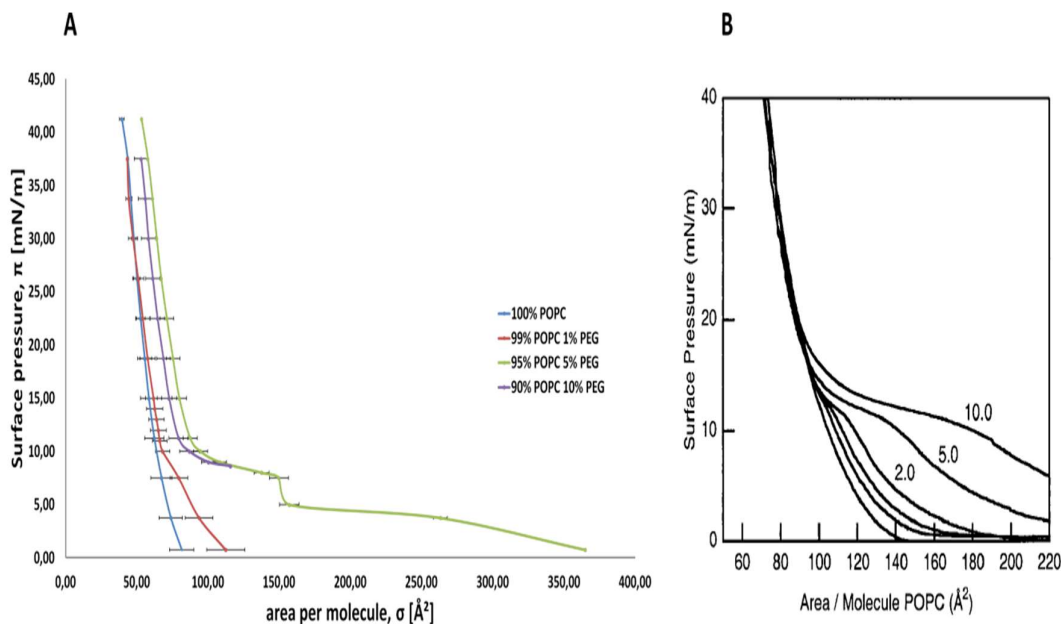


Figure 26: Pressure-area isotherms at 21°C of increasing percentage of DPS in monolayer of POPC on a Langmuir trough. A are the experimental Isotherms graphs recorded with 0 mol% (blue), 1 mol% (red), 5 mol% (green) and 10 mol% (purple) of DPS and B are the Isotherms graphs extracted from (Wagner and Tamm 2000).

The same experiment was repeated with 1,2-dipalmitoylphosphatidylcholine (DPPC) lipid monolayer and we observed the effect of adding DSPE-PEG-Silane (DPS) to the monolayer. We observed in Figure 27, that in both cases, POPC or DPPC, that when we increase the molar percentage of DPS in the monolayer, the longer is the slope corresponding to expanded liquid – condensed liquid phase transition. This is due to the fact the more molecules of DPS are added to the monolayer, the more pressure is needed to overcome the repulsive force between the PEG chains as they are condensed. We also observed that between 15 to 40 mN/m of surface pressure, all the different monolayer compositions are in the condensed liquid phase, which is the region where we deposited the monolayers during this work.

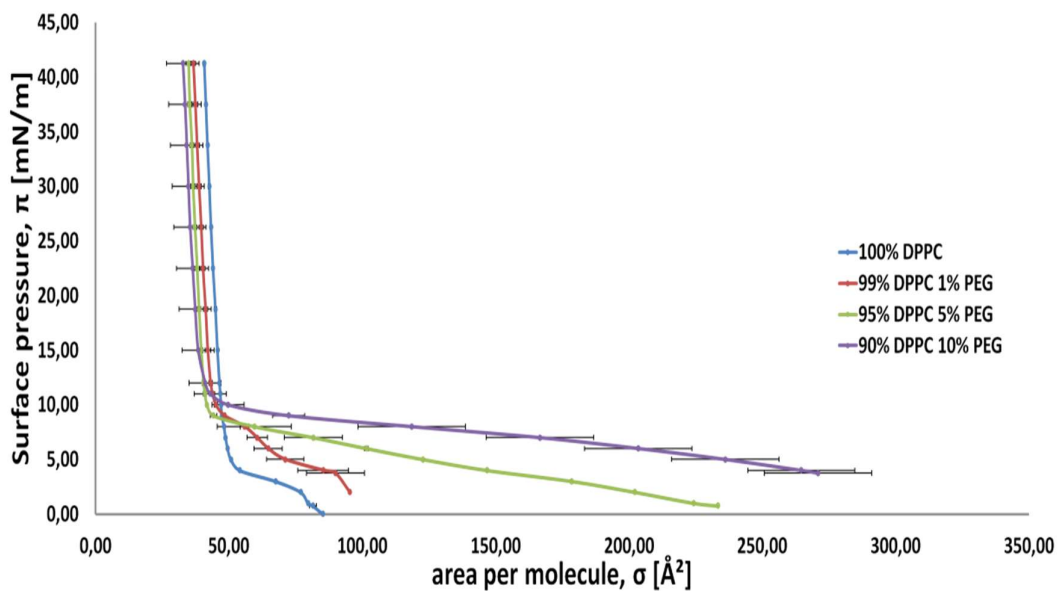


Figure 27: Pressure-area isotherms at 21°C of increasing percentage of DPS in monolayer of DPPC on a Langmuir trough. Isotherms were recorded with 0% (blue), 1% (red), 5% (green) and 10% (purple) of DPS.

Throughout, the remaining of the study, all the monolayer depositions were done at 50mA which corresponds to a surface pressure of 37.5 mN/m on our Langmuir trough using the technique described earlier in chapter 2 section.1. For the remainder of the work, we used mica or glass as substrates, and they needed to be activated. Using air plasma cleaning for ~2-3 minutes, to release the “-OH” molecules for the silane in DPS to tethered to the surface when depositing the first layer. The next two sections of this chapter will centre on the characterisation of the surface prepared throughout this work in term of their outer lipids’ lateral diffusion and their surface structure.

4. Outer lipid leaflet Lateral diffusion

The purpose of the work in this project was to develop artificial membranes that can mimic membranes in a cell. We used 3 types of lipids, listed in Table 1, with the same head group but different tail length and saturation in our membrane development. The 3 lipids chosen have different phase transition temperature (melting temperature). At room temperature ($22 \pm 2^\circ\text{C}$), POPC lipids behave as a liquid, DPPC lipids behave as a gel (solid) and DMPC lipids may be in the transition state between the two.

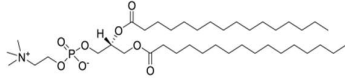
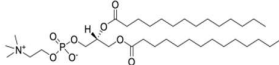
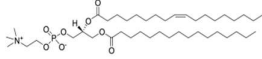
Lipid Name	Label	Molecular Structure	Phase Transition Temperature [$^\circ\text{C}$]
1,2-Dipalmitoyl-sn-glycero-3-phosphocholine (16:0-16:0 PC)	DPPC		41
1,2-Dimyristoyl-sn-glycero-3-phosphocholine (14:0-14:0 PC)	DMPC		24
1-Palmitoyl-2-oleoyl-sn-glycero-3-phosphocholine (16:0-18:1 PC)	POPC		-2

Table 1: Summary of the different Lipids used in the development of the artificial membrane.

The Langmuir Blodgett method was used to deposit, the different artificial membranes, listed in Table 2, on glass substrate for fluorescence microscopy of the membranes.

Artificial Membrane on glass substrate	Artificial membrane system label	
DPS/POPC - POPC	Outer Layer	99% POPC : 1% NBD PE
	Inner Layer	10% DPS:90% POPC
DPS/POPC - DMPC	Outer Layer	99% DMPC : 1% NBD PE
	Inner Layer	10% DPS:90% POPC
DPS/DMPC - POPC	Outer Layer	99% POPC : 1% NBD PE
	Inner Layer	10% DPS:90% DMPC
DPS/DMPC - DMPC	Outer Layer	99% DMPC : 1% NBD PE
	Inner Layer	10% DPS:90% DMPC

Table 2: Summary of the different artificial membranes and their layers deposited on glass substrates.

Using the fluorescence recovery after photo-bleaching (FRAP) method, the lateral diffusion coefficient of the outer layer of each membrane was measured. We used 1 mol% of NBD PE fluorescence lipids to track the diffusion of the lipid on the outer layer.

The FRAP experiments with NBD PE as Fluorescence dye were conducted as followed:

- 10 scans (~0.2s each scan) of Pre-Bleaching at 7-10% laser power
- 1 scan (~0.2s each scan) of bleaching at 100% laser power
- 100 scans (~0.2s each scan) of post-bleaching at 7-10% laser power
- 50 scans (~1s each scan) of post-bleaching at 7-10% laser power

With the excitation wavelength, $\lambda_{exc} = 488\text{nm}$ and the emission wavelength, $\lambda_{em} = 510\text{-}600\text{ nm}$.

To visualise and recover the data obtained during the FRAP experiments; we used the program **LAS X** from **Leica**. The raw FRAP data, $F_{raw}(t)$ were corrected for photofading (Kang et al. 2012) by

$$F_{corrected}(t) = \frac{F_{raw}(t)}{F_{fading}(t)} \quad (\text{Eq 3.4.1})$$

And finally, the corrected data were normalised by the prebleach intensity, $F_{corrected}^i$ as

$$F(t) = \frac{F_{corrected}(t)}{F_{corrected}^i} \quad (\text{Eq 3.4.2})$$

The software program LAS X allowed us to recover the raw data and the photofading data from the recorded images as shown in Figure 28; dotted circle is the raw data set while the solid circle is the photofading data with the same diameter of ROI.

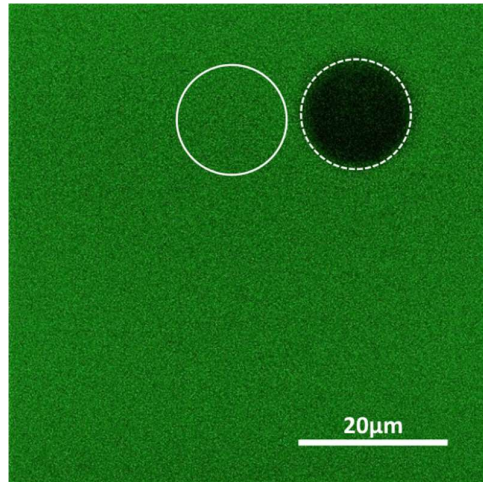


Figure 28: Illustrates a FRAP image of DPS/POPC – POPC membrane just after photobleaching; the dotted circle is the region of the membrane that has been frapped and the solid circle is the region where we measured the fading of the entire surface during post-photobleaching.

In this work, at least 4 samples of each artificial membrane mentioned in the Table 2 were made, on which FRAP measurements were performed. On each sample, at least 4 spots were chosen, where 4 different ROI diameters were used to do FRAP. In Figure 29, recovery images recorded during FRAP experiments are being illustrated for the different artificial membranes manufactured. The membranes have different lipids mixed with 10% DSPE-PEG-Silane deposited in their inner layer followed by 100% of different lipids on the outer layer. The first and last row of images in Figure 29 are symmetric membranes (same lipids in both layers) whereas, the two in the middle are asymmetric membranes. The images at $t = 0.2$ s are the first images recorded just after photobleaching and recovery has already begun in all the membranes. At $t = 3.0$ s, we can see that the top 3 membranes have recovered more than the last one. Just by observing the images, we could already observe that the last artificial membrane has a lower diffusion coefficient

than the others. Finally, at $t = 28$ s, the membranes have mostly recovered from the 15 μm diameter disks shaped bleached.

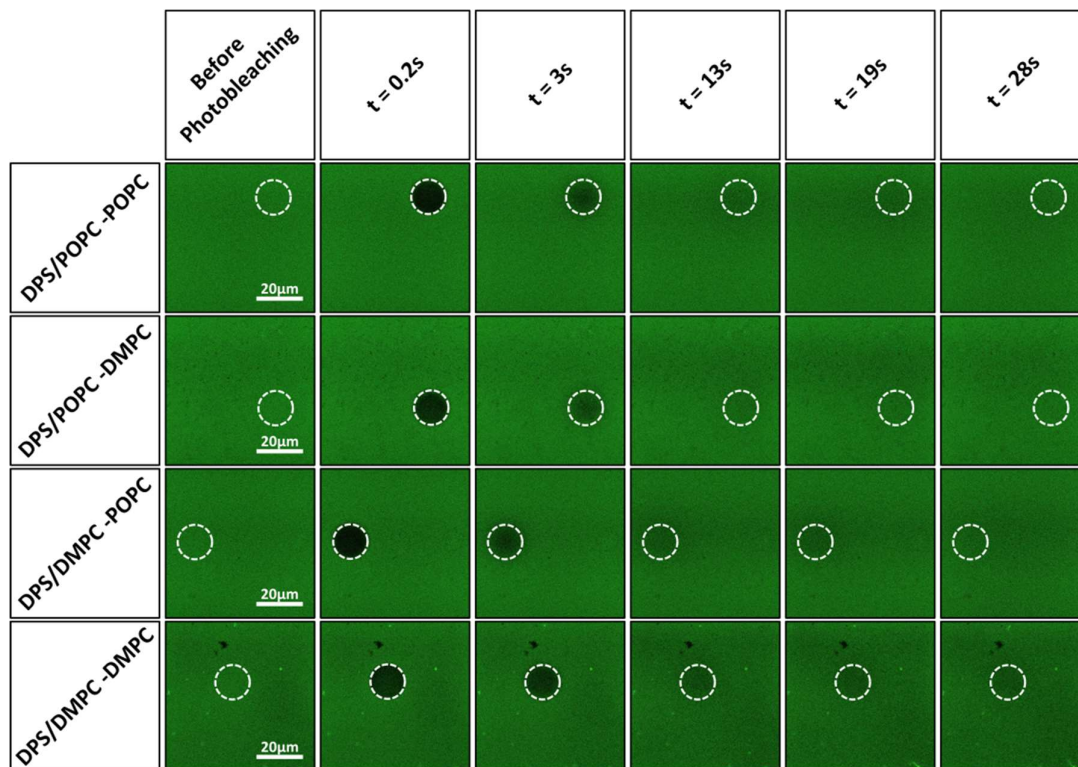


Figure 29: Illustrates the recovery images of the different artificial membranes on which FRAP experiments have been done; the dotted circle is a 15 μm diameter region of interest (ROI) where the surface has been frapped.

Using the fitting program, mentioned in chapter 2 section 3, we extracted the parameter τ , the characteristic diffusion time of each normalized set of data for the different membranes. By plotting the average 16τ values against their corresponding d^2 , ROI diameter square, the inverse gradient of the linear fitting of the data points gives us the diffusion coefficient of the specific membrane. The Table 3, summarised the diffusion coefficient values of all the artificial membrane produced.

Artificial Membrane on glass substrate	Diffusion Coefficient of NBD PE [$\mu\text{m}^2/\text{s}$]
DPS/POPC - POPC	4.3 ± 0.3
DPS/POPC - DMPC	3.4 ± 0.2
DPS/DMPC - POPC	3.4 ± 0.1
DPS/DMPC - DMPC	1.9 ± 0.1
DPS/DPPC - POPC	0.3 ± 0.1

Table 3: Summary of the diffusion coefficient of different artificial membrane developed.

The Table 4 summarized the diffusion coefficient values of NBD-PE fluorescent lipids in different artificial membrane environment published in (Pincet et al. 2016) and (Motta et al. 2015). The fastest diffusing membrane is the first one, DPS/POPC – POPC, composed of fluid lipids in both the inner and outer leaflet of the membrane. However, in comparison to the values published in the literature, the diffusion coefficient of the fastest membrane system made, is still halfway to that of a free giant unilamellar vesicles (GUVs). Even if the polymer, PEG has created a cushioned between the solid substrate

and the membrane, the inner layer of the membrane is still tethered to the solid surface. This reduced the diffusion of the outer layer since, the membrane is not completely free like in GUVs. As for the DPS/DMPC – DMPC membrane system, the diffusion coefficient obtained is similar to that of a fluid membrane deposited straight onto a solid substrate (shown in Table 4), as DMPC lipids are in gel phase at room temperature.

Artificial Membrane Environment	Diffusion Coefficient of DOPE-NBD [$\mu\text{m}^2/\text{s}$]
Supported bilayers on glass substrate	1.9 ± 0.4 (Langmuir Blodgett)
Giant liposomes held through micromanipulation	6.9 ± 1.3 (Osmotic shock) 7.2 ± 0.4 (Electroformation)

Table 4: Summary of diffusion coefficient values of different artificial membrane in different environment. The value on the top row was extracted from (Pincet et al. 2016) and the bottom row was extracted from (Motta et al. 2015).

The phase behavior of the lipid bilayer plays a big role on the lipid mobility. This behavior is largely dictated by the strength of the attractive Van der Waals interactions between nearby lipid molecules. This strength is governed by how long the lipid tails are, how well are they packed and the degree of unsaturation within the lipid tails. Moreover, an unsaturated double bond in the lipid tail can produce a kink in the alkane chain, disrupting the regular periodic structure, making the bilayer more flexible and mobile. The DPS/DMPC – POPC and the DPS/POPC – DMPC have identical diffusion coefficient. This is due to the strength of interaction between the inner and outer leaflet is similar. Whether POPC lipids are in the inner layer and DMPC lipids are in the outer layer, or vice versa, the tails length, the lipid compaction and even the degree of unsaturation within the 2 layers have not changed. Finally, the lipid diffusion of DPS/DPPC – POPC is very slow since DPPC has longer lipid tails and a high transition temperature.

5. Cushioned supported membrane surface characterisation by

AFM

This AFM characterization of the CSLBs was performed at the School of Science department, at RMIT University, Melbourne, Australia. In the previous subchapter, we observed that most of the artificial membranes fabricated are diffusive. In this subchapter, we are imaging, with a special type of AFM that has sub-Angstrom resolution, the surface of these membranes listed in Table 5 below, which have been deposited on mica substrate. Using amplitude modulated atomic force microscopy (AM-AFM) in aqueous medium, we observe the surface morphology of these membranes at high resolution. During this study, a Cypher ES Atomic Force Microscope (Oxford Instrument, Asylum Research, Santa Barbara, CA, USA) at room temperature (22°C) was used. We used ArrowUHF cantilevers, commercially available from NanoWorld, Switzerland with a nominal spring constant, $k_c = 6 \text{ N/m}$, and a sharp tip attached at the end with a resolution of $\sim 0.05 \text{ nm}$ (Page et al. 2014). Since we are dealing with soft surfaces, we set the cantilevers' free amplitude, A_0 (amplitude of oscillation of the cantilevers in buffer away from the surface) to be as small as 1 nm. When imaging the samples, we minimise the imaging force by applying a setpoint ratio (Imaging Amplitude (A) / free amplitude (A_0)) of $>0.7 - 0.8$ was maintained (Elbourne et al. 2019). The cantilevers are calibrated using thermal spectrum method (Sader et al. 1995), in buffer prior to use, and the lever sensitivity was determined using force spectroscopy. In order to confirm that the images

taken during this study were not a result of scanning artifacts, the experiment was repeated on same membrane systems prepared on different days with different tips. We took scan at different spots on the surface (at least 3 spots) with three different scan sizes. The same results for each membrane were observed. During image acquisition both the trace (scanning left to right) and retrace (scanning right to left) profiles were superimposed, meaning that a reliable representation of the surface was obtained.

Artificial Membrane on glass substrate	Artificial membrane system label	
DPS/POPC - POPC	Outer Layer	100% POPC
	Inner Layer	10% DPS:90% POPC
DPS/POPC - DMPC	Outer Layer	100% DMPC
	Inner Layer	10% DPS:90% POPC
DPS/DMPC - POPC	Outer Layer	100% POPC
	Inner Layer	10% DPS:90% DMPC
DPS/DMPC - DMPC	Outer Layer	100% DMPC
	Inner Layer	10% DPS:90% DMPC

Table 5: Summary of the different artificial membranes and their layers deposited on mica substrates.

With the AM-AFM, we are able to record two sets of data; a topographic image (height image) and a phase image. The topographic image gives us information on the roughness of the membranes and the phase image gives us information on the softness of the matter between the sample's surface and the tip. The data sets shown in Figure 30 are from the two symmetric membranes made.

The DPS/POPC – POPC topographic image reveals some faint structures; beads with sub-nanometer separation distance, and hills and valleys with typical separation distance of a few nanometers. As for its phase image, it shows better defined features as the AM-AFM phase signal is more sensitive to minor compositional variations than the height signal (García 2010). The DPS/POPC - POPC phase image shows some repeated beads like structures aligned parallel next to each other as shown in the dotted yellow box in Figure 30. As for the DPS/DMPC – DMPC height and phase images, they do not show any particular repetitive features.

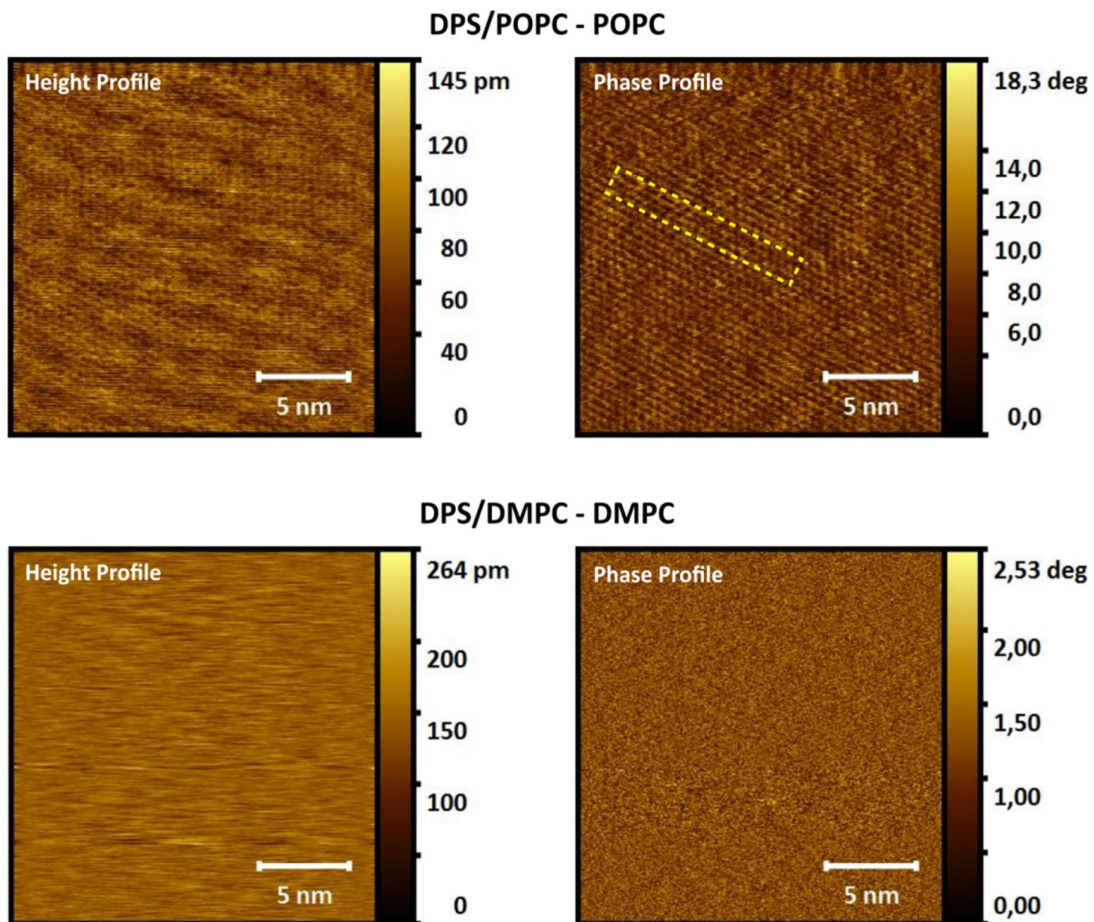
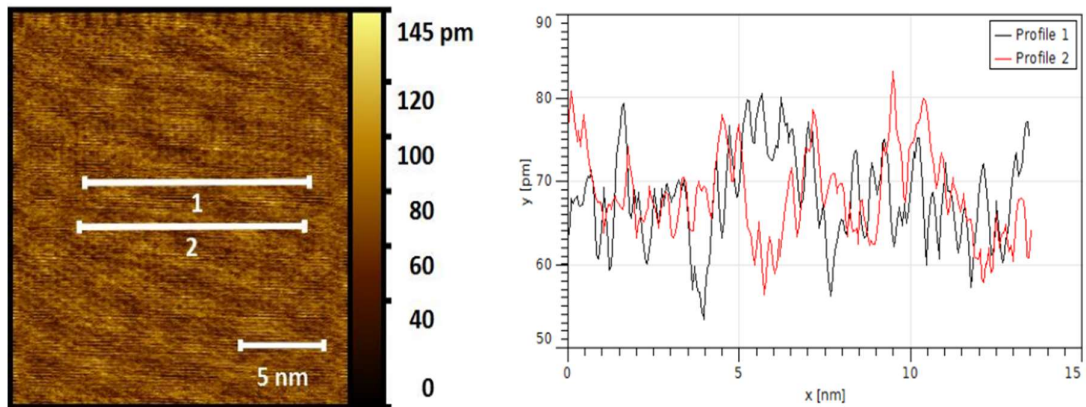


Figure 30: Illustrates the AM-AFM results on 2 different symmetric lipid bilayer systems; top row POPC lipids in both leaflets and bottom row DMPC lipids.

In Figure 31, we compared the height image of the two symmetric membranes along with their profiles. The height variations in Figure 31 are in the picometer range. This means that both membranes are atomically flat on the surface, even if the DPS/POPC – POPC membrane height image shows some hills and valleys. The same observations were made with the asymmetric membranes. Since no deep valleys were seen in any of the samples,

this implies that the membranes were homogeneously covered with no defects at the length scales examined here.

DPS / POPC - POPC



DPS / DMPC - DMPC

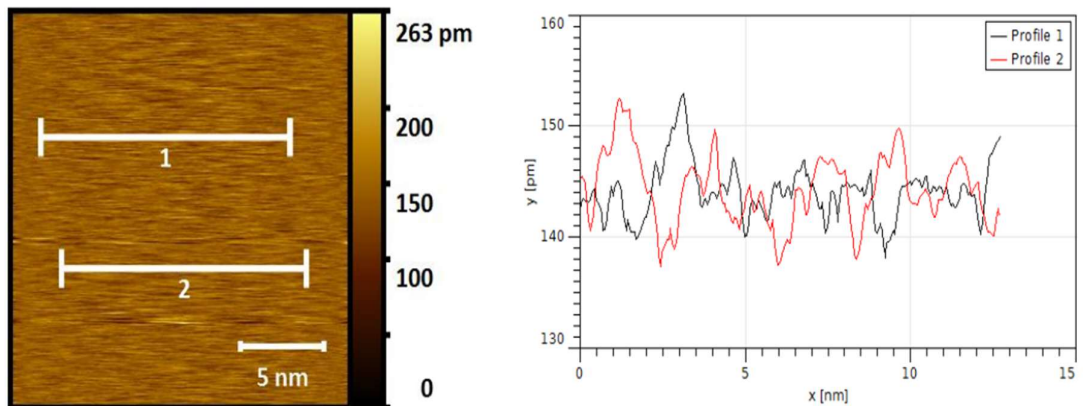


Figure 31: Illustrates the height images of the 2 symmetric membranes and their profiles at 2 different areas.

In Figure 32, we compare the phase images from all four membranes. A and C phase images are from the membranes containing DPS/POPC (a fluid membrane at 22°C) in their inner leaflet. They show some repeated structural features. As for the membrane in B

and D, they contain DPS/DMPC (a gel membrane at 22°C) in their inner leaflet and they show no repetitive features.

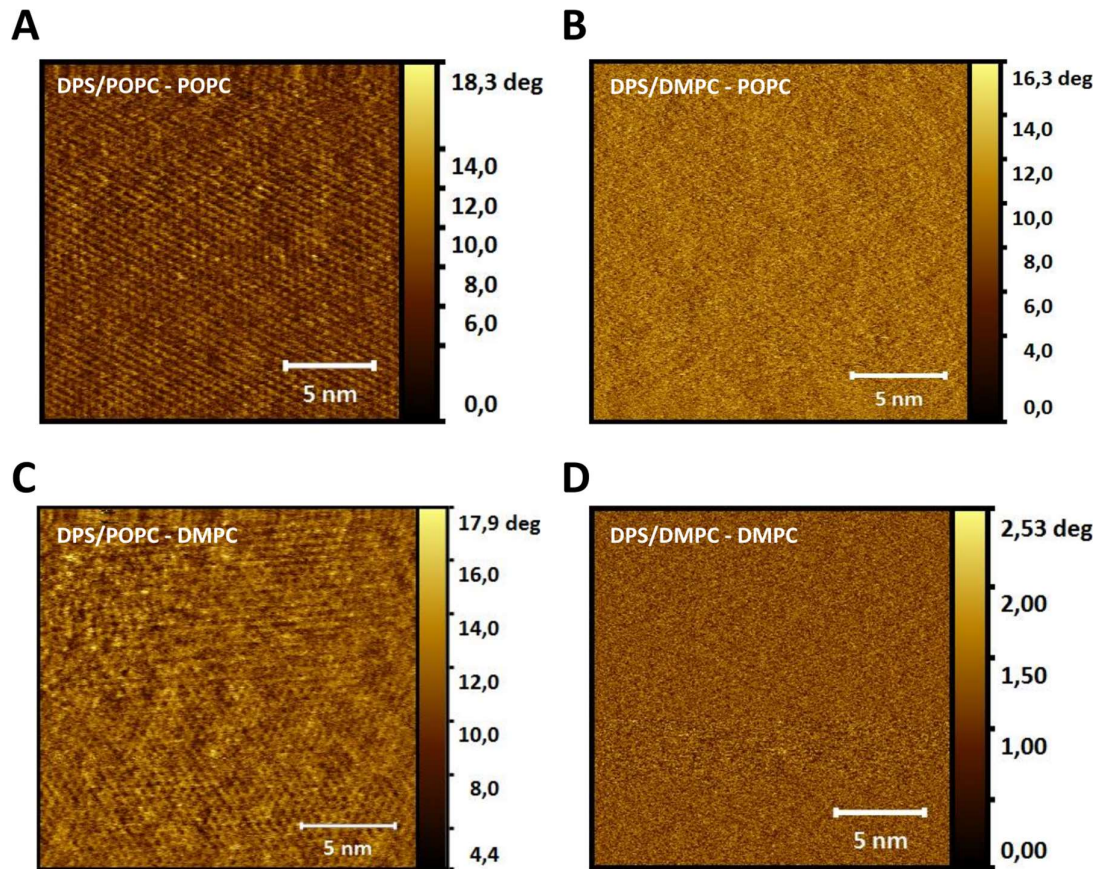


Figure 32: Illustrates the phase images of the different membrane surfaces; (A) DPS/POPC – POPC, (B) DPS/DMPC – POPC, (C) DPS/POPC – DMPC, and (D) DPS/DMPC – DMPC.

We performed Fourier transform analysis on the phase images to confirm whether or not there are repetitive structures on these membranes and to quantify the repetitive distance when they were found as shown in Figure 33. The output of the transformation represents the image in the Fourier space, while the input image is the spatial domain equivalent. In the Fourier space image, each point represents a particular frequency

contained in the spatial domain image. What the Fourier analysis revealed is the occurrence of repetitive patterns, represented by bright dots, in the Fourier space. The more frequent these patterns or structures are in the spatial domain, the brighter are the dots in the Fourier domain. Moreover, by measuring the distance between a dot and the centre of the Fourier domain image, we can inversely calculate the distance between two of these repeating structures in the spatial domain. The closer the dot is in Fourier domain from the centre, the further apart are the repeating structures in the spatial domain.

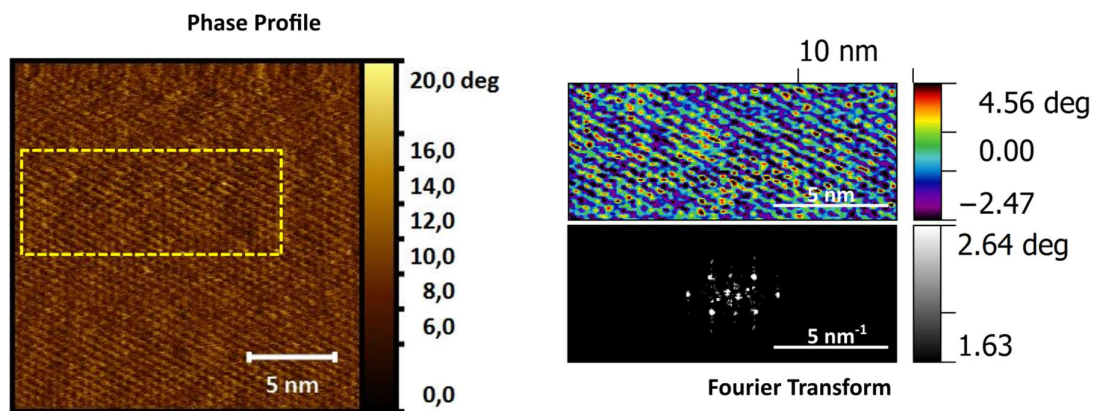


Figure 33: Illustrates the Fourier transform analysis of the phase image of DPS/POPC - POPC. On the left is a 25 nm by 25 nm phase image. On the top right is a cut off of the phase image represented by the yellow box and it is in spectral colour to detail the different degree of softness of the surface. Finally, the bottom right is the Fourier transform of the cut off.

In Figure 34, we summarized the Fourier Transform performed on the different membrane systems' phase images. We also did Fourier Transform on the systems' substrate, Mica to compare. We observed that only the membrane systems with fluid lipids (POPC) in their inner leaflet, show repeated features in their phase images. Moreover, when comparing them to Mica, they show some similarity in their Fourier domain, with 6 bright dots placed in hexagonal pattern in the Fourier domain. However,

when we looked at the DPS/POPC – POPC system more carefully, we noticed 2 dots very close to the centre indicating that there are structures in the spatial domain that are further apart. By measuring and reversely calculating the distance between the dots and the image's centre, we found out that these repeating structures are approximately 3.90 ± 0.01 nm apart. Since, we know the molar percentage of PEG in the membrane inner leaflet; we can say that the 3.90 ± 0.01 nm is the distance between 2 PEG molecules, corresponding to an area per molecule of 15 nm^2 for the PEG molecules within the monolayer. Knowing that there is 10% of PEG and 90% POPC in the inner layer composition, this gives us an area per PEG lipid of 1.5 nm^2 . This is a too small density when comparing to the area per lipid measured, from the pressure-area isotherms in Figure 26 for this particular PEG/Lipid composition, to be $\sim 5.5 \text{ nm}^2$ at the surface pressure the layers were deposited. Therefore, what is likely to happen is that not all the PEG in the inner layer anchored on the mica during the Langmuir Blodgett deposition.

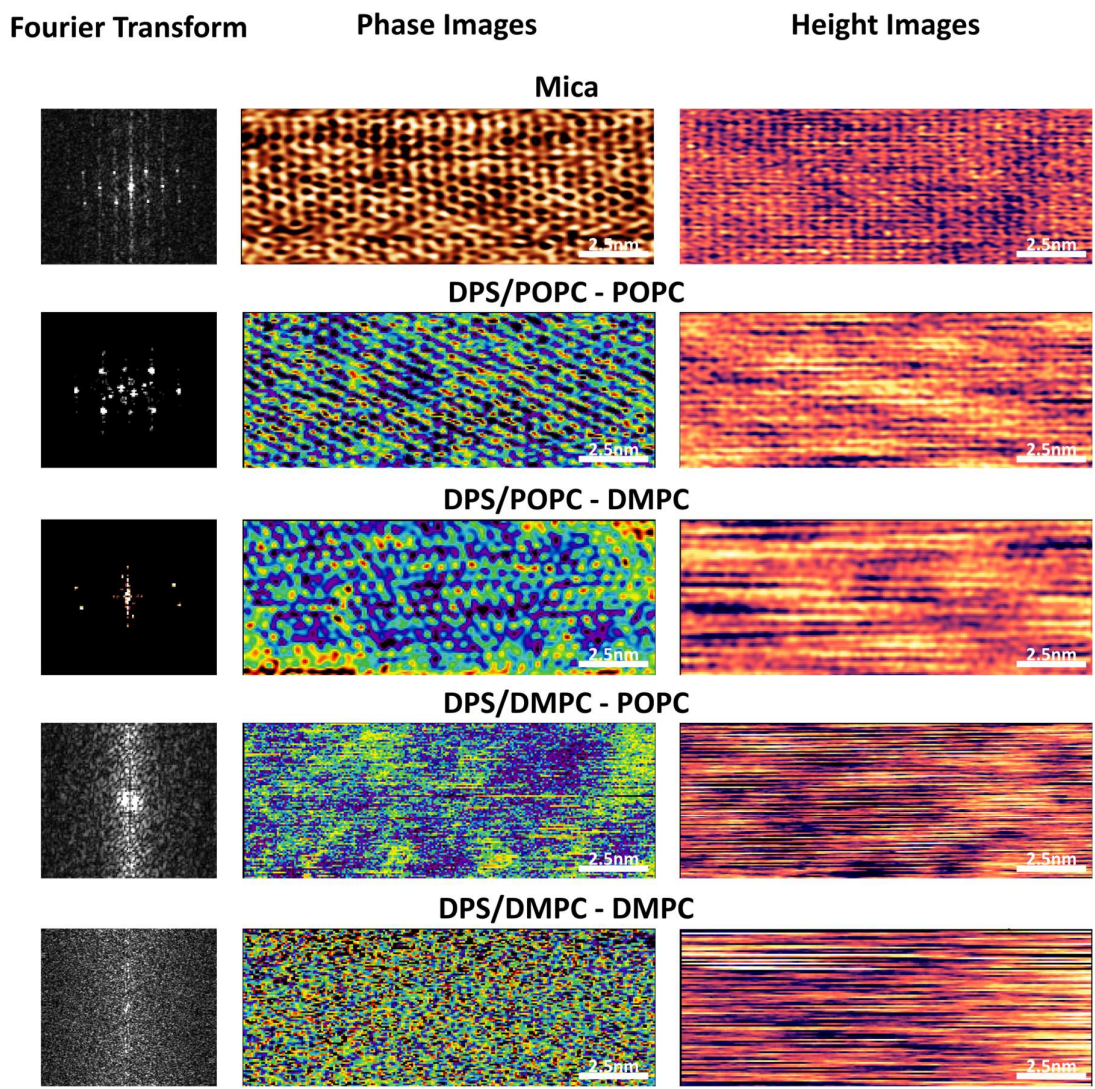


Figure 34: Illustrates the Fourier transforms of the phase images of the different membranes.

In Table 6, we summarized our measurements of the dots in the Fourier domain of the membranes similar to that of mica. We observe that the membranes with gel lipids (DMPC) in their inner leaflet do not exhibit any repeated features. We also could see that the average distance of the dots in the other membranes are smaller than that of Mica.

	2D – Fourier Transform Coordinates		Inverse space (nm ⁻¹)	Real space (nm)	Average (nm)
	x	y			
DPS/POPC - POPC	1.19	2.08	2.40	0.42	0.44
	0.08	2.19	2.19	0.46	
DPS/POPC - DMPC	1.8	1.23	2.18	0.46	0.46
	2.02	0.86	2.20	0.46	
DPS/DMPC - POPC	No Repeat structure				
DPS/DMPC - DMPC	No Repeat structure				
Mica	0.9	1.74	1.96	0.51	0.52
	1.19	1.46	1.88	0.53	
	1	1.7	1.97	0.51	

Table 6: Summary of measured distance of the dots in the different artificial membranes.

If we compare the average distance with what we know about lipid, we can say that the values represent the average radius of the lipid heads (Anton et al. 2013). Furthermore, the membranes were prepared and kept within 150 mM KCl buffer. Comparing our measurements to the study made in (Fukuma, Higgins, and Jarvis 2007), we can say that each bead features (as shown in Figure 35), that can be seen on the phase images, represent either the choline or the phosphate part of the lipid head. The choline and phosphate molecules bind with the ions in the KCl buffer which are seen on the phase images. Since we cannot distinguish between the two molecules on the phase image, we can only assume that the lipids are oriented in such a way to minimise their interaction energy. This is done by arranging the choline of one lipid adjacent to the phosphate of another lipid as shown within the white dotted rectangle on the phase image in Figure 35. The radius of one lipid head can therefore be measured as the distance between the

centre of one bead to the centre of the next, which gives us an average radius for a lipid head of 0.41 ± 0.03 nm. This corresponds to the data obtained from the Fourier analysis data, where the repeat distances in Table 6 correspond to the centre to centre distance between the beads and which correspond to the average radius of the PC (Phosphate choline) head.

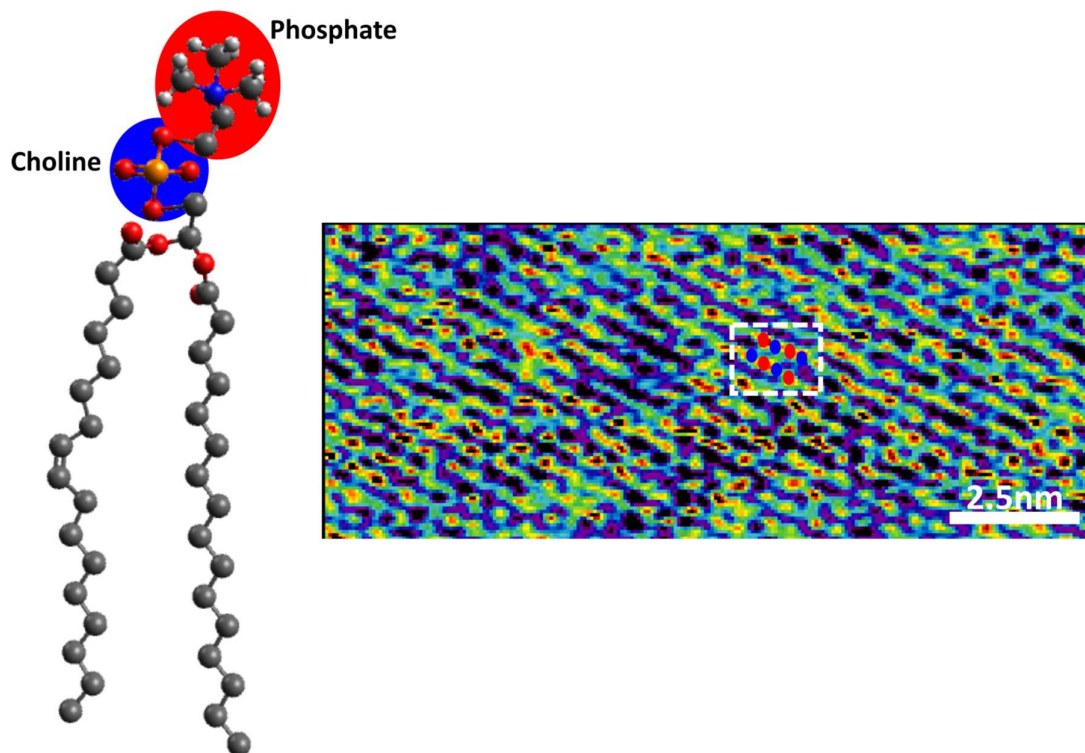


Figure 35: Illustrates the phase image of an AM-AFM measurements of DPS/POPC-POPC membrane. Each beads on the phase images show either a Choline or Phosphate molecules in a particular pattern as shown with the white dotted rectangle.

Chapter 4:

Surface Force measurements on different Cushioned supported bilayer systems

In this chapter, we are going to detail the surface force apparatus (SFA) measurement results obtained in the different configuration of the surfaces. The operational details of the SFA were explained in chapter 2.4. To summarise, an SFA measurement consists of an approach and a separation sequence between 2 surfaces. During the measurement, the distance between the surfaces is measured via interferometry (distance resolution $\sim 1 \text{ \AA}$) along with their corresponding forces exerted on the cantilever spring (force resolution $\sim 1 \text{ \mu N}$). We performed measurements on 3 different systems:

- an asymmetric system with a cushioned bilayer on one surface and a clean mica surface on the other one as shown in Figure 36 (A)
- a symmetric system with a cushioned bilayer on each surface as shown in Figure 36 (B)

- a system with protein incorporated in a bilayer on one side, and a cushioned bilayer on the other side as shown in Figure 36 (C).

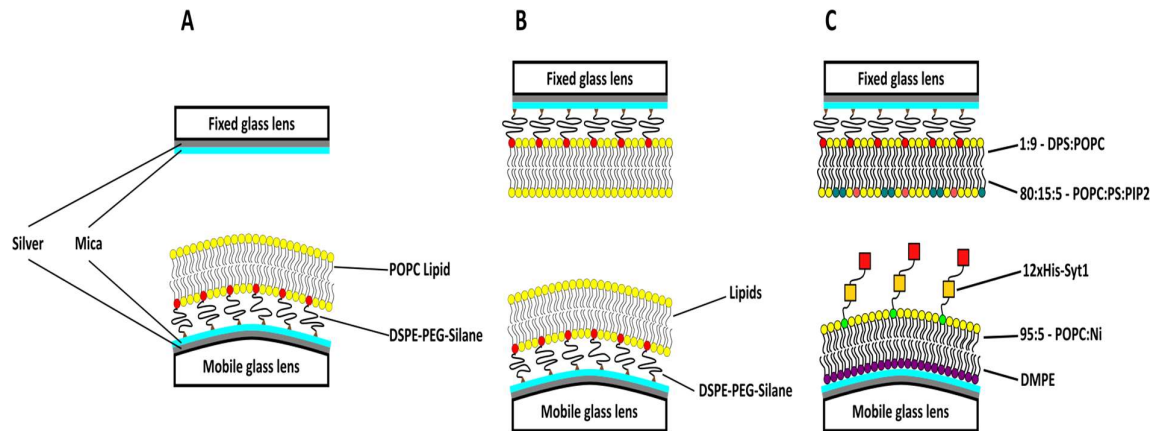


Figure 36: Illustrates the different configurations of surfaces on which we did some force measures. (A) an asymmetric system. (B) a symmetric system. (C) a system with protein incorporated in a bilayer on one side.

For each case, we performed at least three experiments with new mica surfaces (glued on lenses) and bilayers and for each new experiment, we explored at least three regions of the bilayers. Exploring a new region of the bilayer was done by separating the surfaces and by shifting sideways one surface relative to the other and then measuring the force/distance profiles. During the analysis of the SFA force/distance profiles, we observed that there is a shift between the data points collected from one contact region and the ones collected from the next contact region, while the trend of the force curves are similar. This is due to the optical anisotropy of mica that splits the FECOs into doublets, with a different polarisation, in which one fringe corresponds to the extraordinary refractive index while the other corresponds to the ordinary one. When the optical axes of the two mica sheets are parallel, the doublets have the maximal

spacing and when they are perpendicular, the fringes are superimposed. The zero-distance position of the fringes was first taken with clean mica surfaces, and then, the cushioned bilayers were deposited. As the angle between the mica sheets is not controlled, a change of angle during the experiment could have happened at two instances: after the transfer of a bilayer on the lenses and also during the change of contact region. In our SFA experiment, we take our zero-distance reference when the two cleaned back-silvered mica sheets are in contact, inside the empty SFA. Then, the lenses are taken out to deposit the different membranes on them and put back inside the buffer filled SFA. During this transfer, as the angular position of the lenses is not controlled, the lenses may be slightly rotated causing the misalignment of the mica lenses. Another instance where this happens is when we changed contact spots during the experiment; by moving the upper lens forward (or backward) and left (or right) movements. If there was a slight rotation, this causes a shift in the force curve as the reference would not be the same as shown in Figure 4.0 (a).

If the lenses are well aligned after the deposition of the membranes, the contact distance measured correspond to the thickness of the membrane between the two mica surfaces as shown in the first case in Figure 37. However, if there is a rotation, it may cause either an over or under estimation of the membrane thickness as shown in the other cases. This is indeed what the data below shows.



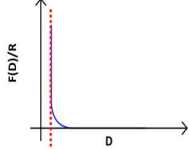


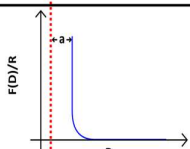


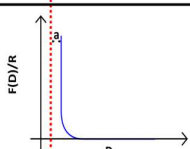

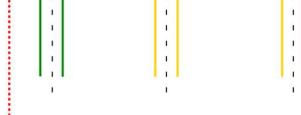
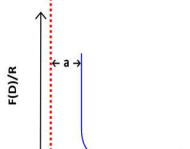
Description	Lenses Alignment	Fringes Alignment	Force curves corresponding
Initial contact cleaned Mica - Mica measurements			
Contact 2 surfaces with bilayer deposited without any rotation			
Contact 2 surfaces with bilayer deposited with a rotation where the optical axes of the mica sheets nearly overlap			
Contact 2 surfaces with bilayer deposited with a rotation with larger angle between the two optical axes of the mica sheets			

Figure 37: Illustrates the different shifting possibilities if there is a misalignment on the lenses between the initial mica-mica contact measurement and the experimental contact measurements.

1. Force measurements on an asymmetric system

Firstly, we observed the behaviour of the force curves of an asymmetric system as shown in Figure 38. In this asymmetric system, a cushioned supported bilayer is deposited on the bottom lens of the SFA, facing the mica of the top lens, within an SFA chamber filled with 150 mM KCl buffer. In this system, the separating distance **D** refers to the distance between the mica surface (on the top lens) and the bilayer (on the bottom lens) as shown in Figure 38. This is achieved by taking the reference distance to be when the bilayer and

the mica surface are in contact with each other, which is done manually by turning the coarse level slowly until flat fringes are seen in the spectrometer. The measurement was performed on one symmetric membrane (membrane with the same lipids in the inner and outer layer) system only, where the cushioned supported membrane consists, in the inner leaflet, of a mixture 10% DSPE-PEG-silane with 90% POPC lipids and in the outer leaflet 100% POPC lipids. In order to solve the fact that we have a distance shift in our experimental measurements, we took the average measured distances of the different contact regions used in one experiment to represent average distance of all the curves. Then, all the curves were shifted to that representative average distance. This means for each contact region, we measure the average distance of all the curves for the same $F^{(D)}/R$ value and then calculate the average of all the contact regions. Finally, we shifted all the curves of each region to that average distance.

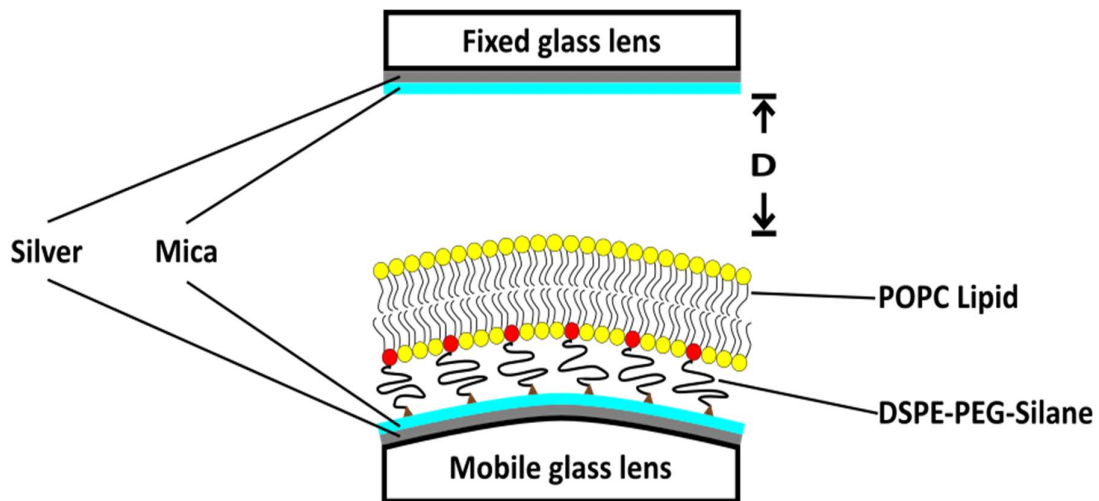


Figure 38: Illustrates the SFA setup for the asymmetric system; a cushioned supported bilayer on one lens and mica on the other.

For the asymmetric system, we obtained the force curve shown in Figure 39. The filled dots represent the approach run and the empty ones represent the separation run. During the approach run, no significant force was measured until the surfaces were brought to a distance of ~ 25 nm. Then, a small repulsive force is observed ($F > 0$) when $D \sim 25 \pm 2$ nm corresponding to the thickness of an unstrained cushioned supported bilayer on the bottom lens.

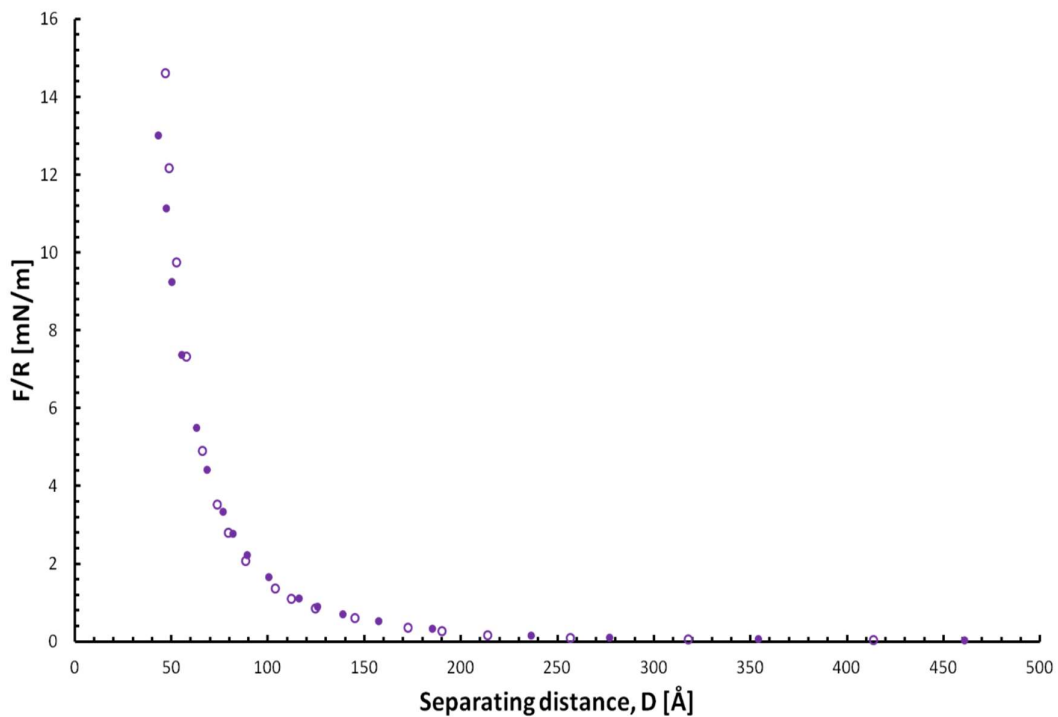


Figure 39: Illustrates the force curve of an asymmetric system; DPS/POPC-POPC on one side and mica on the other side. The filled dots are the approach run and the empty ones are the separation run.

With electrolyte solution like KCl buffer, diffuse cloud of positively charged counterions are accumulated near mica surface which is negatively charged, known as the electrical double layer. The characteristic decay length of this electrical double layer is called the

Debye length λ_D and is proportional to the ionic strength of the aqueous solution. For our experiment, the Debye length of our 150 mM KCl buffer is about 0.8 nm, which indicates the electrostatic forces are negligible at the repulsive distances measured here ($D \sim 25$ nm). Therefore, this interaction is mainly caused by the steric interaction between the anionic membrane surface and the mica surface. When the first significant repulsive force was measured, an unstrained cushioned supported bilayer just started interacting with the mica surface. As the surfaces are compressed, an exponential repulsion is measured.

Therefore by subtracting an approximated value for a bilayer (~ 5 nm) from the thickness of the cushion, we can estimate that the height of the polymer, PEG-5 kDa, is $\sim 20 \pm 2$ nm. We can theoretically calculate the contour length of the polymer by the following equation:

$$L = l * n \quad \text{(Eq 4.1.1)}$$

Where L is the extended length of the polymer, in nm, l is the net length of 1 subunit of the polymer ranging from 0.278 nm to 0.358 nm depending on the orientation of the bonds (Oosterhelt, Rief, and Gaub 1999) and n is the number of subunits within the polymer chain, which calculated from the molar mass of PEG, $(18.02 + 44.05 \times n)$ g/mol. We thus can estimate the contour length of PEG-5 kDa to be between 31 nm to 40 nm.

The approach and separation curves were fitted against a first order exponential curve;

$$f(x) = Ae^{Bx} \quad (\text{Eq 4.1.2})$$

And the extracted values of A and B were used to calculate the radius of gyration, of the cushion and the molecular density, using the polymer mushroom equation (Gruget et al. 2018):

$$\frac{F(D)}{R} = 72\pi\Gamma k_B T \exp\left(-\frac{\sqrt{3}D}{R_g}\right) \quad (\text{Eq 4.1.3})$$

Where **F** is the measured force in mN, **R** ~2 cm is the radius of curvature of the surface, **D** is the separating distance, in Å, between the two mica surfaces, **k_B** is the Boltzmann constant, 1.38x10⁻²³ m²kgs⁻²K⁻¹, **T** is the temperature in °K (298.15°K), **Γ** is the molecular density, molecules per unit area and **R_g** is the radius of gyration for the cushion supported bilayer, in nm. For our system, we got an average **R_g** of 5.34 ± 1.1 nm and a molecular density, **Γ** of 6.34x10¹⁶ molecule/area. By using the relationship between molecular density **Γ** and **s**, the distance between the attachment of two PEG molecules, in nm:

$$\Gamma = \frac{1}{s^2} \quad (\text{Eq 4.1.4})$$

We calculated an average distance, **s** of 4.0 ± 0.8 nm, corresponding to the value that we obtained from the AM-AFM experiment, which is 3.90 ± 0.01 nm.

2. Force measurements on a symmetric system

The next set of SFA results we analysed are the symmetric systems as shown in Figure 40, where identical membranes are deposited on both lenses. We deposited the same membranes compositions as we did AM-AFM measurements (listed in Table 7 below) on the lenses and observed their interactions as the lenses are approached and separated.

Artificial Membrane on glass substrate	Artificial membrane system label	
	DPS/POPC - POPC	Outer Layer
Inner Layer		10% DPS:90% POPC
DPS/POPC - DMPC	Outer Layer	100% DMPC
	Inner Layer	10% DPS:90% POPC
DPS/DMPC - POPC	Outer Layer	100% POPC
	Inner Layer	10% DPS:90% DMPC
DPS/DMPC - DMPC	Outer Layer	100% DMPC
	Inner Layer	10% DPS:90% DMPC

Table 7: Summary of the different artificial membranes and their layers deposited on mica substrates.

In this symmetric system, the separating distance D refers to the distance between the two cushioned supported bilayers as shown in Figure 40. Like the asymmetric system, the reference point is taken to be when both bilayers are slowly brought into contact using the coarse control until flat fringes are seen in the spectrometer. Then for each contact region, we measure the average distance of all the curves for the same $F(D)/R$ value and then calculate the middle of all the contact regions. Finally, we pulled all the curves of each region to that middle distance.

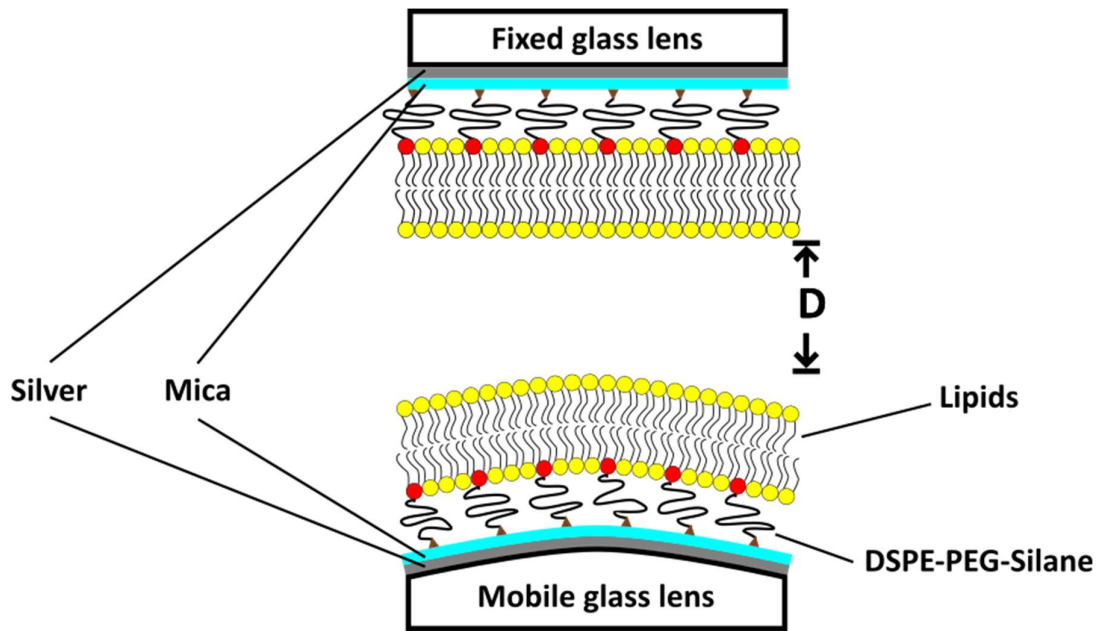


Figure 40: Illustrates the SFA setup for the symmetric system; the same cushioned supported bilayer on both lenses.

The first symmetric system measured was a symmetric membrane of DPS/POPC in the inner layer and POPC lipids in the outer layer on both lenses as shown in Figure 42. On the approach run, a small repulsive force is observed ($F > 0$) when $D \sim 20\text{-}18$ nm corresponding to the distance where both membrane interact with each other. The two membranes keep coming closer to each other, until a point where there is an inward jump at quasi-constant force which is observed. The distance of the jump is approximately 4 nm, corresponding to the thickness of a bilayer. This means that the jump corresponds to the hemi-fusion of the two membrane outer layers (as shown in Figure 41) and it happens at an average force value, normalized by the radius of curvature, of 0.60 ± 0.1 mN/m. On the separation run, we confirm that we had an attraction force from the sudden jump of the curve of ~ 25 nm corresponding to when the two surfaces completely separate. The adhesion energy measured was $W = -F/2\pi = -0.18 \pm 0.04$ mJ/m². This adhesion is

most likely due to the molecule interlacing of the lipids in the two outerlayers and also the polymer “bridging” forces (Wong et al. 1999)

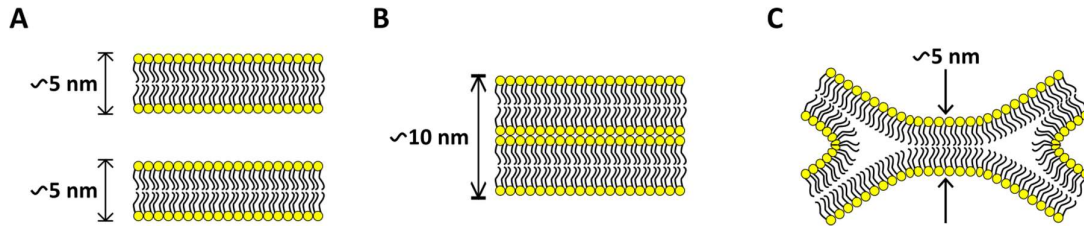


Figure 41: Illustrates the hemifusion process. (A) Two lipid bilayers are apart from each other by a distance D. (B) The two membranes are in contact with each other and they still are approaching. (C) The two membranes hemifused by missing the lipids of their outer layers and make the hydrophobic tails of their inner layers interact.

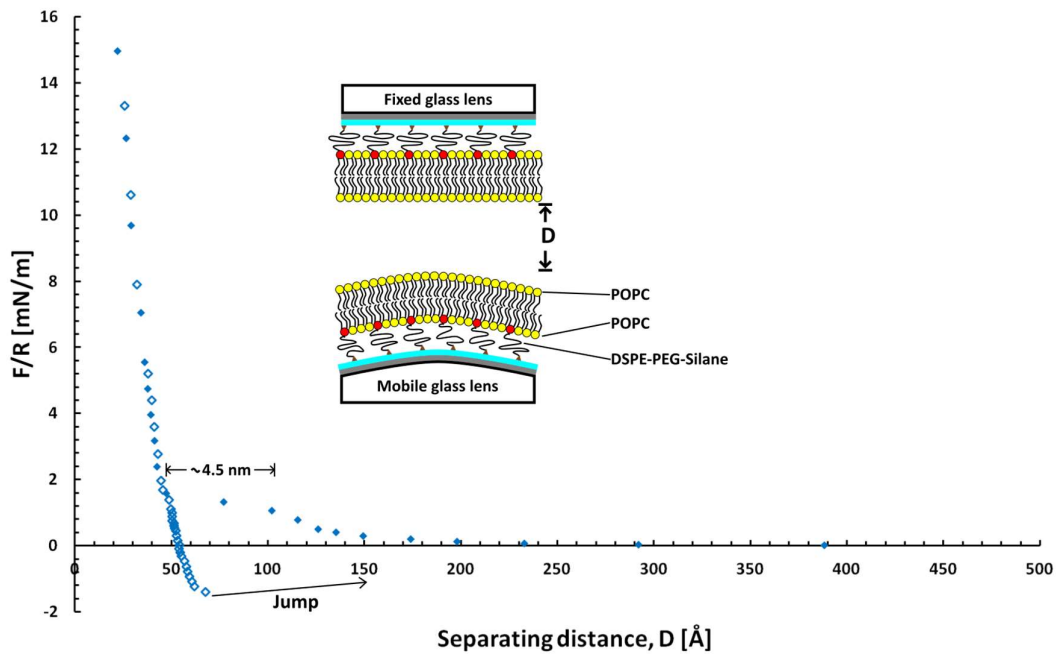


Figure 42: Illustrates the force curve of a symmetric system; with a symmetric membrane DPS/POPC-POPC on both sides. The filled dots are the approach run and the open symbols are the separation run.

At least 3 successive measurements were taken at the same contact, within at least 10 min intervals from each measurement. What was observed, was that the curves, for the

same contact point, overlay on each other even after hemi-fusion. This means that the bilayer healed really fast due to its high fluidity at room temperature of (22°C).

The following symmetric systems which were observed are the symmetric membrane of DPS/DMPC in the inner layer and DMPC lipids in the outer layer, shown in Figure 43 and the asymmetric membrane of DPS/DMPC in the inner layer and POPC lipids in the outer layer, shown in Figure 44 both membranes deposited on both lenses for the different experiments. In both cases, we were dealing with a completely repulsive system as explained earlier in the Chapter 2 section 4.6. This means that the approach and separation run overlap with no apparent hemi-fusion or complete fusion phenomena. It also means that there is no case of molecular entanglement in these cases. These experiments were performed at room temperature (22°C), at which DMPC lipids are in the gel phase and POPC lipids are in the fluid phase. This suggests that for hemi-fusion to happen in these sort of system without the presence of fusogenic proteins (proteins inducing fusion), that the lipids within the membrane has to be naturally fluid at room temperature.

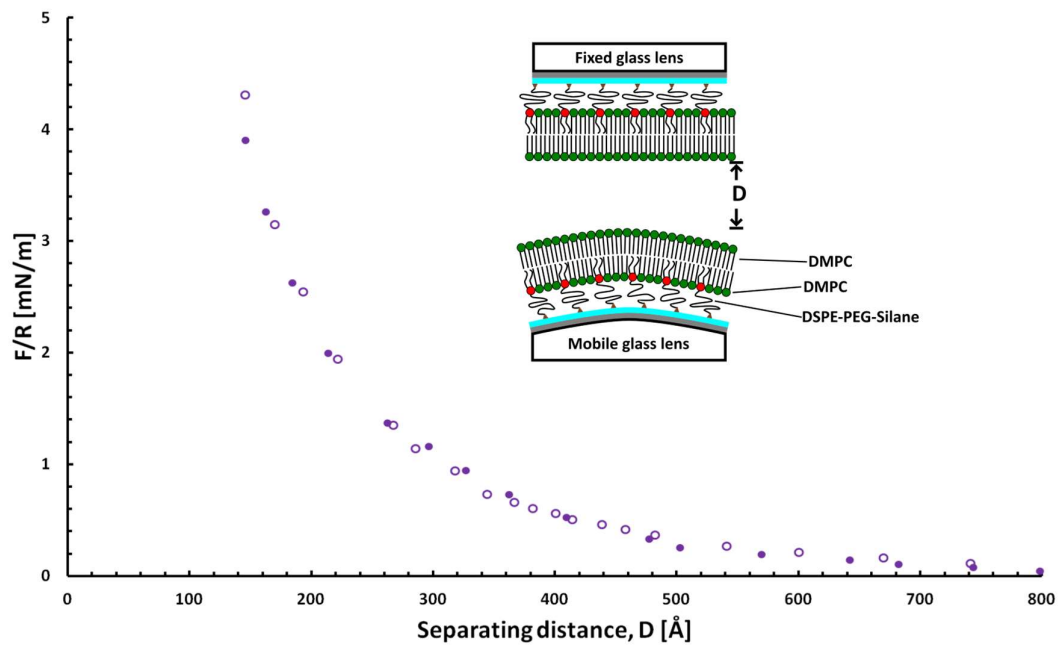


Figure 43: Illustrates the force curve of a symmetric system; with a symmetric membrane DPS/DMPC-DMPC on both sides. The filled dots are the approach run and the open symbols ones are the separation run.

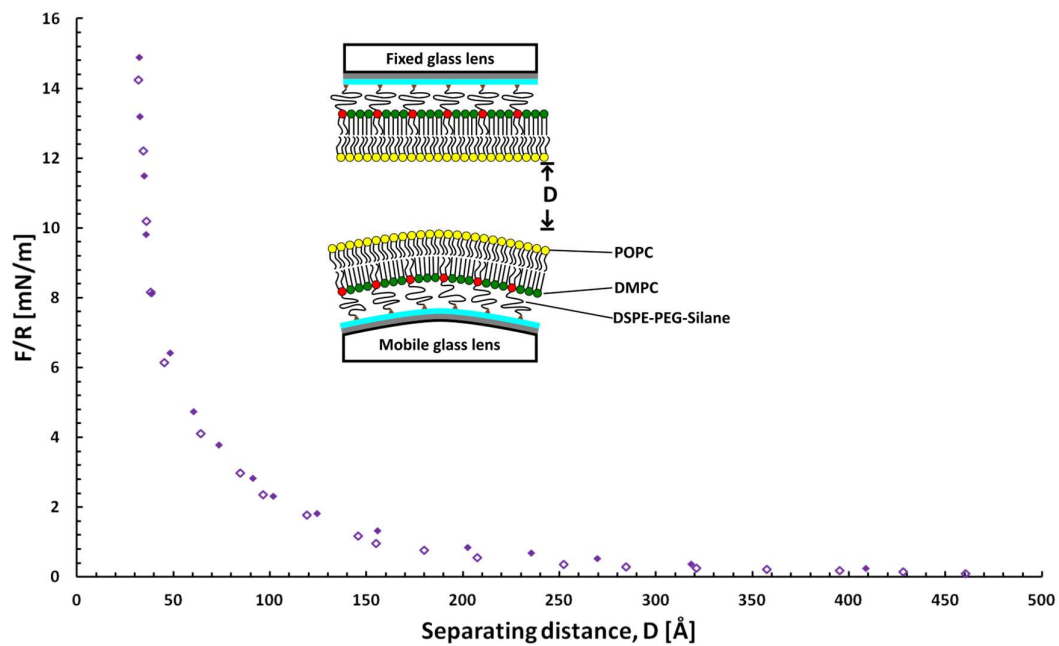


Figure 44: Illustrates the force curve of a symmetric system; with an asymmetric membrane DPS/DMPC-POPC on both sides. The filled dots are the approach run and the open symbols ones are the separation run.

3. Force measurements on a Hybrid system with Protein

incorporated

This project was focused on developing an artificial membrane, which mimics the same physiological characteristics of a biological membrane and incorporate biochemically active proteins in it. Then, using the surface force apparatus (SFA) to simulate the mechanism during exocytosis and observe the forces in play during membrane fusion. Therefore, final last set of SFA results are measurements made on a system in which Synaptotagmin-1, Syt1, a calcium sensor protein present in the synaptic vesicles to regulate the release of neurotransmitters. For this experiment, we used a modified version of the wild type synaptotagmin-1 (WT-Syt1), where 12x Histidine residues tag replaced the transmembrane domain of the full-length WT-Syt1. This modification allowed for the protein to bind DGS-NTA (Ni) lipids present in the Cis-membrane. Figure 45 shows the configuration of the system containing the protein; a Cis-membrane with Syt1, which represents the membrane of the synaptic vesicles, in which the neurotransmitters are encapsulated and a Trans-membrane, which represents the plasma membrane around the neuron's cell with DOPS and PIP2. The trans-membrane consists of the following lipids composition: 80% POPC lipids, 15% DOPS lipids and 5% PIPS. As for the Cis-membrane, it consists of 95% POPC lipids and 5% DGS-NTA (Ni) lipids, to which 2-3 histidines would bind per Ni NTA molecules. We can theoretically approximate the maximum surface density of Syt1 molecules per m^2 by doing the

following. Firstly, using the De Gennes theory for grafts neutral polymer (Wagner and Tamm 2000; de Gennes 1987), we calculated the average distance, s in nm, between two Ni NTA molecules using the following:

$$s = \left(\frac{A}{f} \right)^{1/2} \quad \text{(Eq 4.3.1)}$$

Where A , is the area of a single lipid molecule ($\sim 58 \text{ \AA}^2$ for a POPC lipid according to the experimental data from Figure 26) and f , is the mol fraction of Ni NTA molecules in the membrane. This gives us an average distance between two Ni NTA molecules to be ~ 4 nm. Now, using the following equation:

$$\Gamma = \frac{1}{s^2} \quad \text{(Eq 4.3.2)}$$

Where Γ , is the number of Ni NTA molecules per m^2 , which we calculated to be $\sim 8.6 \times 10^{16}$ molecules per m^2 . Knowing that 1 molecule of Syt1 binds with a minimum of 4 molecules of Ni NTA; we theoretically calculated the maximum surface density of protein is $\sim 2.2 \times 10^{16}$ Syt1 molecules per m^2 .

In this system, the separating distance D refers to the distance between the Cis- and Trans- membranes as shown in Figure 45. In order to do so, we subtracted the thickness of a bilayer ~ 5 nm (representing the thickness of the Cis-membrane) and the thickness of

the cushioned supported bilayer, $\sim 25 \pm 2$ nm measured from the asymmetric SFA experiments (representing the thickness of the Trans-membrane). Similar to the previous experiments, the set of curves are pulled towards the average separating distance of each experimental contact corresponding to the same particular $F(D)/R$ value.

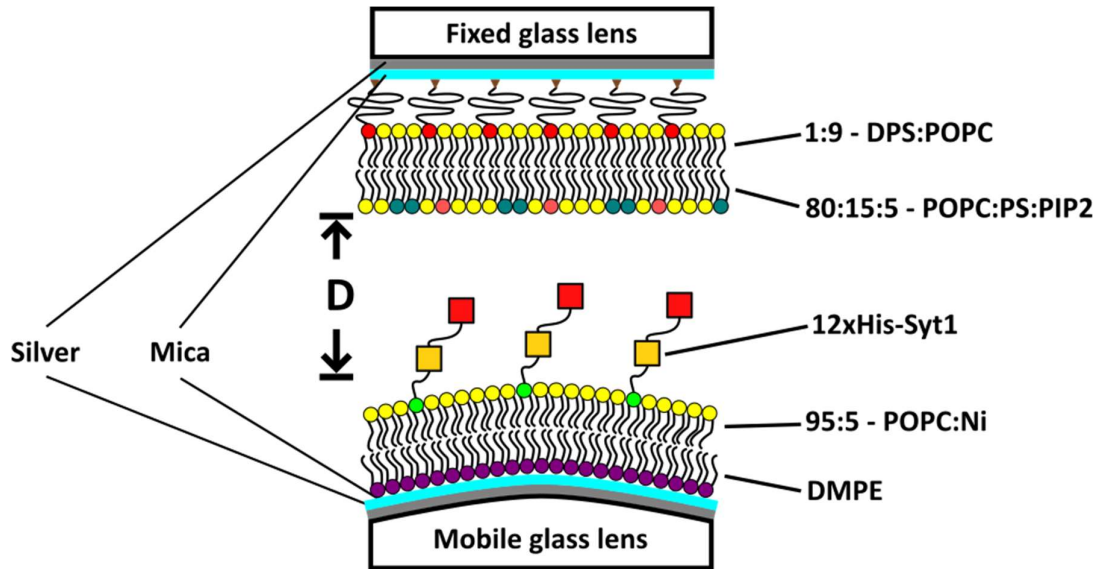


Figure 45: Illustrates the SFA setup for the system containing proteins; the mobile bottom lens represents the vesicle membrane (Cis-membrane) and the fix upper lens represents the plasma membrane (trans-membrane).

The experiments were conducted under well-established conditions to cause an adhesion force of the Syt1, already studied by (Gruget et al. 2018), where the buffer solution contains 150 mM KCl, 0.5 mM of EGTA and 0.5 mM of free Ca^{2+} . We compared the results obtained in our experiments to those published in (Gruget et al. 2018). All the results shown below are from at least 3 independent experimental setups and for at least 3 different contact spots with at least 4 runs each. The first set of measurements shows the results of approach and separation run done with 15 mN/m maximum force set point as

shown in Figure 46. It shows that the interaction between the 2 surfaces is completely repulsive as the approach and the separation run overlap each other.

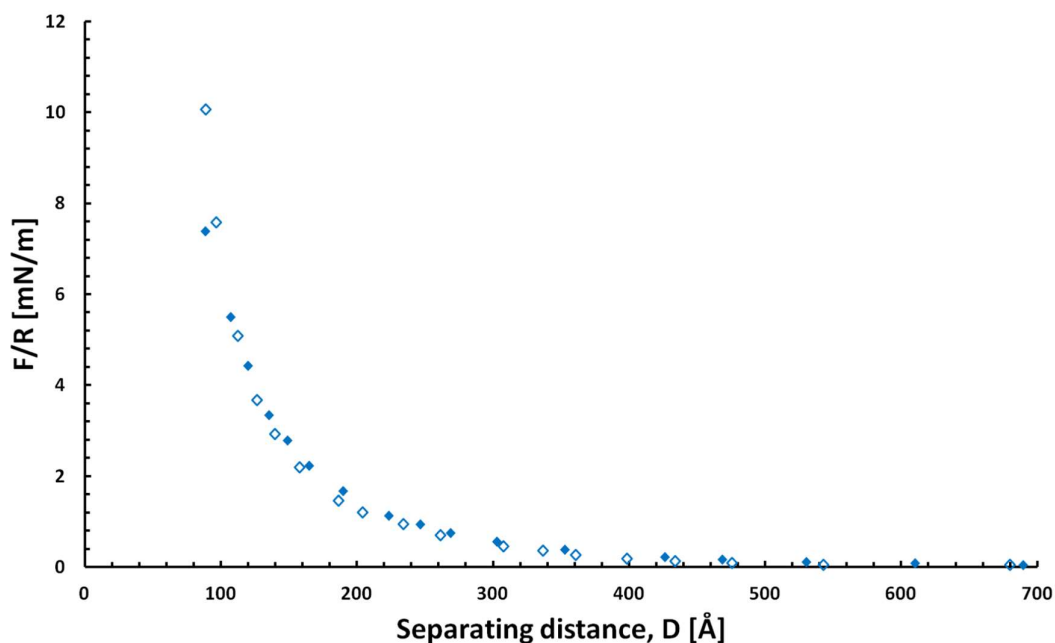


Figure 46: Illustrates the force curve of Syt1 system at 15 mN/m maximum forces applied. It shows a completely repulsive system with no adhesion force present.

In the next set of data, the maximum force set point was at 30 mN/m as shown in Figure 47 & Figure 48. Both figures show that at high maximum force, there is an adhesion force between the surfaces represented by the different path taken by the separation run compared to its approach. The normalised adhesion force measured was -1.3 ± 0.5 mN/m, corresponding to an adhesion energy of $W = -F/2\pi = -0.20 \pm 0.08$ mJ/m². Concerning the adhesion force, no difference was observed between having 1 hour waiting time between the approach and separation run, or not. However, during the 1 hour waiting time between the approach and separation run shown in Figure 48, there is

a slight inward shift of the separation force curve. This may indicate that during the 1 hour shift, there has been a modification of the protein structure or it can also be due to the lateral diffusion of the lipids around the protein molecule allowing it to insert into the membrane.

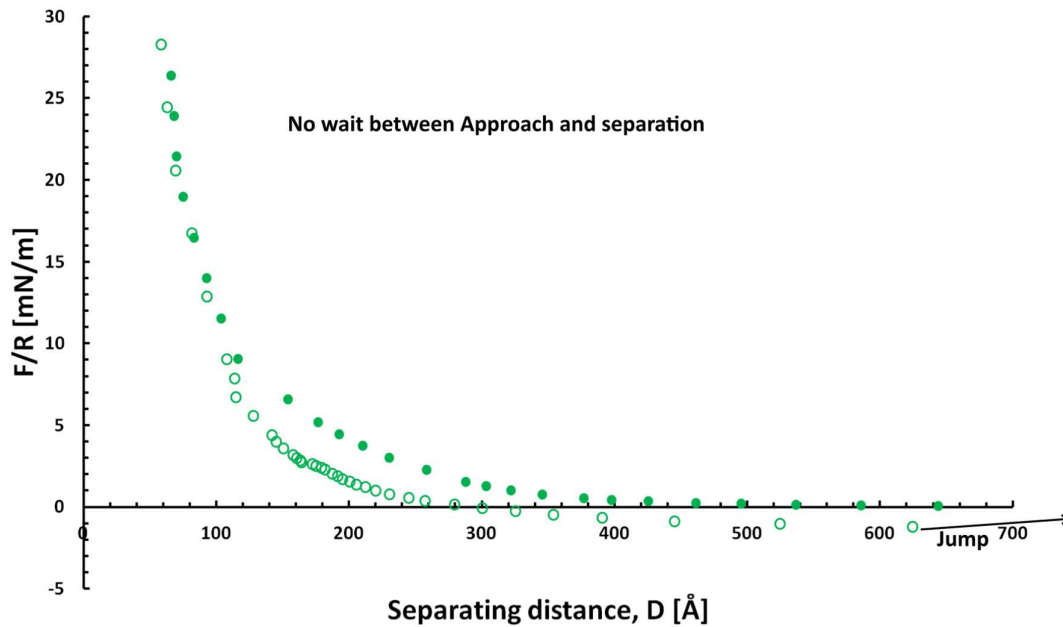


Figure 47: Illustrates the force curve of Syt1 system at 30 mN/m maximum forces applied with no waiting time between the approach and separation run. It shows an adhesion force during the separation run and also a long stretch of the system from ~30 nm to ~61nm before the 2 surfaces jump apart.

During the course of this experiment, we model the force interaction using the polymer mushroom model from **Eq 4.1.3**. From, this model, we extracted the radius of gyration, R_g , the molecular surface density, Γ . With this model, we obtained a normalised R_g value of 10.5 ± 1.1 nm and average molecular surface density, Γ of $(4.4 \pm 1.6) \times 10^{16}$ molecules/m² equivalent to a distance between to end-grafted protein, $s = \frac{1}{\sqrt{\Gamma}} = 4.8 \pm$

0.9 nm. Since, the value $s < R_g$, this means that we are in a high coverage of protein regime, and therefore in the polymer brush model, instead of the polymer mushroom model. So, we used the polymer brush model described in (de Gennes 1987) where the approximation equation at D , the separating distance between the 2 surfaces is equal or less than twice the thickness of the protein, L is given as follows:

$$\frac{F(D)}{R} = 200 \Gamma^{3/2} L K_B T \exp^{-\frac{\pi D}{L}} \quad (\text{Eq 4.3.3})$$

Where, K_B is the Boltzmann constant, $1.38 \times 10^{-23} \text{ m}^2 \text{ kgs}^{-2} \text{ K}^{-1}$ and T is the temperature in °K (298.15°K). With this model, we obtained , an average molecular surface density, Γ of $(1.9 \pm 0.5) \times 10^{16}$ molecules/m² equivalent to a distance between to end-grafted protein, $s = \frac{1}{\sqrt{\Gamma}} = 7.3 \pm 1.0$ nm and also obtained a normalised thickness of the protein, L of 19.3 ± 2 nm and a Flory radius of PEG polymer, $R_f = \left(L * s^{2/3} \right)^{5/3}$ of 13.1 ± 1.5 nm.

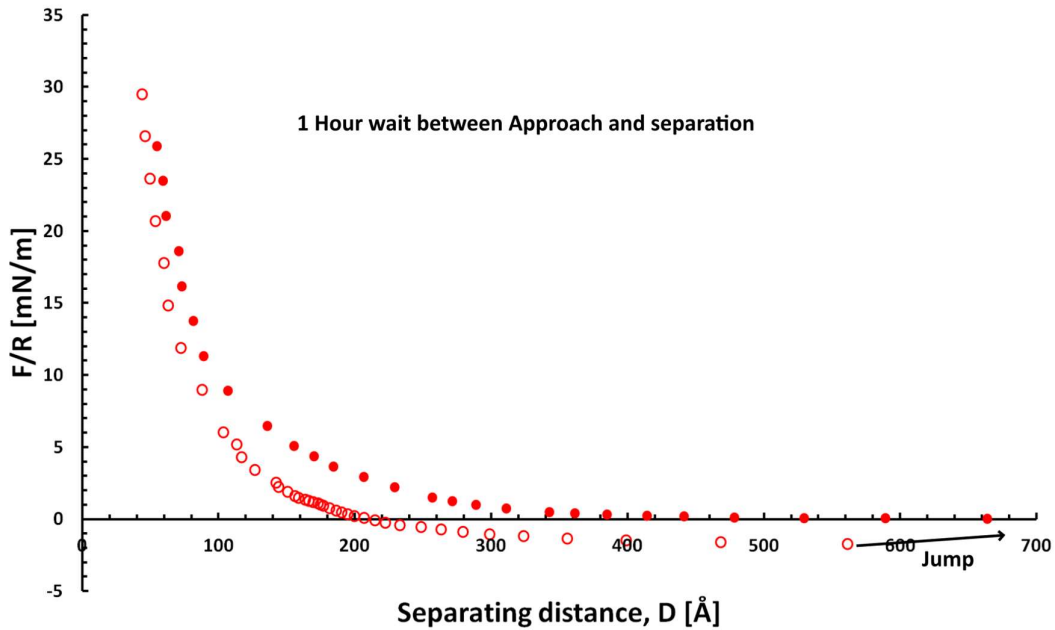


Figure 48: Illustrates the force curve of Syt1 system at 30 N/m maximum forces applied with 1 hour waiting time between the approach and separation run. It shows an adhesion force during the separation run and also a long stretch of the system from ~20 nm to ~56nm before the 2 surfaces jump apart. Moreover, there is a slight shift between the approach and separation curves that accounts to the restructuring of the protein during the 1 hour wait.

Moreover, if we compare the curves obtained from the studies of the same system in (Gruget et al. 2018) but on solid surface, we observe a difference on the separation run, from the point where $\frac{F(D)}{R} = 0$ till the surfaces detached (where the 2 surfaces jump away from each other). In the published study, we can see that there is roughly a 4 nm extension of the protein before the surfaces separates. However, in our study with the polymer cushioned on one side, that extension is approximately 36 nm, which we can suggest that before complete separation, the polymer and the protein has to extend without breaking and then detach. Finally, the last comparison that we made between the 2 studies is that the energy per molecule, E obtained in our experiments is low compared to the previous study; with solid surface system, $E = 17.6 \pm 1.4 k_B T$,

whereas with cushioned supported bilayer system, $E = 2.7 \pm 0.6 k_B T$. This also suggests that energy has been dissipated in the extension of the polymer during this study.

Conclusion

In this project, we were able to develop a cushioned supported lipid bilayer (CSLB), as a new model mimicking biological membranes, for studying membrane interaction involving protein. The difference with the solid supported lipid bilayer is the thin layer of polymer deposited in between the solid substrate and the lipid bilayer in the CSLB model. With the CSLB model, we obtained a higher mobility of the lipids, as attested by the diffusion coefficients measured during the study. Knowing that the lipids were diffusing faster in the CSLB model suggests that incorporated transmembrane proteins in this system would also be able to diffuse faster; in contrast to when they were in SLB model in which case they were immobile. Therefore, this CSLB model is a better physiological matrix for studying the interactions of membrane proteins and receptors, compared to previous model membrane system, the solid supported lipid bilayer (SLB) model.

Through amplitude modulated atomic force microscopy (AM-AFM), we were able to observe the topography of the different CSLB surfaces we made with a very high spatial resolution. Firstly, the AM-AFM images confirmed that a membrane was well deposited on the substrate when compared to a clean mica substrate under the same conditions. Secondly, the observations revealed that there were no defects on any of the membranes at the nanometric length scales studied here. The phase profiles unveiled a strong effect

between the lipid natural phase (at room temperature) in the inner layer and the structural organisation of lipids in the outer layer of the membrane. If the lipids in the inner layer are in the fluid phase, the topography images showed some structural motifs on the outer layer of the membrane. These motifs enabled us to locate the polyethylene glycol (PEG) molecules anchored into the membrane and measure the distance between two end grafted PEG molecules to be $\sim 3.9 \pm 0.1$ nm and a similar value of the distance was obtained independently by the fits of the force/distance profiles to polymer theory. These observations confirmed that the Langmuir Blodgett deposition method was the appropriate fabrication technique of this membrane model. It has enabled us to control the surface pressure at which each layer of the membrane was deposited in order to obtain a homogeneous membrane.

The developed membranes are subjected to surface force measurements in three different configurations: an asymmetric, a symmetric and a protein anchored configuration. From the asymmetric configuration results, we obtained 2 interesting results on the structure of these membranes. First, we confirmed that the distance between two end grafted PEG molecules to be $\sim 4.0 \pm 0.8$ nm. Secondly, was the height of the polymer cushion, which we measured to be $\sim 20 \pm 2$ nm. This elevation of the membrane would allow incorporating transmembrane proteins that have the freedom to diffuse laterally within the membrane. Thus, making the CSLB the appropriate model for the study of biochemically active membrane and furthermore, study the structure and

function of transmembrane proteins receptors in a more physiological matrix with the surface force apparatus (SFA).

The SFA measurements were also done in a symmetric configuration, where similar membranes were deposited on both lenses. The results obtained during the measurements showed that when 2 symmetric fluid membranes (same lipids composition in the inner and outer layer) are brought into contact, hemifusion happens (in our case at a normalised force of 0.60 ± 0.1 mN/m) when surfaces suddenly jumped inward by ~ 4.5 nm. This was also confirmed by the measured adhesion energy of -0.18 ± 0.04 mJ/m² obtained when the two lenses are separated. This adhesion is due to the molecular mixing of the lipids as the hydrophobic tails of apposing inner monolayer come into contact (as shown in Figure 49).

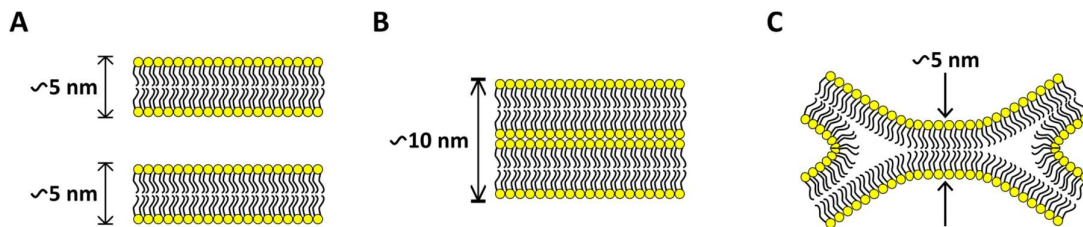


Figure 49: Illustrates the hemifusion process. (A) Two lipid bilayers are apart from each other by a distance D . (B) The two membranes are in contact with each other and they still are approaching. (C) The two membranes hemifused by missing the lipids of their outer layers and make the hydrophobic tails of their inner layers interact.

Moreover, membrane healing was observed after hemifusion as consecutive runs overlap each other. These observations suggest that membrane fusion may readily happen in absence of fuseogenic proteins if the lipids in the membrane are fluid.

Finally, with the last configuration as shown below in Figure 50, where we anchored protein to a SLB membrane on one lens and make it interact with a CSLB membrane on the other lens, we compared the results to a previous study where both sides were made of SLB membranes. We observed four distinct differences. Firstly, we only observed an adhesion force when the applied normalised force was greater than 30 mN/m. Secondly, we found that the anchored proteins created a shield between the two membranes and a long range repulsive interaction. This implies that for fusion to happen in the synapse there should be proteins that would pull the Syt1 protein closer to the target vesicle membrane and other to bring the transport vesicle membrane and target vesicle membrane into contact. Thirdly, we found that there is an extension of both the polymer cushion and the protein before they separate. Finally, the energy per molecule we measured with our system is low compared to that obtained in the previous studies, which suggest that energy has been dissipated during the extension of the polymer.

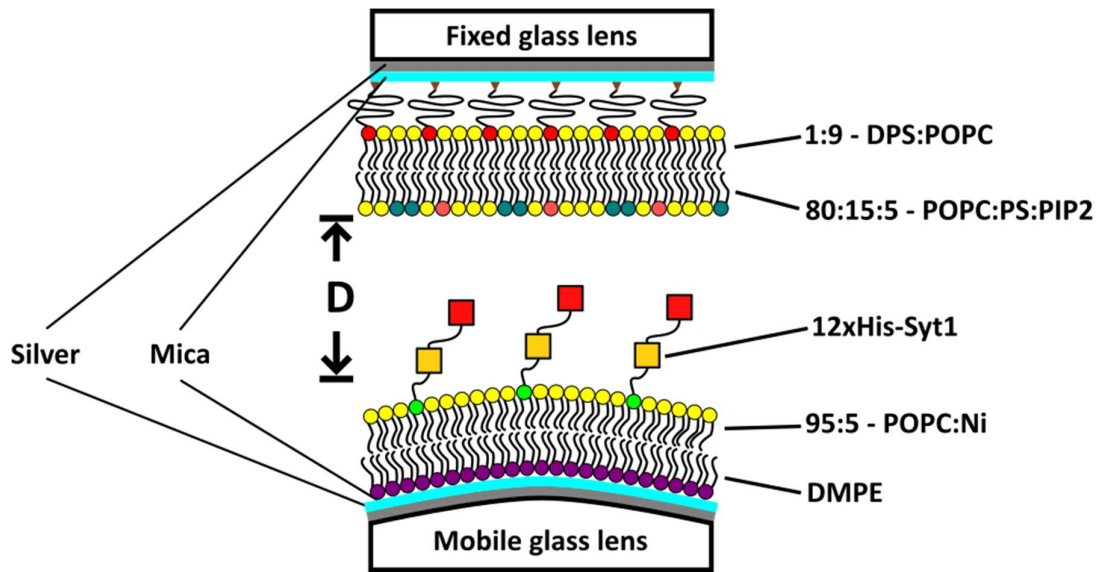


Figure 50: Illustrates the SFA setup for the system containing proteins; the mobile bottom lens represents the vesicle membrane (Cis-membrane) and the fix upper lens represents the plasma membrane (trans-membrane).

Since we were using the Langmuir Blodgett to deposit the membrane onto the lenses, and as a transmembrane protein does not insert naturally in a lipid monolayer at the air/water interface, we were unable to incorporate full transmembrane proteins. This is the reason why we started by using anchored proteins first. The future work would require finding a way to incorporate transmembrane proteins in the CSLBs model. This could be tested by depositing the first monolayer of the CSLBs with the Langmuir Blodgett deposition technique and then using vesicle fusion of proteoliposomes to spread a second layer of lipids with transmembrane proteins incorporated in them. Having a CSLB on both lens with transmembrane proteins incorporated in one of them, is a closer mimic of real biomembranes. For example, Syt1 is involved in the interaction of a neurotransmitter vesicle close to the neuron membrane, in a synapse. The full incorporation of a transmembrane Syt1 should provide an insight on the function of the

transmembrane domain during membrane fusion and should also provide the possibility of membrane deformation to ease membrane fusion.

Bibliography

- Alberts, J., Lewis, Raff, Roberts, and Walter. 2008. *Molecular Biology of Cell*. 5th ed. papers2://publication/uuid/0BF210E2-70B3-4CC9-A859-111EF841687B.
- Anton, Nicolas, Philippe Pierrat, Luc Lebeau, Thierry F. Vandamme, and Patrick Bouriat. 2013. 'A Study of Insoluble Monolayers by Deposition at a Bubble Interface'. *Soft Matter* 9 (42): 10081–91. <https://doi.org/10.1039/c3sm51688a>.
- Berg, J. M., J. L. Tymoczko, G. J. Gatto, and L. Stryer. 2019. *Biochemistry. Journal of Chemical Information and Modeling*. 8th ed. Vol. 53. <https://doi.org/10.1017/CBO9781107415324.004>.
- Bouar, Tugdual Le, Yongmin Zhang, Jacques Esnault, Jean-maurice Mallet, Eric Perez, and Pierre Sinay. 2001. 'Ultraweak Sugar-Sugar Interactions for Transient Cell Adhesion' 80 (March): 1354–58. [https://doi.org/10.1016/S0006-3495\(01\)76108-5](https://doi.org/10.1016/S0006-3495(01)76108-5).
- Corbalan-garcia, Senena, and Juan C Gómez-fernández. 2014. 'Biochimica et Biophysica Acta Signaling through C2 Domains : More than One Lipid Target ☆'. *BBA - Biomembranes* 1838 (6): 1536–47. <https://doi.org/10.1016/j.bbamem.2014.01.008>.
- Derjaguin, BV, VM Muller, and YP Toporov. 1975. 'Effect of Contact Deformation on the Adhesion of Elastic Solids'. *Journal of Colloid and Interface Science* 53 (2): 314–26. [http://linkinghub.elsevier.com/retrieve/pii/0021979775900181%0Apapers3://publication/doi/10.1016/0021-9797\(75\)90018-1](http://linkinghub.elsevier.com/retrieve/pii/0021979775900181%0Apapers3://publication/doi/10.1016/0021-9797(75)90018-1).
- Eeman, Marc, and Magali Deleu. 2010. 'From Biological Membranes to Biomimetic Model Membranes'. *Biotechnology, Agronomy and Society and Environment* 14 (4): 719–36.
- Elbourne, Aaron, Madeleine F. Dupont, Simon Collett, Vi Khanh Truong, Xiu Mei Xu, Nandi Vrancken, Vladimir Baulin, Elena P. Ivanova, and Russell J. Crawford. 2019. 'Imaging the Air-Water Interface: Characterising Biomimetic and Natural Hydrophobic Surfaces Using in Situ Atomic Force Microscopy'. *Journal of Colloid and Interface Science* 536: 363–71. <https://doi.org/10.1016/j.jcis.2018.10.059>.
- Fukuma, Takeshi, Michael J. Higgins, and Suzanne P. Jarvis. 2007. 'Direct Imaging of Lipid-Ion Network Formation under Physiological Conditions by Frequency Modulation Atomic Force Microscopy'. *Physical Review Letters* 98 (10): 1–4. <https://doi.org/10.1103/PhysRevLett.98.106101>.
- G. Roberts, G. 2006. 'Langmuir-Blodgett Films'. *Contemporary Physics* 25 (August): 109–28. <https://doi.org/10.1080/00107518408230324>.
- García, Ricardo. 2010. 'Phase Imaging Atomic Force Microscopy'. *Amplitude Modulation Atomic Force Microscopy*, 91–101. <https://doi.org/10.1002/9783527632183.ch7>.
- Gennes, P. G. de. 1987. 'Polymers at an Interface; a Simplified View'. *Advances in Colloid and Interface Science* 27 (3–4): 189–209. [https://doi.org/10.1016/0001-8686\(87\)85003-0](https://doi.org/10.1016/0001-8686(87)85003-0).
- Gourier, Christine, Frørdoric Pincet, Eric Perez, Yongmin Zhang, Zhenyuan Zhu, Jean-maurice Mallet, and Pierre Sinab. 2005. 'The Natural Lewis' 05: 1683–87. <https://doi.org/10.1002/anie.200461224>.
- Gruget, Clémence, Jeff Coleman, Oscar Bello, Shyam S. Krishnakumar, Eric Perez, James E. Rothman, Frederic Pincet, and Stephen H. Donaldson. 2018. 'Rearrangements under Confinement Lead to Increased Binding Energy of Synaptotagmin-1 with Anionic Membranes in Mg 2+ and Ca 2+'. *FEBS Letters* 592 (9): 1497–1506. <https://doi.org/10.1002/1873-3468.13040>.
- Heo, Paul, Sathish Ramakrishnan, Jeff Coleman, James Rothman, Jean-Baptiste Fleury, and Frederic Pincet. 2019. 'Highly Reproducible Physiological Asymmetric Membrane with Freely Diffusing Embedded Proteins in a 3D-Printed Microfluidic Setup'. *Small*, April, 1900725. <https://doi.org/10.1002/sml.201900725>.
- Israelachvili, J. N. 1973. 'Thin Film Studies Using Multiple-Beam Interferometry'. *Journal of Colloid And Interface Science* 44 (2): 259–72. [https://doi.org/10.1016/0021-9797\(73\)90218-X](https://doi.org/10.1016/0021-9797(73)90218-X).
- Israelachvili, Jacob N, and Gayle E Adams. 1978. 'Measurement of Forces between Two Mica Surfaces in Aqueous Electrolyte Solutions in the Range 0–100 Nm'. *Journal of the Chemical Society, Faraday Transactions 1: Physical Chemistry in Condensed Phases* 74 (0): 975–1001.

- <https://doi.org/10.1039/F19787400975>.
- Jagtap, R. N., and A. H. Ambre. 2005. 'Atomic Force Microscopy (AFM): Basics and Its Important Applications for Polymer Characterization: An Overview'. *Journal of Polymer Materials* 22 (1): 1–26.
- Jahn, Reinhard, and Dirk Fasshauer. 2012. 'Molecular Machines Governing Exocytosis of Synaptic Vesicles'. *Nature* 490 (7419): 201–7. <https://doi.org/10.1038/nature11320>.
- Kang, Minchul, Charles A Day, Anne K Kenworthy, and Emmanuele DiBenedetto. 2012. 'Simplified Equation to Extract Diffusion Coefficients from Confocal FRAP Data.' *Traffic (Copenhagen, Denmark)* 13 (12): 1589–1600. <https://doi.org/10.1111/tra.12008>.
- Katz, B Y B, and R Miledi. 1969. 'SPONTANEOUS AND EVOKED ACTIVITY OF MOTOR NERVE ENDINGS IN CALCIUM RINGER', 689–706.
- Leica TCS SP5 Leica TCS SP5 X User Manual*. n.d.
- Li, Feng, Frédéric Pincet, Eric Perez, William S. Eng, Thomas J. Melia, James E. Rothman, and David Tareste. 2007. 'Energetics and Dynamics of SNAREpin Folding across Lipid Bilayers'. *Nature Structural and Molecular Biology* 14 (10): 890–96. <https://doi.org/10.1038/nsmb1310>.
- Motta, Isabelle, Andrea Gohlke, Vladimir Adrien, Feng Li, Hélène Gardavot, James E. Rothman, and Frederic Pincet. 2015. 'Formation of Giant Unilamellar Proteo-Liposomes by Osmotic Shock'. *Langmuir* 31 (25): 7091–99. <https://doi.org/10.1021/acs.langmuir.5b01173>.
- Mouritsen, Ole G, Kai Simons, Julio L Sampaio, Dominik Schwudke, Kai Schuhmann, Clifford A Lingwood, Annette Shewan, et al. 2012. 'Model Answers to Lipid Membrane Questions'. <https://doi.org/10.1101/cshperspect.a004622>.
- Oesterhelt, F., M. Rief, and H. E. Gaub. 1999. 'Single Molecule Force Spectroscopy by AFM Indicates Helical Structure of Poly(Ethylene-Glycol) in Water'. *New Journal of Physics* 1.
- Page, Alistair J., Aaron Elbourne, Ryan Stefanovic, Matthew A. Addicoat, Gregory G. Warr, Kislon Voitchovsky, and Rob Atkin. 2014. '3-Dimensional Atomic Scale Structure of the Ionic Liquid-Graphite Interface Elucidated by AM-AFM and Quantum Chemical Simulations'. *Nanoscale* 6 (14): 8100–8106. <https://doi.org/10.1039/c4nr01219d>.
- Palfreyman, Mark T, and Erik M Jorgensen. n.d. 'Roles of SNARE Proteins in Synaptic Vesicle Fusion SNARE Discovery : A Convergence of Genetics', 35–59.
- Perez, Eric, Feng Li, David Tareste, and Frédéric Pincet. 2008. 'The Surface Force Apparatus to Reveal the Energetics of Biomolecules Assembly. Application to DNA Bases Pairing and SNARE Fusion Proteins Folding'. *Cellular and Molecular Bioengineering* 1 (4): 240–46. <https://doi.org/10.1007/s12195-008-0025-7>.
- Perez, Eric, and Joe Wolfe. 1994. 'A Simple, Cheap, Clean, Reliable, Linear, Sensitive, Low-Drift Transducer for Surface Pressure'. *Langmuir* 10 (3): 974–75. <https://doi.org/10.1021/la00015a062>.
- Pincet, Frédéric, Vladimir Adrien, Rong Yang, Jérôme Delacotte, James E. Rothman, Wladimir Urbach, and David Tareste. 2016. 'FRAP to Characterize Molecular Diffusion and Interaction in Various Membrane Environments'. *PLoS ONE* 11 (7): 1–19. <https://doi.org/10.1371/journal.pone.0158457>.
- Prashar, Deepak. 2012. 'Self Assembled Monolayers -a Review'. *International Journal of ChemTech Research* 4 (1): 258–65.
- Sader, John E., Ian Larson, Paul Mulvaney, and Lee R. White. 1995. 'Method for the Calibration of Atomic Force Microscope Cantilevers'. *Review of Scientific Instruments* 66 (7): 3789–98. <https://doi.org/10.1063/1.1145439>.
- Schweizer, F. E., and G. J. Augustine. 1998. 'SNARE Proteins and the Timing of Neurotransmitter', 293–97.
- Singer, S. J., and G. L. Nicolson. 2016. 'The Fluid Mosaic Model of the Structure of Cell Membranes' 239 (4843): 17–18.
- Söllner, T., SW. Whiteheart, M. Brunner, Erdjument-Bromage Geromanos S H., P. Tempst, and JE. Rothman. 1993. 'SNAP Receptors Implicated in Vesicle Targeting and Fusion.' *Nature* 362 (6418): 318–24. <http://www.nature.com/nature/journal/v362/n6418/abs/362318a0.html>.
- Soumpasis, D. M. 1983. 'Theoretical Analysis of Fluorescence Photobleaching Recovery Experiments'.

- Biophysical Journal* 41 (1): 95–97. [https://doi.org/10.1016/S0006-3495\(83\)84410-5](https://doi.org/10.1016/S0006-3495(83)84410-5).
- Südhof, Thomas, and James Rothman. 2009. 'Membrane Fusion: Grappling with SNARE and SM Proteins'. *Science (New York, N.Y.)* 323 (February): 474–77. <https://doi.org/10.1126/science.1161748>.
- Szoka, Francis. 1980. 'COMPARATIVE PROPERTIES AND METHODS OF PREPARATION OF LIPID VESICLES (LIPOSOMES)', 467–508.
- Wagner, Michael L., and Lukas K. Tamm. 2000. 'Tethered Polymer-Supported Planar Lipid Bilayers for Reconstitution of Integral Membrane Proteins: Silane-Polyethyleneglycol-Lipid as a Cushion and Covalent Linker'. *Biophysical Journal* 79 (3): 1400–1414. [https://doi.org/10.1016/S0006-3495\(00\)76392-2](https://doi.org/10.1016/S0006-3495(00)76392-2).
- Weber, Thomas, Boris V. Zemelman, James A. McNew, Benedikt Westermann, Michael Gmachl, Francesco Parlati, Thomas H. Söllner, and James E. Rothman. 1998. 'SNAREpins: Minimal Machinery for Membrane Fusion'. *Cell* 92 (6): 759–72. [https://doi.org/10.1016/S0092-8674\(00\)81404-X](https://doi.org/10.1016/S0092-8674(00)81404-X).
- Wong, Joyce Y., Chad K. Park, Markus Seitz, and Jacob N. Israelachvili. 1999. 'Polymer-Cushioned Bilayers, II. An Investigation of Interaction Forces and Fusion Using the Surface Forces Apparatus'. *Biophysical Journal* 77 (3): 1458–68. [https://doi.org/10.1016/S0006-3495\(99\)76993-6](https://doi.org/10.1016/S0006-3495(99)76993-6).

Résumé

Les membranes à support solide sont des bicouches lipidiques déposées directement sur un substrat solide. Elles sont généralement utilisées comme modèles de membranes biologiques pour l'étude des interactions membranaires comprenant des protéines et des récepteurs. Un problème majeur de ces modèles de membranes est le fait que les protéines transmembranaires ne peuvent pas interagir physiologiquement en raison des interactions défavorables induites par la proximité du support solide. Pour résoudre ce problème, nous avons développé un système de membranes sur coussin de polymères compatible avec l'incorporation intégrale de protéines transmembranaires avec une mobilité latérale. Nous utilisons une bicouche lipidique sur un coussin mince de polymère de polyéthylène glycol (PEG), qui constitue un support souple et, avec une bonne stabilité grâce à la liaison covalente des membranes au substrat solide par l'intermédiaire du PEG. Les bicouches ont été formées sur des substrats solides tels que le mica ou le verre selon la technique de dépôt de Langmuir Blodgett: une première monocouche composée de silane-PEG-lipide (10%) et de lipide (90%) a été déposée, suivie d'une seconde couche lipidique (100%). Leur morphologie a été observée en utilisant la microscopie à force atomique à ultra haute résolution (AFM). Nous n'avons observé aucun défaut de structure à l'échelle sub-nanométrique sur ces bicouches sur coussin de polymère. La diffusion latérale des lipides dans la bicouche a été mesurée par recouvrement de fluorescence après photoblanchiment (FRAP). Selon la phase des lipides (gel ou fluide) dans chaque couche de la membrane, nous avons observé une augmentation des coefficients de diffusion latérale (de 1,9 à 4,3 $\times 10^8$ cm² / s) en allant de la phase gel à la phase fluide à température ambiante.

En utilisant l'appareil de force de surface (SFA), nous avons pu observer l'interaction de ces modèles de membrane dans différentes configurations (bicouches dans l'état gel ou fluide, configuration symétrique ou asymétrique des surfaces en interaction dans le SFA). Les mesures montrent que l'épaisseur du coussin de polymère était d'environ 20 nm en milieu aqueux. Elles montrent également que l'hémi fusion entre les membranes (où la couche externe de chaque membrane fusionne et se déplace dans le réservoir aqueux afin de ne mettre en contact que les couches internes) ne se produit que lorsque les lipides sont fluides dans les couches interne et externe. Une protéine, Synaptotagmin-1 (Syt1), a ensuite été ancrée sur la bicouche sur coussin de polymère. Il a été démontré que cette protéine se liait aux lipides d'une membrane opposé lors d'expériences précédentes sur des membranes à support solide. Les mesures effectuées avec des protéines ancrées à la bicouche de lipides sur coussin polymérique révèlent une diminution de l'énergie par molécule de l'étude précédente réalisée avec un modèle de bicouche de lipide à support solide : de $17,6 \pm 1,4$ kBT pour la bicouche supportée à $2,7 \pm 0,6$ kBT pour la bicouche sur coussin. Ceci suggère que lors de la séparation des lentilles, le polymère et les protéines sont étirés au moment de la séparation et que l'énergie perdue est dissipée dans l'extension du polymère. Les travaux menés dans le cadre de ce projet nous donnent une première étape dans la construction d'une couche lipidique sur coussin polymérique avec des protéines transmembranaires incorporées.

Mots Clés

Membranes sur coussin
Polymère de polyéthylène glycol
Microscopie à force atomique
Appareil de force de surface

Abstract

Solid Supported membranes, lipid bilayers that are directly deposited on a solid substrate, are generally used as models of biological membranes for the study of membrane interactions involving proteins and receptors. A primary problem with these model membranes is the fact that transmembrane proteins cannot interact physiologically due to unfavourable interactions induced by the proximity of the solid support. To solve this problem, we have developed a cushioned supported bilayer system that is compatible with the incorporation of integral membrane proteins in a laterally mobile form. We use a lipid bilayer on a thin polyethylene glycol (PEG) polymer cushion, which provides a soft support, and for increased stability, covalent linkage of the membranes to the solid substrate mediated by the PEG. The bilayers were formed on solid substrates like mica or glass using Langmuir Blodgett deposition technique: a first monolayer composed of silane-PEG-lipid (10%) and lipid (90%) was deposited, followed by a second lipid (100%) monolayer. Their morphology was observed using ultra-high-resolution atomic force microscopy (AFM). We observed no structural defects on these cushions supported bilayers at a sub nanometric scale. The lateral diffusion of the lipids in the bilayer was monitored by fluorescence recovery after photobleaching (FRAP). Depending on the phase of the lipids (gel or fluid) within each layer of the membrane, we observed an increase in lateral diffusion coefficients (from 1.9 to 4.3 $\times 10^8$ cm²/s) upon going from gel like lipids to fluid like lipids at room temperature.

Using the surface force apparatus (SFA), we were able to observe the interaction of these membrane models in different configurations (bilayers in a gel or fluid phase, symmetric or asymmetric configuration of the interacting surfaces in the SFA). The measurements show that the thickness of the polymer cushion was ~ 20 nm in an aqueous medium. They also show that hemifusion between the membranes (where the outer layer of each membrane fuse and move into the aqueous reservoir in order to bring only the inner layers into contact) occurs only when there are fluid lipids in both the inner and outer leaflets. Then, one protein, Synaptotagmin-1 (Syt1), was attached to the cushioned lipid bilayer. This protein has been shown to bind to the lipids of an opposing membrane in previous experiments on solid supported membranes. The measurements made with Syt1 anchored to the cushioned lipid bilayer reveal a lowering of the energy per molecule compared to the previous study done with solid supported lipid bilayer model; from 17.6 ± 1.4 kBT on solid supported membrane to 2.7 ± 0.6 kBT on cushioned bilayer. This suggests that during the separation of the lenses, the polymer and the proteins are stretched before separating and the lost energy is dissipated into the polymer extension. The work in this project gives us an initial start on building a cushioned supported lipid bilayer with transmembrane proteins incorporated in them.

Keywords

Cushion supported Bilayer
Polyethylene Glycol
Atomic Force Microscopy
Surface Force Apparatus

